



Helen Verstraelen

CORROSION IN BALLAST TANKS ON BOARD OF MERCHANT VESSELS

Study of the relation between steel quality and corrosion

Universiteit Antwerpen
Associaiefaculteit Nautische Wetenschappen
Faculteit Wetenschappen
Departement Bio-ingenieurswetenschappen

CORROSIE IN BALLASTTANKS VAN KOOPVAARDIJSCHEPEN
Studie naar de relatie tussen staalkwaliteit en corrosie

Proefschrift voorgedragen tot het behalen van de graad van
doctor in de Nautische Wetenschappen aan de universiteit Antwerpen te verdedigen door

Helen Verstraelen

Antwerpen, 2013

Promotoren Universiteit Antwerpen: Prof. dr. Silvia LENAERTS
Hogere Zeevaartschool Antwerpen: Prof. kapt. dr. Kris DE BAERE

Associatiefaculteit Nautische Wetenschappen

**Faculteit Wetenschappen
Departement Bio-ingenieurswetenschappen**

**CORROSION IN BALLAST TANKS ON BOARD OF MERCHANT VESSELS
Corrosie in ballasttanks van koopvaardij schepen**

Study of the relation between steel quality and corrosion

Studie naar de relatie tussen staalkwaliteit en corrosie

**Proefschrift voorgelegd tot het behalen van de graad van doctor in de Nautische
Wetenschappen aan de Universiteit Antwerpen te verdedigen door**

Helen Verstraelen

Promotoren: Prof. dr. Silvia LENAERTS

Prof. Kapt. dr. Kris DE BAERE

Antwerpen, 2013

Print: Silhouet, Maldegem

© 2013 Helen Verstraelen

2013 Uitgeverij VUBPRESS Brussels University Press

VUBPRESS is an imprint of ASP nv (Academic and Scientific Publishers nv)

Ravensteingalerij 28

B-1000 Brussels

Tel. +32 (0)2 289 26 50

Fax +32 (0)2 289 26 59

E-mail: info@vubpress.be

www.vubpress.be

ISBN 978 90 5718 278 5

NUR 950/969/974

Legal deposit D/2013/11.161/040

All rights reserved. No parts of this book may be reproduced or transmitted in any form or by any means, *electronic, mechanical, photocopying, recording, or otherwise*, without the prior written permission of the author.

Examination board

Prof. dr. Roeland Samson – President of the doctoral jury (University of Antwerp)

Prof. dr. Silvia Lenaerts – Supervisor (University of Antwerp)

Prof. dr. Kris De Baere – Supervisor (Antwerp Maritime Academy)

Prof. dr. Geert Potters – Assessor (Antwerp Maritime Academy)

Prof. dr. Marc Vantorre – Assessor (University of Ghent)

Prof. dr. Karolien De Wael - Assessor (University of Antwerp)

dr. Chao Wei – Assessor (American Bureau of Shipping)

Thank you

After a lot of hard work, experimenting, drawing wrong conclusions, suffering setbacks and putdowns, experiencing joy, discovering interesting opportunities and savoring “Eureka!” moments, the results of all that effort is presented in this manuscript. Let me take the opportunity to thank those who have participated in this work.

Capt. Dr. Kris De Baere drives the research into corrosion at the AMA and is the in-house promoter of this thesis. He has always proved a highly enthusiastic and extremely thorough investigator. No stone was left unturned! He helped me from beginning to end and this work would never have been possible without his contribution.

From the start of this research program in 2007, the department of bio-engineers at UA, represented by Dr. Silvia Lenaerts, my promoter at UA, Dr. Geert Potters and Dr. Roeland Samson believed in this research project. They have provided the academic input to the subject and have taught an inexperienced researcher the tricks of the trade.

Many experts specializing in different aspects of corrosion, chemical, metallurgical, economic and statistical science, helped me to understand the basics of their particular fields of study. All of this was previously untrodden ground for me. Ir. Jean- Pierre Smet, Dr. Deidre Luyckx, Dr. Ann De Vyt, Dr. Yves Van Ingelghem, Dr. Lucien Lemmens, Dr. Philippe Rigo, Dr. Steven Van Passel, Dr. Marc Vantorre, Dr. Karolien De Wael, Dr. Chao Wei, and many others from the universities of Antwerp, Ghent, Leuven, Brussels and Liège, have supported me with their professional knowledge and expertise.

The Antwerp Maritime Academy, Antwerp Ship Repair, the Belgian shipping companies and ABS all opened doors and sponsored this project with material, facilities and/or financial support.

And finally, you can't live without love and Bart, Simon and William, my family, have given me all the love and appreciation I need. The smiles, jokes and cuddles, the everyday needs, keep everything in perspective.

Summary

Corrosion in ballast tanks represents a major cost in the operation of merchant ships. On board of every ship, the crew is doing its utmost to fight the spontaneous electrochemical reaction of iron, oxygen and seawater. But ultimately, the ship loses its strength and is sent to scrap. Many of the components are recycled and the steel is molten again, ready to be reused, maybe for the construction of another vessel. For this new or recycled steel of different chemical composition, it is interesting to know whether there is a difference in corrosion performance and whether a new corrosion resistant material gives a possible economical alternative for ballast tank construction. Three distinctive elements that are dealt with in the major parts of this work.

First, an economic study evaluates five possibilities for ballast tank construction and protection against corrosion. Five options were considered: Standard epoxy coating and zinc sacrificial anodes, increased scantlings, a life lasting coating system, the use of corrosion resistant steel and a standard epoxy coating with lifetime aluminum sacrificial anodes. The life cycle cost of every option was calculated and a sensitivity analysis was performed. An interesting conclusion was that the steel quality used might be an important element in the economic life expectancy of the vessel.

Therefore, the second part focuses on the quality of ship construction steel used in ballast tanks of merchant vessels. To examine this, ballast tank construction plates were collected from vessels performing steel work in dry-dock. These plates were investigated thoroughly to define the chemical composition, the metallic structures and the inclusions. The corrosion rate was monitored at defined intervals for a period of two years. Experimental corrosion resistant steel quality for use in ballast tanks was added to the sample collection in the experimental set up. This resulted in three clusters of steel qualities: grade A steel, high tensile steel and corrosion resistant steel. The grade A and AH steel samples have similar corrosion rates, a conclusion that is supported by many laboratory studies on new construction material. The corrosion resistant steel, which has notable higher concentrations of chromium, molybdenum and aluminum and a small Cu concentration, performs much better with a corrosion rate reduction of more than 30% (up to 50%).

It is therefore relevant to know whether this corrosion resistant steel has the mechanical and chemical properties required to be used as ship ballast tank construction material. This is dealt with in the third part. Hardness, tensile strength and yield stress, notch toughness and weldability are measured and evaluated.

This research emphasizes the need for steel mills to develop steel qualities for ballast tank construction that can eliminate the need for protective coating and/or sacrificial anodes, being beneficial for the environment as it reduces the introduction of heavy metals from

the sacrificial anodes and solvent emission from coatings. An economic advantage, as maintenance costs can be reduced significantly.

Samenvatting

Corrosie in ballasttanks van koopvaardij schepen vertegenwoordigt een belangrijke kost in de exploitatie van een schip. De scheepsbemanning doet zijn uiterste best om de spontane elektrochemische reactie van ijzer, zeewater en zuurstof tegen te gaan. Maar uiteindelijk verliest het schip zijn stevigheid en wordt het gesloopt. Vele componenten worden gerecycleerd en het staal wordt opnieuw gesmolten en hergebruikt, misschien bij de constructie van een nieuw schip. Het zou interessant zijn om de verschillen in corrosieweerstand te kennen van deze nieuwe of gerecycleerde staalsoorten en te bepalen of nieuw, corrosieresistent materiaal een economisch aanvaardbaar alternatief kan bieden voor de constructie van ballast tanks. Drie belangrijke elementen, die elk behandeld worden in de drie grote delen van dit werk.

Het eerste deel vergelijkt de manier zoals schepen vandaag gebouwd en tegen corrosie beschermd worden met vier mogelijke alternatieven: de standaardtank met epoxyverf en zinkanodes, een tank met een dubbele corrosietoeslag, een tank met een verbeterd verfsysteem, een tank gebouwd uit corrosieresistent materiaal en ten slotte met een tank waar de zinkanodes vervangen zijn door aluminiumanodes die levenslang meegaan. De kosten voor de volledige levenscyclus van elke optie werden berekend en een sensitiviteitsanalyse werd uitgevoerd. Een interessant besluit hieruit is dat de staatkwaliteit die gebruikt wordt wel een belangrijke rol zou kunnen spelen in de levensverwachting van de schepen.

Daarom richt het tweede deel van deze studie zich op de gebruikte staalsoorten bij de constructie van ballasttanks aan boord van koopvaardij schepen. Hiervoor werden staalplaten verzameld uit de scheepsromp van schepen die laswerkzaamheden uitvoerden in droogdok. Deze platen werden grondig onderzocht om de chemische samenstelling, de microstructuur en de insluitsels te bepalen. De corrosievorming werd bestudeerd op vastgestelde tijdsintervallen voor een totale periode van twee jaar. Een experimenteel corrosieresistente staal, ontwikkeld voor gebruik in ballasttanks werd aan de stalenset toegevoegd. Dit resulteerde in drie clusters: gewoon staal, staal met verhoogde sterkte en het corrosieresistent staal. Het gewone staal en het staal met verhoogde sterkte roesten met gelijkaardige corrosiesnelheden, een conclusie die door verschillende experimenten in laboratoria op nieuw staal bevestigd wordt. Het corrosieresistente staal, welk een duidelijk hogere concentratie chroom, aluminium en molybdenum heeft een verminderde corrosiegraad van 30 tot 50%.

In het derde deel wordt dit corrosieresistente materiaal verder geanalyseerd om te bepalen of de mechanische en chemische eigenschappen voldoende zijn om als staal te gebruiken voor de constructie van ballast tanks. De hardheid, de rek en breeksterkte en ook de lasbaarheid werden bepaald.

Dit onderzoek toont de noodzaak aan voor verder onderzoek naar staalsoorten die bescherming door verfsystemen en opofferingsanodes overbodig maakt. Dit is niet enkel zeer voordelig voor het maritieme milieu om dat de aanvoer van zware metalen en polymeren sterk wordt verminderd. Ook economisch is dit een goede zaak, omdat de onderhoudskosten drastisch kunnen worden verlaagd.

General outline of the study

The origin of this work lies back in 2007, when scientific research was initiated at the Antwerp Maritime Academy.

A constant challenge for ship owners is the proper maintenance of the ballast tanks of their ships. They are divided into small compartments and are in constant contact with an aggressive chloride rich environment, ideal for corrosion. The owner wants to keep its tanks in an acceptable condition for the complete lifespan of his ship, at minimum cost. If he can limit repair and maintenance work, the operating cost can significantly be reduced. The environment benefits as well from a good, long lasting ballast tank protection system, as epoxy coatings contain a large number of chemicals and organic solvents. These all end up in the air or the water. Sacrificial zinc anodes introduce heavy metals in the water. The accumulation of zinc less important in open sea, but not in port areas, where the water circulation is limited.

The research with regard to corrosion in ballast tanks was initially funded by the Flemish "Bijzonder Onderzoeks Fonds" (BOF). The first project comprised an in situ study of more than 140 tanks and was elaborated in the Ph D thesis of Capt. K. De Baere, defended July 2011.

The last chapter of his work consisted of a limited economic study. This was later developed further in close cooperation and forms the link between his and this work. It compares five possible options for ship construction. This study revealed that today's method of construction is economically the best option. But it is a close call, with some uncertainties. A promising line of research is the study of the steel quality for ship construction and the use of alternative and corrosion resistant steel (CRS). In this work CRS is defined as a steel quality that is more resistant to corrosion than ordinary steel. There is still corrosion, but at a lower rate.

This comprehensive economic study, submitted for publication in Marine Structures, is used as an introductory chapter (Chapter 1). It raises some interesting questions: What is the influence on the corrosion rate of the different steel types used in ship construction today? Do ships, built at major ship building sites all over the world have different life expectancies, based on the steel used for their tank construction? What properties define and discern the steel types used and do they have an influence on their corrosion performance?

Figure I shows of the different parts elaborated in this work:

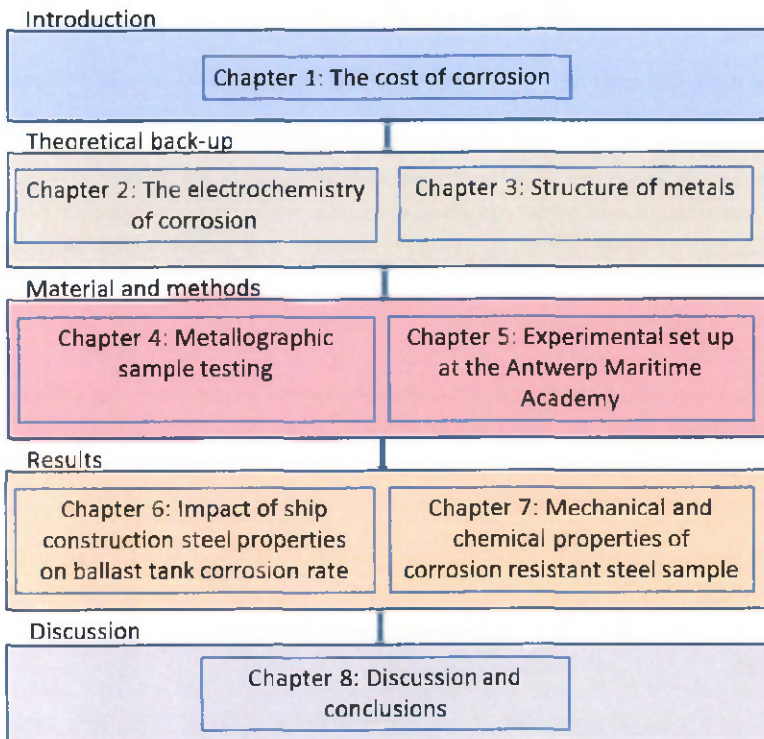


Figure I: schematic overview different chapters.

It is the objective of this research to unveil how different steel qualities used in ballast tank construction corrode and to compare this with the characteristics of an experimental steel quality, designed for use in these tanks. To achieve this goal, more than 40 steel plates from ballast tanks of existing ships were collected and examined through a period of two years.

The words “steel quality” comprise a collection of properties, all responsible for the characteristics of the specific steel. All these properties are considered.

Figure II gives an overview of the conditions applicable to this research and the experiments performed to achieve the goals set and to be able to examine, weigh and compare them with accepted scientific references.

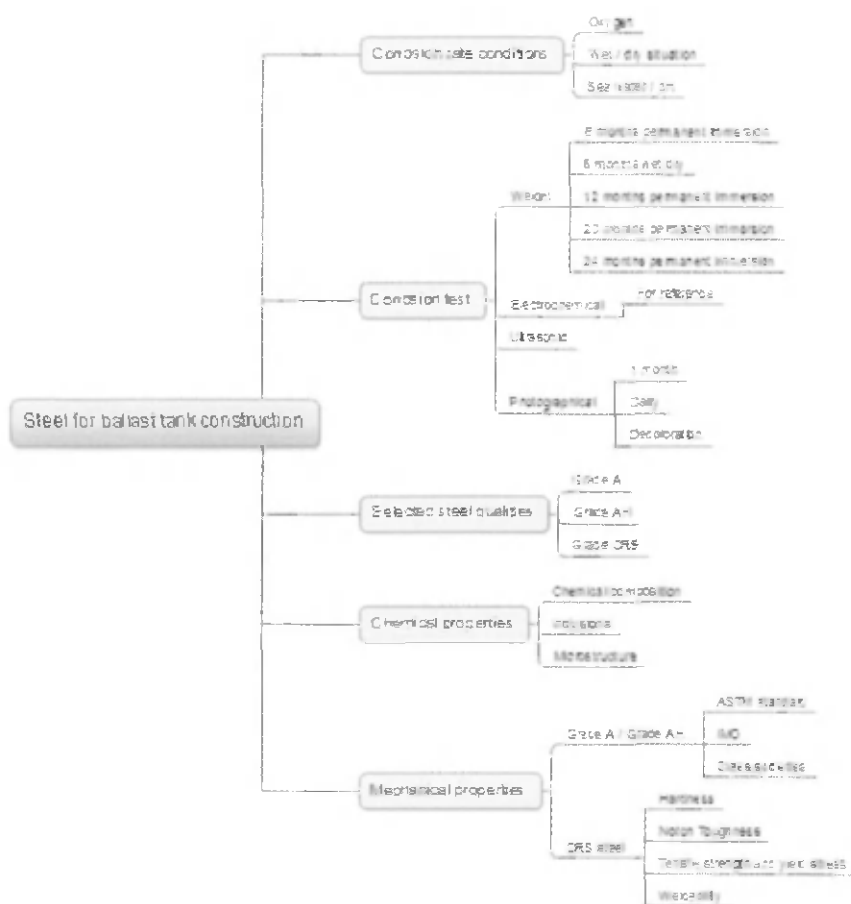


Figure II: schematic overview experiments and conditions.

After the introduction, two general chapters are included in this work, to give the reader a theoretical background. Chapter 2 handles the electrochemistry of the corrosion process, starting from the first law of thermodynamic. The Nernst equation, the Pourbaix and the Evans diagrams are explained. Chapter 3 discusses the structure of metals, where the lattice structures are studied. They are an important element in the formation of solid metals at different temperatures, given by the Fe-C diagram and the TTT (Time Temperature Transformation) curves. Steel is composed out of iron, with alloy elements, all having their specific characteristics and influences on the steel quality. When foreign material enters the metallic matrix, this is called inclusions. A large number of these inclusions can disrupt the homogeneity of the metal, thus influencing the characteristics.

Chapter 4 and 5 reflect extensively the experimental set up, both for the metal analysis and the corrosion measurements. Metal analysis was performed under the supervision

of specialists from OCAS, the scientific research center of Arcelor Mittal in Belgium. SEM, GDOES, EDX and XRD sample testing was used.

The corrosion rate tests were performed at the Antwerp Maritime Academy and at the Karel de Grote university college. They comprise electrochemical, ultrasonic, photographic and weight measurements. For every measurement technique, sample preparation and procedures are explained.

The results of the experiments and a first discussion are given in the following 2 chapters. Chapter 6 elaborates the corrosion measurements after 6, 10, 20 and 24 months of permanent immersion and after 6 months of wet/dry exposure. This chapter is mainly based on an article which was written after 6 months of permanent immersion and was submitted for publication in *Materials Performance*, 2012, a NACE publication. The results of the subsequent experiments are also included and the discussion and conclusions are adapted accordingly.

Chapter 7 comprises the results of the extensive mechanical and chemical testing of the corrosion resistant steel. The outcomes are compared with the rules and regulations for ship construction steel of classification societies to determine whether this steel could be approved for use in ballast tanks. It discusses the corrosion mechanisms and gives an explanation for the reduced corrosion rate of this corrosion resistant steel. This work will also be submitted for publication.

All the elements are finally evaluated in the last part of this work. Chapter 8 summarizes the important elements, discusses the different opinions encountered in literature, comes to conclusions, reflections and recommendations and sets out possibilities for new lines of research.

The included articles have been written and reviewed by a team of specialists. Based on our research results and conclusions, they provided the necessary scientific support. The purpose is certainly not to assume credit for their intellectual efforts but to reflect the solid basis on which the conclusions are founded (De Baere, 2011).

Table of contents

1	The cost of corrosion	5
1.1	Introduction: the problem of ballast tank corrosion	5
1.2	Research objective	6
1.3	Methodology	7
1.3.1	Total cost of ballast tanks (TCB)	9
1.3.2	Sensitivity analysis and Monte Carlo simulation	15
1.4	Case study	16
1.4.1	Model selection	16
1.4.2	Calculations	16
1.4.3	Financial parameters used throughout the calculations	20
1.5	Statistical analysis of the model results	21
1.5.1	Model results	21
1.5.2	Sensitivity analysis	22
1.5.3	Monte Carlo analysis	24
1.6	Consequences for future ship construction	26
1.7	Conclusion	28
2	The electrochemistry of corrosion	29
2.1	Introduction	29
2.2	Fundamentals	30
2.3	Thermodynamic principles	32
2.3.1	Reduction potential $[E]$ and standard reduction potential at 298K $[E_{298}^0]$	32
2.3.2	The Nernst equation	33
2.4	Relation Pourbaix diagrams - Nernst equation	34
2.5	Corrosion kinetics	36
2.5.1	Overpotential or polarization	36
2.5.2	Ohmic drop: iR	37
2.5.3	Concentration polarization	37
2.5.4	Activation polarization	39
2.5.5	Linear polarization measurement (LPR)	42

2.5.6	Graphical presentation of kinetic data – $E/(\log)i$ diagrams or Evans Diagrams	43
2.5.7	Tafel Curve	44
2.5.8	Determination of mass loss and corrosion rate	45
3	Structure of metals	47
3.1	Crystal structure.....	47
3.1.1	Body centered cubic (BCC).....	48
3.1.2	Face centered cubic (FCC).....	48
3.1.3	Hexagonal close-packed (HCP)	49
3.1.4	Body-centered tetragonal (BCT) and orthorhombic.....	49
3.1.5	Monoclinic.....	50
3.1.6	Overview	50
3.2	The Fe-C diagram (iron-carbon) and time temperature transformation (TTT) curve	51
3.2.1	Introduction	51
3.2.2	The Fe-C diagram	51
3.2.3	The TTT diagram	57
3.3	Alloy elements	61
3.4	Inclusions	65
4	Metallographic sample testing	69
4.1	Introduction	69
4.2	Chemical composition.....	69
4.2.1	Atomic emission spectroscopy (AES)	69
4.2.2	Glow discharge optical emission spectroscopy (GD-OES)	72
4.3	Nonmetallic inclusions	72
4.3.1	ASTM E45-05.....	72
4.3.2	Scanning electron microscope (SEM)	73
4.3.3	Testing.....	74
4.4	Phase analysis	76
4.5	Microstructure	77
5	Experimental set up at the Antwerp Maritime Academy	79
5.1	Introduction	79

5.2	Sample collection	79
5.3	Sample preparation	79
5.4	Sample number	80
5.5	Test facility	81
5.6	Electrochemical measurements	83
5.6.1	Determination of the equilibrium potential E_{eq}	84
5.7	Weight loss method	85
5.8	Ultrasonic measurement	87
5.9	Photographical measurement	87
6	Impact of ship construction steel properties on ballast tank corrosion rate.....	89
6.1	Introduction	89
6.2	Results & discussion.....	93
6.2.1	Exploratory data analysis.....	93
6.2.2	Statistical interpretation	93
6.2.3	Use of electrochemical measurements	99
6.2.4	Applicability of the different steel types in corrosion prevention	103
6.3	Conclusions	104
7	The chemical, mechanical and physical properties of the Korean Corrosion Resistant Steel (CRS)	105
7.1	Introduction	105
7.2	Overview of the performed tests	106
7.2.1	Chemical properties.....	106
7.2.2	Mechanical properties.....	107
7.2.3	Weldability.....	110
7.3	Results & discussion.....	111
7.3.1	Chemical properties.....	111
7.3.2	Mechanical properties.....	122
7.4	Conclusions	127
8	Discussion and conclusions	129
9	Bibliography.....	140
10	List of figures.....	157
11	List of tables.....	161

12	Abbreviations	163
13	CV + list of publications.....	169

1 The cost of corrosion

1.1 Introduction: the problem of ballast tank corrosion

The degradation of metallic surfaces due to corrosive environments (atmospheric, immersive and chemical) is a well-known problem for many steel structures such as bridges, storage tanks and pipelines. Sea water is an aggressive environment for corrosion. Nevertheless, merchant vessels, carrying cargo all over the seven seas, are mostly built of steel. In the absence of cargo, or when the ship is only partly loaded, a vessel carries seawater in her ballast tanks to ensure maneuverability and to control draft, stress and stability. As necessary as they are for the operation of a ship, though, the fact that ballast tanks are prone to corrosion poses an important challenge for ship owners.

Corrosion is expensive. The total direct costs associated with metallic corrosion, provoked by production interruptions, incidents and repairs, in nearly every U.S. industry sector in 1998 was about \$276 billion among which \$2.7 billion was from ships. (Koch et al., 2002, Johnson et al., 2001). This cost is divided into cost associated with new construction (\$1.12 billion), maintenance and repairs (\$810 million) (De Baere, 2001), and corrosion-related downtime (\$785 million; (Koch, 2002, Johnson, 2001). Corrosion can become a safety issue in ships. Statistics show that 90 % of ship failures are attributed to corrosion (Melchers, 1999).

Corrosion is a major cause of marine structural failures. Corrosion results in loss of structural strength at local and global levels, and leads to fatigue failure and stress corrosion cracking. Some marine incidents with tankers have been directly linked to accelerated corrosion (Brown, 1996). Localized corrosion is among the major types of physical defects found largely on ship structures. The areas of the ship most susceptible to corrosion are the ballast tanks, due to the intense contact with seawater and the chloride-rich environment. Because of the double hull configuration required by the Oil Pollution Act of 1990 (Tator, 2004, OPA, 1990, Kim, 2002), ballast tanks are difficult to maintain. The access to ballast tanks is restricted, the environment is unfriendly, the light is scarce, large parts are hard to reach. The cost of inside maintenance is high, partly because the working conditions are troublesome. In short, double hull ballast tanks act as the Achilles' heel of the ships lifetime expectancy. The introduction of the double hull tankers in the nineteen nineties resulted in longitudinal stiffeners being placed in the ballast tanks (Brown, 1996). This configuration aggravates the corrosion problem on board. The rate of corrosion in ballast tanks is therefore a decisive factor for ending the economic life of the ship and sending her to the scrap yard (LR, 2006).

Today, ship's ballast tanks are constructed in mild steel and protected with hard coatings with zinc anodes. These serve to reduce and in some instances effectively defer

corrosion and mitigate corrosion consequences (Wang, 2003). Such a construction has been applied without significant changes for decades. The goal of this study is to compare this traditional approach with some potential alternatives through an analysis of the total cost from new construction, exploitation and maintenance of the ballast tanks, hereinafter called total cost of ballast tanks (TCB). As such, the impact of any structural investments can be investigated in the design stage of the vessel. Important elements in such an analysis are the selection of appropriate construction, equipment and protection material.

1.2 Research objective

The objective of this economic study is to construct a cost-based model outlining some aspects in the construction of a double hull ship to achieve minimal corrosion effects during the economic life time of the ship (25 years).

Based on this model, five different options of ballast tank construction (cases I-V in Table 1) are compared, within the currently available techniques and materials, in order to obtain cost reductions.

Table 1: summary of the five cases in the economic analysis in terms of construction, equipment and maintenance criteria.

	Case I	Case II	Case III	Case IV	Case V
Steel	Grade A	Grade A	Grade A	Corrosion resistant	Grade A
Paint system	IMO PSPC ₁₅	IMO PSPC ₁₅	TSCF ₂₅	1 coat white epoxy	IMO PSPC ₁₅
Nominal dry film thickness	320µm	320µm	350µm	160µm	320µm
Paint quality	Pure epoxy	Pure epoxy	Pure epoxy	Pure epoxy	Pure epoxy
Anodes	Yes (Zn)	Yes (Zn)	Yes (Zn)	No	Yes (Al)
Replacement of the anodes	Every 5 years	Every 5 years	Every 10 years	NA	Every 25 years
Coating repair	Yes	Yes	Yes	Yes	Yes
Increased scantlings	No	Yes	No	No	No
Steel replacement	Yes	NA	NA	NA	Yes

Selection of cases I to IV occurred on the basis of Safinah (Safinah, 2009), option V is based on experience and information we obtained while working on this article (Smoljko, 2007). The cases are applied to a typical Panamax tanker, a ship constructed according to the size limits for ships travelling through the Panama Canal (Vantorre, 2011).

Case I is the typical tank as constructed today in ordinary grade A steel, 14 mm thickness, coated with a standard PSPC₁₅ coating (IMO RES MSC.215(82), 2006) and equipped with zinc sacrificial anodes. Such a tank remains intact for approximately five years (Verstraelen, 2009a, Verstraelen, 2009b); then the coating starts to degrade and corrosion appears requiring eventually steel replacement and paint restoration at a certain point of time. The anodes have to be replaced every five years.

In case II, the core element is corrosion allowance. The corrosion allowance is the maximum steel thickness loss allowed by the classification society, meaning that in the lifespan of a ship a certain quantity of corrosion is tolerable without endangering the structural integrity of the ship. As a rule of thumb, steel will be replaced, in dry dock, when its thickness has been reduced to 80 % of the initial value (ABS SVR 7-A4). The present corrosion allowances from even the most conservative classification societies are marginally adequate for a 20-year design life vessel (except tankers, 25 years (ABS, pers comm.)) (Gratsos, 2007). Hence, case II has been chosen to provide for an additional corrosion allowance of 3 mm, as in case I, a standard PSPC₁₅ coating was applied, and the anodes have to be replaced every five years.

In case III, ships receive the currently experimental TSCF₂₅ coating on top of 14 mm grade A steel. This coating system is postulated to have a lifetime expectancy of 25 years, the economic lifetime of the ship, by a better surface preparation of the steel, improved coating application conditions and an increased coating thickness (ABS, 2007, Shell, 2000). Consequently, there is no more need for steel replacement, and coating repair needs are reduced. Since the surface attacked by corrosion is reduced, so will be the consumption of the sacrificial anodes. The anodes will be replaced only once every ten years.

For case IV, the tanks are constructed in corrosion resistant steel (CRS) and painted with an aesthetical white coating as per IMO PSPC₁₅ (IMO, 2006). Coating repair remains necessary, although reduced. Anodes become redundant and are not used.

The case V tanks are again constructed in ordinary grade A steel and protected with a standard PSPC₁₅ epoxy coating. Cathodic protection is obtained by aluminum sacrificial anodes of sufficient mass to last 25 years, the full economic lifespan of the selected model.

1.3 Methodology

To assess all possibilities a total cost of ballast tanks model is developed. In a next step, uncertainties are taken into account by a sensitivity analysis, including Monte Carlo sensitivity analysis. For each of the equations, Table 2 gives the applicable variables.

Table 2: TCB variables per model and per equation, used in the economic model.

	CASE I	CASE II	CASE III	CASE IV	CASE V
INITIAL INVESTMENT - STEEL COST					
Surface area	AREA	AREA	AREA	AREA	AREA
Thickness	PT	PT+CA	PT	PT	PT
Density	DENS	DENS	DENS	DENS	DENS
Cost new building steel	CAN	CAN	CAN	CNCRS	CAN
INITIAL INVESTMENT - COATING COST					
Initial coating cost per m ²	PSPC ₁₅	PSPC ₁₅	TSCF ₂₅	CCRS	PSPC ₁₅
INITIAL INVESTMENT - ANODE COST					
Number of anodes	ZA	ZA	ZA	\	AA
Initial installation cost per anode	IZA	IZA	IZA	\	IAA
STEEL RENEWAL COST					
Lightweight	LWT _T	\	\	\	LWT _T
Cost of steel repair per ton	RAS	\	\	\	RAS
COATING REPAIR COST					
Surface	AREA	AREA	AREA/2	AREA/4	AREA
Cost of recoating per square meter	RSPC	RSPC	RTSCF	RCCRS	RSPC
ANODE REPLACEMENT COST					
Number of anodes	ZA	ZA	ZA	\	AA
Installation cost per anode	IZA	IZA	IZA	\	IAA
COST OF UNAVAILABILITY DUE TO DRYDOCK					
Factor f	1	2	4	4	1
Lightweight	LWT _T	LWT _{III}	LWT _T	LWT _I	LWT _T
Time charter equivalent	TC	TC	TC	TC	TC
Cost of dry dock per day	CDD	CDD	CDD	CDD	CDD
RESIDUAL VALUE					
Lightweight	LWT _T	LWT _{III}	LWT _T	LWT _T	LWT _T
Value of scrap iron	SCI	SCI	SCI	SCRS	SCI

1.3.1 Total cost of ballast tanks (TCB)

The TCB equals the initial investment plus the operating costs through 25 years minus the residual value when the ship is sold for scrap and with DR as discount rate.

$$\text{TCB} = \text{Initial investment} + \sum_1^{25} \frac{\text{operating cost}}{(1+\text{DR})^n} - \frac{\text{residual value}}{(1+\text{DR})^{25}} \quad \text{Eq. 1}$$

1.3.1.1 Initial investment

The initial investment for each of the cases can be calculated as follows:

$$\text{Initial investment} = \text{steel cost} + \text{coating cost} + \text{anode cost} \quad \text{Eq. 2}$$

$$\text{Steel cost} = \text{lightweight (Eq. 4)} \times \text{cost new building steel} \quad \text{Eq. 3}$$

$$\text{Lightweight} = \text{surface area} \times \text{thickness} \times \text{density} \quad \text{Eq. 4}$$

$$\text{Coating cost} = \text{surface area} \times \text{initial coating cost per m}^2 \quad \text{Eq. 5}$$

$$\text{Anode cost} = \text{number of anodes} \times \text{initial installation cost per anode} \quad \text{Eq. 6}$$

1.3.1.2 Operating cost

The calculation of the operating cost takes five elements into account: steel renewal cost, coating repair cost, the cost to replace the anodes, the cost of unavailability of the ship due to dry dock and the loss of cargo carrying capacity due to an increased lightweight (for case II ships).

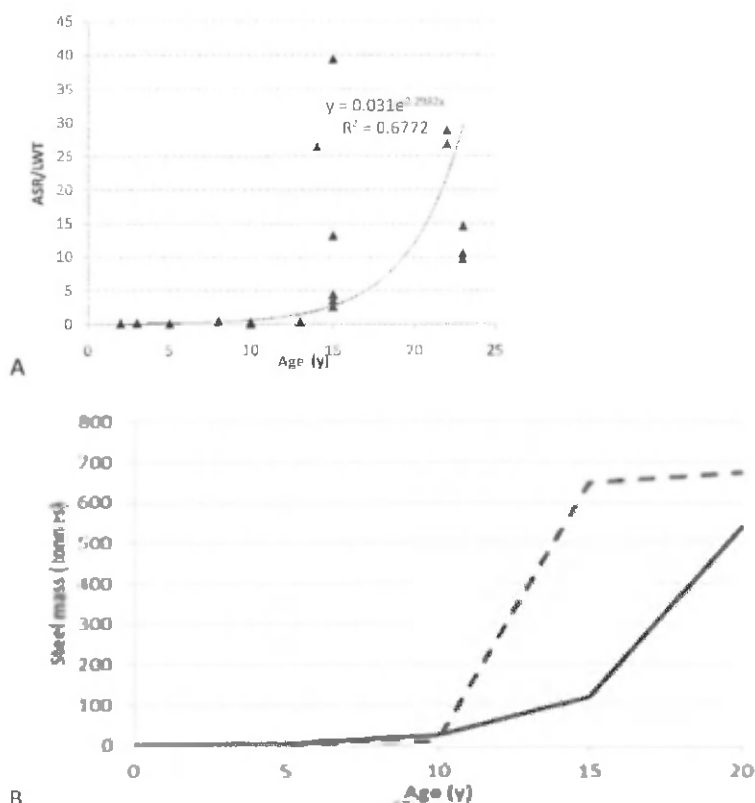
Steel renewal cost

Effective ship maintenance can only be carried out during dry docks. A ship has to visit dry docks two times every five years, during one of which steel and coating repair jobs are performed. A rough estimate of the steel renewal cost has been derived from data obtained from a population of 18 ships (Figure 1), taken from three separate shipping companies who were willing to share their information on past maintenance repairs.

These ships were maintained in a normal way and repairs had been carried out during every previous dry dock visit. The quantity of steel replaced during dry dock resulting from damage by corrosion, cracks and deformation but excluding accidents can be represented by the following regression (Aloui, 2010):

$$\text{ASR}/\text{LWT} = 0.031e^{0.2982t} \text{ or } \text{ASR} = \text{LWT} \times 0.031e^{0.2982t} \quad \text{Eq. 7}$$

with ASR being the quantity of steel in ton replaced per dry dock in function of the age of the ship in years (t) and the light weight in ton (LWT).



A. quantity of steel in terms of the quantity of steel replaced per dry dock, per unit lightweight of the ship, in function of the age of the ship (Aloui, 2010).

B. comparison of the predicted steel replacement in according with the observed replacements by Løseth (1994). Solid line: own model (Eq.7) upsized to a VLCC of 300.000 DWT Dashed line: Data taken from Løseth (1994), for a double hull VLCC, with the effect of maintenance taken into account.

Figure 1: steel replacement (tonnes) in function of the age (y) of the ship (Alaoui (2010) + Løseth (1994))

In this model (Figure 1A), an important amount of scatter shows up for ships older than 15 years. Next to our in situ experience in the ballast tanks of more than 150 ships, this type of scatter turns out to be rather common among older ships, and the difference in the condition of the ballast tanks of two similar ships of the same age could be strikingly huge. This can be related to the observations of Paik and Kim (Paik, 2012), where the distribution of corrosion wastage statistics for any structural member is highly scattered at any corrosion exposure time and changes with time. Indeed, the condition of a ballast tank is not only age-dependent but other important factors are involved such as substrate preparation, application conditions, mechanical damages, maintenance and many more. Other, previously published time dependent corrosion models (Paik, 2004, Guo, 2008, Southwell, 1979, Soares, 1999, Qin, 2003, Ivanov, 2004, IACS, 2005), note a similar high variability for older ships.

Data collected by Løseth (1994) can be used for a validation of equation 7 (Figure 1B). As it turns out, these data show a comparably large variation for steel renewal per dry dock for fifteen-year-old vessels, ranging from 6 to 1700 tons.

It is necessary to reduce the total quantity of steel work per dry dock to the steel replacement exclusively imposed by corrosion. Steel repair work can be a consequence of deformations, corrosion and cracks. In the context of this research we are only interested in steel repair work inflicted by corrosion. A polynomial regression (Figure 2) of the data obtained by Kawano & Hirakata (2003) offers the following expression for the fraction of ASR/LWT caused exclusively by corrosion in function of the time, represented by C1 ($R^2 = 0.911$):

$$C1 = -0.0325t^3 + 1.1299t^2 - 4.465t + 1.1866 \quad \text{Eq. 8}$$

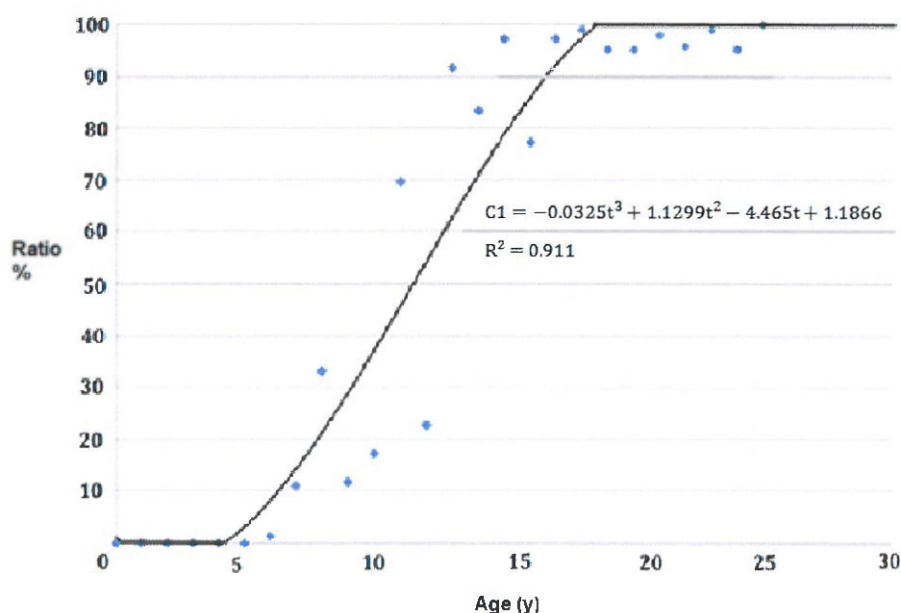


Figure 2: C1 (portion steel replacement due to corrosion (%)) in function of the age (y) of the ship (graphical presentation by Kawano & Hirakata 2003).

Multiplication of Eq. 7 and Eq. 8 leads to the quantity of corroded steel to be replaced per dry-dock.

Finally, steel renewal cost can be calculated as follows:

$$\begin{aligned} \text{Steel renewal cost} &= 0.031 e^{0.2982t} \times \text{lightweight} \\ &\times (-0.0325t^3 + 1.1299t^2 - 4.465t + 1.1866) \\ &\times \text{cost of steel repair per ton} \end{aligned} \quad \text{Eq. 9}$$

Coating repair cost

With regard to coating repair, the data presented in Verstraelen et al. (2009a, 2009b) allows to determine the percentage of the surface to be recoated, through the following equation:

$$CI = 1.682t - 7.145 \quad \text{Eq. 10}$$

With the corrosion index CI representing the surface of the coating damaged by corrosion in % and function of the time (Verstraelen, 2009a, 2009b). This formula shows that a coating remains nearly intact during approximately the first 5 years. Afterwards the paint degrades in a nearly linear way with approximately 1.7 % surface per year.

$$\text{Coating repair cost} = \text{Surface} \times (1.682t - 7.145) \times \text{cost of recoating per m}^2 \quad \text{Eq. 11}$$

At this moment TSCF₂₅ is seldom applied and certainly not generally accepted by the shipping world as being the ultimate solution for the corrosion problem in ballast tanks (Damen Shipyard, 2011, pers. comm.). Consequently, statistical data on the effective lifetime of this coating are still lacking. The result of this study rests upon the basic assumption that the TSCF₂₅ lives up the promised characteristics. When applying a TSCF₂₅ (case III) instead of PSPC₁₅ the surface to be re-coated and number of dry-days to do this are diminished with 40% following the predicted lifetime of the coating system. For corrosion resistant steel (case IV) a similar reasoning is followed seen the nature of the substrate.

Anode replacement cost

Anodes should normally be replaced every 5 years. However, due to the expected good performance of the TSCF₂₅ coating (case III), it can be surmised that replacement is only required once every 10 years. Tanks built in corrosion resistant steel (case IV) do not require any anodes at all. Case V ships are equipped with aluminum sacrificial anodes lasting the economic lifespan of the ship. Anodes replacement is not considered.

$$\text{Anode replacement cost} = \text{number of anodes} \times \text{installation cost per anode} \quad \text{Eq. 12}$$

Cost of unavailability of the ship due to dry dock

Time in dry dock as a consequence of corrosion is the sum of the time needed to replace the steel plus the time needed to restore the coating and replace the anodes.

The steel replacement time equals (Eq.7) x (Eq.8) divided by the yard capacity in t/day. Research (data obtained from 20 ship repair yards worldwide) revealed a huge variation in capacity ranging from 2 to 40 tons of steel per day. An average of 16.7 t/day was calculated and rounded to 20t/day.

The calculation of the coating maintenance and repair time in dry dock is complicated since a lot of variables are involved. Maintenance is normally done at sea or in port by the crew while repair work in ballast tanks does not necessarily require the vessel to enter dry-dock, all the work can be done afloat at a repair base or at sea using a riding squad.

$$\sum_{t=1}^5 (1.682(5t) - 7.145) \quad \text{Eq. 13}$$

The algebraic sum of the outcome of (Eq.10) after 5, 10, 15, 20 and 25 years indicates that 90.4% of the coating is repaired during the complete lifecycle of the ship.

It would take typically two months dry-dock to recoat the ballast tanks completely (Kattan, Safinah Ltd., pers. comm). Moreover, the coating of a ship accounts for 12-25% (average 18.5%) of the total man hours for the construction, with approximately 50% of the coated surface being inside the ballast tanks (Baldwin, 1995).

Applied to a Panamax tanker, which takes around 21 mh cgt⁻¹ (manhour per compensated gross tonnage) to be built (Lloyds shipping economist, 2006), or, with a cgt of 21,000 (OECD, 2006), around 441,000 mh for the total construction and 41,000 mh to (re)coat the ballast tanks. With 3 teams of 10 men working each 3 shifts of 10 hours per day, this complete recoating is finished in 45 working days, which corresponds to the amount of time devoted to it in practice (Kattan, Safinah Ltd., pers. comm). These 45 days will be divided following the appearance of corrosion as represented by equation 10 and over the major 5-year dry dock periods, as represented in Table 3.

Table 3: number of days needed for recoating in function of ship's age (y).

Moment of drydock (years)	Number of days re-coating (DRC)
5	0
10	3
15	9
20	14
25	19*
Total	45

* Will not be taken into account since the ship is sold for scrap at that time.

Finally, the time in excess of a standard dry dock of 6 days (Antwerp Ship Repair, 2012, pers. comm.) is allocated to the corrosion problem.

Dry dock time can then be calculated according to eq. 14:

Dry dock time =

$$\left[\frac{[0.031 e^{0.2982t} \times \text{lightweight} \times (-0.0325t^3 + 1.1299t^2 - 4.465t + 1.1866)]}{20} + \text{DRC} \right] - 6$$

Eq. 14

The equivalent cost then comes down to:

Dry dock cost =

$$[\text{Dry dock time} \times (\text{Time Charter Eq} + \text{cost of dry dock / day})] \quad \text{Eq. 15}$$

When applying a TSCF₂₅ (case III) instead of PSPC₁₅ the number of days is diminished with 40% following the predicted lifetime of the coating system. When using corrosion resistant (case IV) steel a similar reasoning is followed seen the nature of the substrate. In case II, III and IV no dry dock time is provided for corroded steel replacement based on the fundamental assumptions of these alternative ways of construction.

Loss or gain of cargo carrying capacity due to an increased or decreased lightweight

A final exploitation cost, calculated in Eq. 16, is the loss of income (LI) due to an increased LWT as a consequence of the increase of the corrosion allowance. This cost is only applicable to option II. Increasing the corrosion allowance increases the lightweight of the ship while the cargo carrying capacity is diminished with the same amount. As this loss is only applicable during loaded voyages, the tanker is here supposed to be loaded 50% of the time (McNulty, 2011).

$$LI = (TC \times 365 \text{ days}) / \text{total load} \times (LWT_{TII} - LWT_T) \times 0.5 \quad \text{Eq. 16}$$

For an assessment of the parameters linked to the use of corrosion-resistant steel (CRS), an experimental steel type was obtained. Experiments show that the corrosion rate of this alloy is more than 30% lower than grade A ship construction steel (Chapter 6).

1.3.1.3 Residual value

After 25 years of service the ship is sold at the value of the scrap iron. As it is improbable that the higher concentrations of valuable alloys will influence the scrapping price, the same price can also be used for the tanks constructed in CRS (case IV). Residual value can then be calculated as follows:

$$\text{Residual value} = \text{lightweight} \times \text{value of the scrap iron} \quad \text{Eq. 17}$$

1.3.2 Sensitivity analysis and Monte Carlo simulation

1.3.2.1 Sensitivity analysis.

To determine how the optimal solution, the minimum cost of the ballast tanks, is affected by multiple parameters a sensitivity analysis was carried out. Each of the parameters was varied and the variance of the real TCB analyzed.

1.3.2.2 Monte Carlo simulation

To examine how the TCB varies when the value of uncertain assumptions are modified, a Monte Carlo simulation was performed using the software program Crystal Ball (Oracle). When performing a Monte Carlo sensitivity analysis, probability distributions are specified for uncertain values of model input parameters. Then multiple trials are executed, taking each time a random draw from the distribution for each parameter. For each trial, the output is calculated for each set of specified values. When all the trials have been executed, a probability distribution of the model output is obtained (Boardman, 2006).

By applying the Monte Carlo Simulation technique, not consequences but risks are compared and hence, more information is obtained as compared to when a conventional, static model is used. When probability distributions for several defined assumptions are specified, uncertainties are incorporated in the model. Moreover, the results of the model not only incorporate the uncertainties of the input parameters, they also give us their importance (Al-Mansour, 2007).

1.4 Case study

1.4.1 Model selection

The model selected for this study is a Panamax tanker¹. Panamax ships can be considered as a good representation of the medium size merchant ship, representing approximately 48 % of the world fleet (Eurostat, 2012).

More specifically, the calculations presented here are based on an average Panamax tanker of approximately 75,000Mt DWT, a LOA of 228m, and a beam of 32.2m. As the sole interest of this study concerns the ballast tanks, all assessments are limited to the size and weight of the ballast tanks only. Starting point is the surface of the ballast tanks set at 51,000m² (McNulty, 2011). Furthermore, the ship is supposed to have been built in China and to have dry-dock inspections and repairs in Bahrain, due to the availability of recent, suitable and complete data. The economic life of the ship is set at 25 years. Afterwards the ship is sold for scrap iron.

1.4.2 Calculations

Table 4 lists the parameters used in the basic economic model as developed in section 2. To this end, the parameters are sub-divided into 3 categories, viz. the values used to calculate (a) the lightweight of the tanks, (b) the initial investments and (c) the exploitation costs. For each parameter the acronym, a short description, the standard value and unit, source and formula and the type are indicated in the table.

¹ Panamax ship: ship designed with maximum design limits to pass the Panama Canal. The maximum length overall (LOA - the total length of a ship's hull from the foremost to the aftermost points) of the ship is determined by the usable length of the locks being 304.8m. The maximum draft (12.04m in tropical fresh water) is limited by the shallowest depth at the south sill of the Pedro Miguel locks and the maximum air draft of 57.91m (at any state of the tide) is defined by the clearance under the Bridge of the America's at Balboa. The maximum width over outer surface of the shell plating is 32.31m. The deadweight of a Panamax ship varies between 50,000 and 80,000Mt (DWT - total weight of cargo, crew, stores, ballast and bunkers on board a ship).

Table 4: parameters used in the economic model.

* "F" are parameters with a fixed value determined by the selected model, "U" are the parameters with a variable value (Table 5) and "D" are the parameters which are function of one or more other parameters (see Source & Formula column).

Acronym	Parameter	Value	Source & Formula	Type*
Parameters used to calculate the lightweight of the tanks				
AREA	Surface of the ballast tanks	51,000m ²	P. McNulty, 2007	F
DWT	Deadweight	75,000t		F
DENS	Density steel	7.8tm ⁻³	ABS, 2012	F
PT	Plate thickness	14mm	Own measurements	F
CA	Corrosion allowance	3mm	IACS CSR	F
WA	Weight anodes Zn & Al	22kg	Assumption	F
LWT _I	Lightweight Tank I, III & IV	5,569.2t	See total cost of ownership	F
LWT _{II}	Lightweight Tank II	6,762.6t	See total cost of ownership	F
Parameters used to calculate the initial investment				
PSPC ₁₅	Initial coating PSPC ₁₅	40€m ⁻²	P. McNulty, 2008	U
TSCF ₂₅	Initial coating TSCF ₂₅	63€m ⁻²	IHC, pers. comm. TSCF ₂₅ = PSPC ₁₅ x 1.575	D
CCRS	Initial coating CRS	35€m ⁻²	Own estimation CCRS = PSPC ₁₅ x 0.875	D
PZ	Price zinc	4€kg ⁻¹	Z-guard	U
PA	Price Aluminum	8€kg ⁻¹	Z-guard	U
ZA	Number of zinc anodes	325	P. McNulty, 2007	F
IZA	Initial installation zinc anodes	116€anode ⁻¹	IZA = (WA x PZ) + 28 €/piece	D
AA	Number of aluminum anodes	477	Own calculation	F
IAA	Initial installation aluminum anodes	204€anode ⁻¹	IAA = (WA x PA) + 28 €/piece	D
AS	Grade A steel purchase price	900€t ⁻¹	ArcelorMittal, 2009	U

Acronym	Parameter	Value	Source & Formula	Type*
RACRS	Ratio CRS versus grade A	1.3	30% > grade A; POSCO, pers. comm.	U
CRS	CRS steel purchase price	1,170€t ⁻¹	CRS = AS x RACRS	D
CAN	New building in grade A	3,150€t ⁻¹	CAN = AS x 3.5	D
CNCRS	New building in grade CRS	4,095€t ⁻¹	CNCRS = CRS x 3.5	D
\$	Dollar exchange rate	1\$ = 0.68473€	As per 26/04/2011	F
Parameters used to calculate the exploitation costs				
RAS	Repair grade A steel	7,020€t ⁻¹	RAS = AS x 7.8	D
RPSPC	Repair PSPC ₁₅	61.35€m ⁻²	Terkels (ASR) & Hoogenboom (Hempel), pers. comm. RPSPC = PSPC ₁₅ x 1.5338	D
RTSCF	Repair TSCF ₂₅	96.62€m ⁻²	Own estimation RTSCF = PSPC ₁₅ x 2.4156	D
RCCRS	Repair coating CRS	53.8€m ⁻²	Own estimation RCCRS = PSPC ₁₅ x 1.345	D
SCI	Scrap per t grade A steel	585€t ⁻¹	SCI = AS x 0.65	D
SCRS	Scrap per t CRS steel	585€t ⁻¹	SCRS = AS x 0.65	D
CDD	Rental dry dock	2,885€day ⁻¹	Arab Shipbuilding and Repair Yard company, 2011 (LXB0.5\$/dag)	U
TC	Time Charter Equivalent Panamax tanker	15,514€day ⁻¹	Legacy Shipbroking, 2010	U
IR	Inflation rate	2%	Eurostat, 2012	
DR	Discount rate	4%	Pearce, 2003 & pers. Comm. Notteboom	U
DRC	Days Re-Coating	See Table 3	Own estimation	

Three types of variables can be distinguished. The first type gives parameters with a fixed value (F), determined by the selected generic Panamax tanker and constant in all further simulations. The second type shows the uncertain parameters (U). During Monte Carlo analysis, these parameters will be allowed to vary according certain probability distributions between minimum and maximum values (Table 5). The third type describes the parameters which are dependent (D) upon one or more other parameters of either other type.

Table 5: minimum, maximum and most plausible value of the uncertain parameters used during the Monte Carlo Analysis together with the probability distribution.

Uncertain parameter	Symbol	Min.	Most plausible value	Max.	Model	Unit
Initial cost PSPC coating	PSPC ₁₅	40	45	60	Normal	€m ⁻²
Grade A steel (basic price)	AS	900	1,000	1,500	Normal	€t ⁻¹
Ratio CRS versus grade A	RACRS	1.2	1.3	1.5	Normal	
Dry dock/day	CDD	2,597	2,885	3,174	Normal	€day ⁻¹
Time charter equivalent	TC	13,963	15,514	17,065	Normal	€day ⁻¹
Price zinc	PZ	4	5	6	Normal	€kg ⁻¹
Price aluminum	PA	8	10	12	Normal	€kg ⁻¹
Inflation Rate	IR	0.9	2	3.8	Normal	%

The cost of steel renewal, coating repair, the replacement of anodes and the rental cost of the dry dock have been based on the price list of Bahrain ASRY dry docks of 2008 (<http://www.asry.net>). More recent prices were available from other dry dock facilities, but the set of Bahrain was the only complete list for the purposes of this study.

Figure 3 shows the outcome of the basic economic model for each of the 5 cases based on the parameters given in table 4. The numbers represent real values, adjusted for an inflation of 2% and discount rate of 4%.

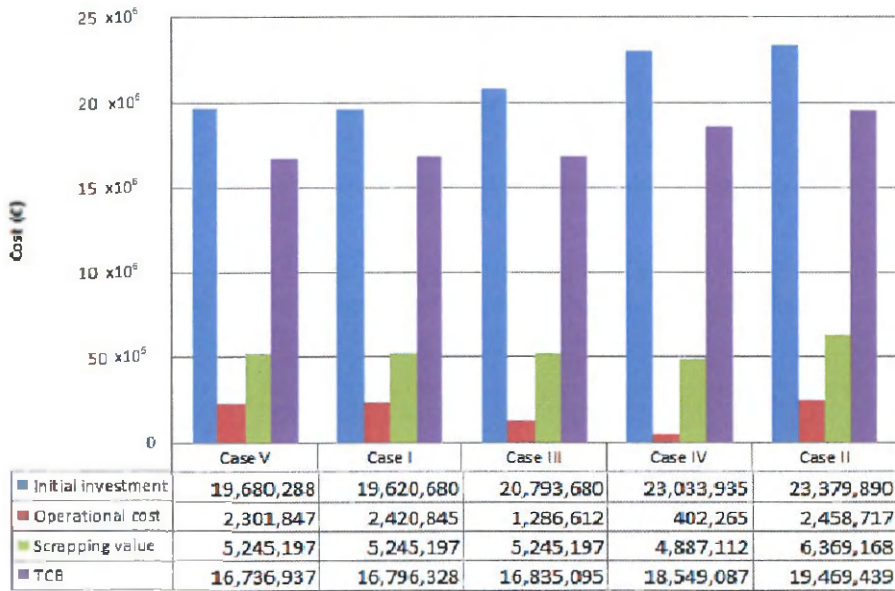


Figure 3: results (€) of the basic model for each of the five cases, inflated with 2% and discounted with 4% per year.

1.4.3 Financial parameters used throughout the calculations

1.4.3.1 Inflation adjustment factor

The result of the model, the sensitivity analysis and the Monte Carlo simulation are real cost. An inflation adjustment factor $(1+P)^t$ was applied. P is the inflation per year and t is the age of the tank. Based on the Harmonized Indices of Consumer Prices (HICP) as published by Eurostat (2012) for the European Union for the period December 1997 till June 2012, P was assumed to vary between 0.9-3.8% with an average value of 2% (Harmonized indices of consumer prices, consulted 2011).

1.4.3.2 Steel price

The steel price is rising steeper than the 2% per annum taken into account by the general inflation rate. This increase in price is caused firstly by the increasing scarcity of raw materials, especially given the growing demand in China. Moreover, the fabrication of ship construction steel is energy consuming and energy is getting ever more expensive. An increase of 8.6% per year was observed for hot rolled steel for the Asian market in a period from August 2005 till April 2011 (Community of European Shipyard Associations, 2011). Hence, an increase of 6% was incorporated in the model. However,

a changing price of grade A means that the price of corrosion resistant steel, steel repair work and scrap are supposed to vary in parallel.

1.4.3.3 Discount rate

Generally, low discount rates favor projects with the highest total benefits while high discount rates favor projects where the benefits are front-end loaded. Based on the European Commission (2009) (social cost-benefit 2% and private investments 15%) a discount rate of 4% was chosen.

This figure is backed up by an analysis of similar, maritime, investments. Eijgenraam (2000), mention in their directives for cost based analysis that the real discount rate should equal average interest rate for risk-free long term loans on the capital market. The figure they put forward is 4% per annum. Pearce et al (2003), also prefer to use a standard discount real discount rate of 4% based on social time preference, and the cost and benefits analysis of major harbor projects in Flanders and the Netherlands, such as Maasvlakte 2, uses a 4% discount rate as well (Notteboom, pers. comm.). A sensitivity analysis of the impact of the discount rate (data not shown) indicates that, although absolute values in the outcome of the calculations change, there is no effect on the differences between the cases analyzed in this text.

1.5 Statistical analysis of the model results

1.5.1 Model results

Comparison of the TCB results in Figure 3 shows that cases I, III, and V were very competitive, whereas, in case II, expanded scantlings might well offer adequate protection against corrosion, but are counterbalanced by the high penalty of an increased loss of cargo carrying capacity. This conclusion is confirmed by Psarros (2009) and Eliasson (2003) who state that it is possible to build ships with thick steel without corrosion protection which would have enough strength left during its designed service life. However, it is generally agreed today that this is no longer a cost efficient way to build and operate ships.

The outcome of cases III, V and even IV increases the number of choices available to the ship owner. A few years ago the classic combination of grade A steel protected with a PSPC₁₅ system coating and backed up with sacrificial anodes, would not have been questioned. This study shows that today it is may be worthwhile to take alternatives III, IV or V into consideration. A sensitivity and Monte Carlo analysis is therefore well placed to shed more light on which parameters are most influential.

1.5.2 Sensitivity analysis

The parameters with substantial impact on TCB are the steel and coating price. Other parameters have a negligible importance.

Table 6 represents the impact of a change in steel price and coating cost on the real value of the TCB and the relative ranking of the cases. The values used in the original basic economic model are in cells with grey shading. Cases are ranked from left to right with ascending TCB value. The difference between I, III and V remains small and nearly unaffected by them. It is inevitable that the price of raw materials, such as ship construction steel, grade A as well as CRS, will rise in the future. The increased scantling method and the construction in CRS will lose ground compared to the cases where the protection of the tanks is based on coating and sacrificial anodes.

Table 6: influence on the real TCB (€) of the evolution of the steel price and coating cost. Cells with grey shading refer to values used in the basic model.

TCB in €					
Steel price					
-50%	Case V 10,168,501	Case I 10,227,892	Case IV 10,368,176	Case III 10,686,203	Case II 12,002,928
-25%	Case V 13,452,719	Case I 13,512,110	Case III 13,760,649	Case IV 14,458,632	Case II 15,736,183
900 EURO/ton	Case V 16,736,937	Case I 16,796,328	Case III 16,835,095	Case IV 18,549,087	Case II 19,469,439
+25%	Case III 19,909,540	Case V 20,021,155	Case I 20,080,546	Case IV 22,639,543	Case II 23,202,694
+50%	Case III 22,983,986	Case V 23,305,373	Case I 23,364,764	Case IV 26,729,999	Case II 26,935,949
+100%	Case III 29,132,877	Case V 29,873,809	Case I 29,933,200	Case II 34,402,460	Case IV 34,910,910
Cost of coating					
-50%	Case III 14,628,568	Case V 15,081,953	Case I 15,141,344	Case IV 17,322,494	Case II 17,814,455
-25%	Case III 15,731,832	Case V 15,909,445	Case I 15,968,836	Case IV 17,935,791	Case II 18,641,947
PSPC _{cr} à 40 EURO/m ²	Case V 16,736,937	Case I 16,796,328	Case III 16,835,095	Case IV 18,549,087	Case II 19,469,439
+25%	Case V 17,564,429	Case I 17,623,820	Case III 17,938,358	Case IV 19,162,384	Case II 20,296,930
+50%	Case V 18,391,921	Case I 18,451,312	Case III 19,041,621	Case IV 19,775,681	Case II 21,124,422

Table 7 represents the influence of cost of CRS to grade A steel and cost of PSPC₁₅ to TSCF₂₅ and the discount on the relative ranking of the cases. It is not surprising that when CRS becomes more expensive compared to grade A steel, the position of case IV becomes less favorable. Additionally, the impact of the relation between the cost of TSCF₂₅ and PSPC₁₅ is not sufficiently important to influence the relative position of the cases significantly. Only when the price of the TSCF₂₅ system drops, case III becomes attractive. The second part of Table 7 shows the influence of the cost of coating. When application of a coating becomes cheaper, the use of sophisticated coating systems (case III) becomes favored compared to the standard PSPC₁₅ coating.

Table 7: influence on the real TCB (€) of the price ratios of CRS to grade A steel and TSCF₂₅ to PSPC₁₅. Cells with grey shading refer to values used in the basic model.

TCB in €					
Ratio cost CRS to grade A steel					
1	Case IV 13,645,487	Case V 16,736,937	Case I 16,796,328	Case III 16,835,095	Case II 19,469,439
1.1	Case IV 15,280,021	Case V 16,736,937	Case I 16,796,328	Case III 16,835,095	Case II 19,469,439
1.2	Case V 16,736,937	Case I 16,796,328	Case III 16,835,095	Case IV 16,914,554	Case II 19,469,439
1.3	Case V 16,736,937	Case I 16,796,328	Case III 16,835,095	Case IV 18,549,087	Case II 19,469,439
1.4	Case V 16,736,937	Case I 16,796,328	Case III 16,835,095	Case II 19,469,439	Case IV 20,183,621
1.5	Case V 16,736,937	Case I 16,796,328	Case III 16,835,095	Case II 19,469,439	Case IV 21,818,154
Ratio cost TSCF ₂₅ to PSPC ₁₅					
1.4	Case III 16,478,095	Case V 16,736,937	Case I 16,796,328	Case IV 18,549,087	Case II 19,469,439
1.575	Case V 16,736,937	Case I 16,796,328	Case III 16,835,095	Case IV 18,549,087	Case II 19,469,439
1.6	Case V 16,736,937	Case I 16,796,328	Case III 16,886,095	Case IV 18,549,087	Case II 19,469,439
1.8	Case V 16,736,937	Case I 16,796,328	Case III 17,294,095	Case IV 18,549,087	Case II 19,469,439

1.5.3 Monte Carlo analysis

1.5.3.1 Input parameters

As indicated previously, the parameters used in the Monte Carlo analysis are divided into three categories. The fixed parameters are model dependent, the dependent parameters are a function of one or more other values and the uncertain parameters are allowed to vary according to a certain probability distribution. For all of the uncertain parameters a normal distribution was selected. Minimum and maximum values and most probable value are listed in Table 5.

1.5.3.2 Results of the Monte Carlo analysis

The bar graphs in Figure 4 show the mean value of the real Total Cost of Ballast tanks (TCB) after 5,000 trials.

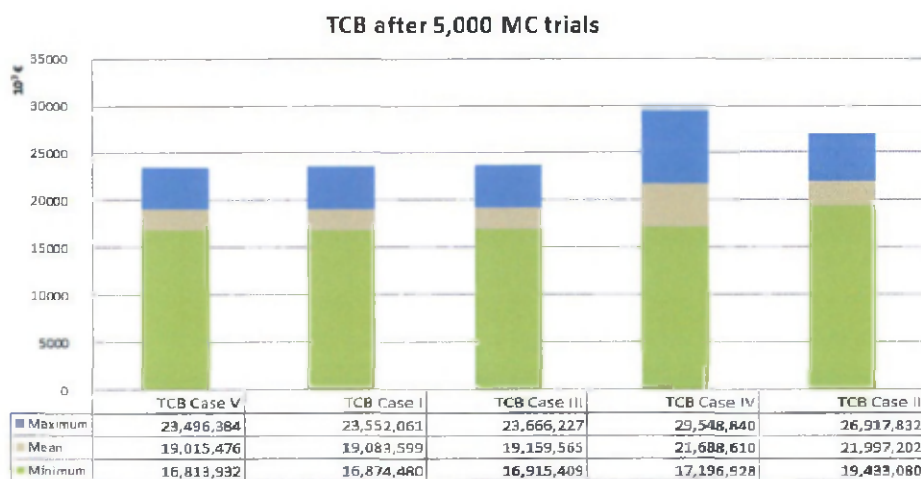


Figure 4: result of the Monte Carlo analysis (€) after 5,000 trials.

Statistical data and sensitivity analysis are shown in Table 8 and Table 9 . Table 8 gives the complete statistical outcome of the Monte Carlo analysis after 5,000 trials as per Crystal Ball software. Table 9 gives the contribution to the variance of certain assumptions. These assumptions are given in the first column and correspond to the uncertain parameters as described in Table 5.

Table 8: statistical outcome of the Monte Carlo Analysis after 5,000 trials.

Statistics	TCB Case I	TCB Case II	TCB Case III	TCB Case IV	TCB Case V
Trials	5,000	5,000	5,000	5,000	5,000
Mean	19,083,599	21,997,202	19,159,565	21,688,610	19,015,476
Median	18,974,364	21,876,340	19,059,431	21,548,482	18,906,595
Mode	---	---	---	---	---
Standard Deviation	1,103,677	1,250,232	1,064,975	1,963,763	1,103,431
Variance	1,218 x10 ⁹	1,563 x10 ⁹	1,134 x10 ⁹	3,856, x10 ⁹	1,218 x10 ⁹
Skewness	0	0	0	0	0
Kurtosis	3	3	3	3	3
Coeff. of Variability	0	0	0	0	0
Minimum TCB	16,874,480	19,433,080	16,915,409	17,196,928	16,813,932
Maximum TCB	23,552,061	26,917,832	23,666,227	29,548,840	23,496,384
Range Width	6,677,581	7,484,752	6,750,818	12,351,912	6,682,452
Mean SD. Err.	15,608	17,681	15,061	27,772	15,605

Table 9: contribution to the variance of certain assumptions in Monte Carlo analysis.

Assumptions	TCB Case I	TCB Case II	TCB Case III	TCB Case IV	TCB Case V
Drydock/day	0	0	0	0	0
Grade A basis	94.1	94.7	88.8	44.3	94.2
Initiele cost $PSPC_{25}$ or $TSCF_{25}$	5.5	4.3	10.9	1.1	5.5
Price aluminium anodes in €/kg	0	0	0	0	0
Price anodes in €/kg	0	0	0	0.00	0
Relation grade A – CRS	0.1	0.1	0.1	54.6	0.1
Time Charter equivalent	0	0.6	0	0	0
Inflation rate	0.2	0.3	0.2	0	0.2

When Figure 3 (outcome of the basic economic model) and Figure 4 (results of the Monte Carlo simulation) are compared we observe an increase in absolute values of the TCB's while the ranking of the cases remains the same. The considered parameters (Table 5) were, amongst others, an increase in the cost of steel, coating, aluminum and zinc over the 25 years to come. If the range and distribution model of these variables are assumed correctly this is reflected by a rise of the mean value of the TCB's with an average of 20% without a change in the relative relation of the cases.

The values shown in Table 9 are the percentages variance or uncertainty in the target forecast due to the respective assumptions. Items with a positive contribution have a positive value; this reflects a direct relationship between the item and the TCB.

Only three assumptions are worth mentioning. The influence of the steel price is decisive for all cases. 11% of the variance of the TCB of Case III is due to the cost of TSCF₂₅ and the TCB of case IV is mainly affected by the price of CRS.

1.6 Consequences for future ship construction

The increased scantling technique (case II), can be classified as economically not healthy, based on the reference model and supported by the sensitivity analysis and the Monte Carlo simulation. Expanded scantlings offer adequate protection against corrosion but the penalty of an increased lightweight and consequently the loss of cargo carrying capacity is simply too important. This conclusion is a confirmation of J. Eliasson's (2003) statement, *"it is possible to build ships with such thick steel that even with free corrosion taking place the ship would have enough strength left to perform its designed service life but that it is generally agreed today that this is no longer a cost efficient way to build and operate ships."*

Construction methods I, III and V are matched and the correct choice will be dependent upon a lot of parameters, the most important being the steel price and the coating cost. The use of corrosion resistant steel (option IV) becomes attractive if the cost of CRS comes down till maximum 1.1 times the cost of ordinary grade A steel.

Case I, the way we are actually constructing ballast tanks, is not the worst of solutions though that there is still a lot of room for improvement.

The average degradation rate of the coating used in the economic model is probably high. 1.7% surface degradation per year is based on our database of 140 ships ranging from 0 to more than 40 years of age. A follow-up study to determine a sound corrosion rate is needed with a focus on PSPC ships without considering older non-PSPC ships.

The average durability of PSPC₁₅ coating can be increased substantially if sufficient attention is given to surface preparation and application conditions.

Case V is a logical evolution of case I. The sacrificial Zn anodes have been replaced by aluminum anodes and the weight has been increased to last the full economic lifespan of the ship.

Zinc has been in use as a sacrificial anode for longer than aluminum and is considered the traditional anode material. However, aluminum has several outstanding advantages (higher current, less weight and less toxicity) as a sacrificial anode material and is fast becoming the material of choice (Cuproban, 2012).

The replacement of zinc by aluminum is ecological beneficial. The negative impact of zinc on the marine environment is well known and documented while this is not the case for aluminum. Aluminum is not considered a pollutant.

However, there are also some drawbacks regarding the use of aluminum as sacrificial material in ballast tanks adjacent to tanks for liquid cargo with flash point $<60^{\circ}\text{C}$. According to DNV Rules for Ships such tanks are considered dangerous areas. Aluminum alloyed anodes are to be so located that a kinetic energy of $\leq 275\text{J}$ is developed in case of their falling down. That means that an aluminum anode weighing for instance 10 kg must be located lower than 2.8m from the tank bottom or stringer deck.

In a forgoing study (De Baere, 2011) we demonstrated that sacrificial anodes are only beneficial if they are installed and maintained in a correct way. Practical experience after many tank surveys indicated that this is not very often the case.

Economically, Case III, the use of a superior paint, seems promising. Yet, what such an improved paint system should look like is still far from clear. Our field research indicates mechanical damage and cracking, besides application shortcomings, as primary cause of corrosion. A protective coating can be made more resistant to deformations by the addition of fibers. Natural or synthetic fibers will be used to mechanically reinforce formulations increasing fatigue properties, strength, and flexibility improving corrosion resistance and increasing the service life of coating.

Also, the performance of TSCF₂₅, used in this study, is questioned by some shipyards. A Dutch shipyard (which requested to stay anonymous) mentioned as follows: *"The wish to reduce and eventually completely eliminate, the maintenance in ballast tanks is fully understandable. I am not aware of any independent scientific proof that the complete removal of the shop primer, the reduction of the allowable quantity of dust, a lowering of the maximal chloride pollution from 50 to 30mg/m², the increase of the layer thickness from 320 to 350 (90/10) micron and 3 full coats instead of 2 will result in an increase of life span of 67%."*

On the other hand, J. Eliasson (ABS, 2012) mentions a number of ships coated according to the precursor of the TSCF₂₅ specifications which are now in service for more than 15 years and are in a near perfect condition.

Case IV studies the use of corrosion resistant materials instead of grade A steel. It is assumed here that CRS will live up to the promised characteristics. At this moment these steel varieties are in an experimental phase and the exact features still remain to be established. Also, the exact retail price is unknown at present. The estimations used in this study are indicative and only based on the value of the composing alloy elements. It is almost certainly that when the demand for this product increases, the retail price will follow.

The data used in this model are an approximation of reality. They provide a platform to compare the different cases and should not be considered as true costs. Differences exist and prices vary in function of geographical location, time and availability. Since the basic commodities are becoming scarcer, the steel price will keep on rising. The CRS obtains its qualities by adding, amongst others, chromium and molybdenum, both becoming increasingly scarce. These arguments are favoring the use of improved coating systems. However, the coating cost is very sensitive. A little change in the cost of TSCF₂₅ is capable of reversing the economical ranking of the hypothetical cases.

1.7 Conclusion

At this moment the best way to protect ballast tanks is by applying a standard PSPC₁₅ coating on a perfectly prepared substrate and under good application conditions. Lifetime lasting aluminum anodes could then be used as a backup system, if they are well distributed across the ballast tank and properly maintained.

In addition, an interesting line of research is the use of alternative construction materials, where the corrosion rate is reduced due to a change in the composition of the steel used. It might eliminate the need for a paint system and sacrificial anodes and might significantly reduce the maintenance and consequently the operation cost.

2 The electrochemistry of corrosion

2.1 Introduction

Corrosion science studies what happens on the interface between electrical and chemical phenomena. It is the interaction between a substance and its environment that results in deterioration of the material (Nace, 2002, Groysman, 2010). Corrosion occurs in all kind of materials but in this work only the corrosion process of steel in a seawater environment is considered. In this context, the definition can be rephrased to: corrosion is the degradation of a metal by an electrochemical reaction with its environment.

It is an unstoppable force that drives the steel back to its most basic and most stable appearance; iron ore. Iron ore is a rock and consequently consist of minerals. Besides (SiO_2) the most important minerals in iron ore are oxides and hydroxides of iron. The two most important iron ore minerals are hematite (Fe_2O_3) and magnetite (Fe_3O_4) (Figure 5).

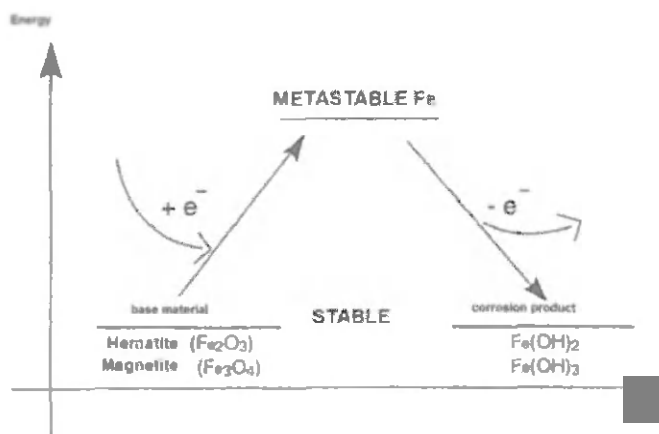


Figure 5: time-energy diagram iron (adapted from Smet, 2008).

It is important to note that the corrosion products are not identical but similar to the original ore. Figure 5 demonstrates that the energy levels are very comparable (Veleva, 2003).

Iron is produced by adding a lot of, mainly thermal, energy to the basic ore. The outcome is a meta-stable product that automatically returns to its ore-like condition if the appropriate protective measures are not taken. This reversing process is called corrosion.

2.2 Fundamentals

Corrosion can only proceed if four elements are present: a cathode, an anode, an electrolyte and a metallic path. The anode is the electrode of an electrochemical cell at which oxidation occurs. Electrons flow away from the anode in the external circuit. Corrosion usually occurs and metal ions enter the solution at the anode (Nace, 2002). The cathode is the electrode of an electrochemical reaction at which reduction is the principal reaction. Electrons flow toward the cathode in the external circuit (Nace, 2002). The electrolyte is the chemical substance containing ions that migrate in an electric field (Nace, 2002). Within the context of this research the electrolyte is invariably seawater. The conductivity of this electrolyte changes in function of a number of parameters such as salinity, temperature and concentration of chlorides (ASM, 2000).

On the same metallic surface, anodic and cathodic microscopic parts can be found. The electrochemical difference is created by small irregularities in chemical composition, the presence of impurities, deposits on the surface, and variations in the electrolyte (Garnett, 1992). The anode is the part of the metal where the bond between the core of the iron atom and the electrons is the weakest. The electrons are easily released and remain in the metal substrate, increasing the electrode potential, while the iron-ions (Fe^{2+} or Fe^{3+}) go into solution causing the loss of material. The material is oxidized.



This is a continuous process if the electrons are consumed. If not, the potential of the metal surface becomes so negative and the transition of the iron-ions to the electrolyte will be impossible. The process is stopped automatically at an equilibrium potential².

If a metallic path exists between anode and cathode, the cathode acts as the electron consumer. At the cathode, the surplus of electrons is used to reduce the oxygen in the seawater. Oxygen is the electron acceptor.



The hydroxide ions react with the iron ions to form iron hydroxide.



² Equilibrium potential: The potential of an electrode in an electrolyte at which the forward rate of a given reaction is exactly equal to the reverse rate; the electrode potential with reference to the standard equilibrium, as defined by the Nernst equation (Nace, 2002).

E_{298} : Cell potential at a temperature of 298K.

Further oxidation results in the final red product $\text{Fe}_2\text{O}_3 \cdot \text{H}_2\text{O}$ known under the common name of rust (Nace, 2002). Whether or not a material corrodes depends on the position if it's potential with respect to the electron acceptor. Only when the potential is lower than the potential of the electron acceptor, corrosion occurs.

In the external circuit, electrons will flow from the most negative point (anode) to the most positive point (cathode) and, by convention; the current will flow in the opposite direction, as presented in Figure 6 (Roberge, 2008).

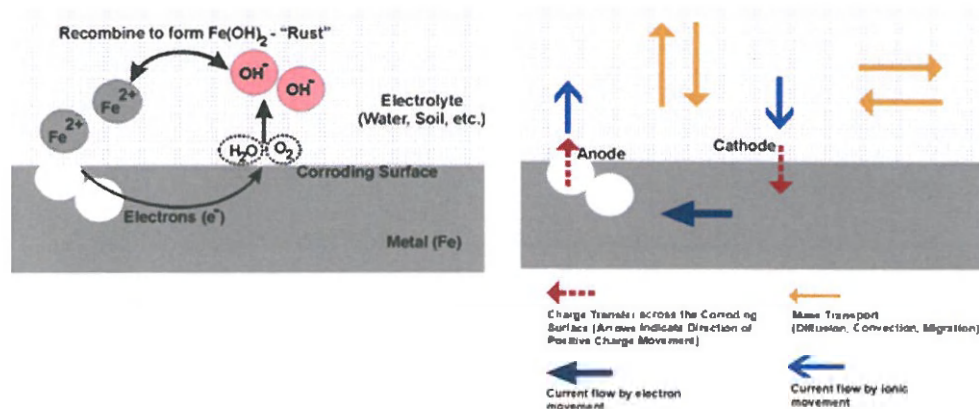


Figure 6: electron and current flow of corrosion cell (<http://amudugowripalan.blogspot.com>).

The above mentioned chemical reactions provide no information regarding the governing environmental conditions and the reaction speed. The thermodynamics and the kinetics of these chemical reactions allow us to develop two important equations forecasting if a reaction will occur and if so at what rate. These formulas are referred to as the Nernst Equation³ and the Butler-Volmer equation⁴. Both equations are given further in this chapter.

³ Nernst Equation: An equation that expresses the exact electromotive force of an electrochemical cell in terms of the activities of products and reactants of the cell (Nace, 2002).

⁴ Butler-Volmer equation: central equation in electrochemistry. It gives the current density as a non-linear function of the overpotential (Ruby, 2003).

2.3 Thermodynamic principles

2.3.1 Reduction potential [E] and standard reduction potential at 298K [E₂₉₈]

The potential difference between the anode and cathode of a galvanic cell can be measured by a voltage measuring device. The absolute potential of the anode and cathode cannot be measured.

Therefore, all reduction potentials are defined in relation to a reference electrode, the standard hydrogen electrode (SHE) (Table 10). The SHE itself has been assigned an arbitrary half-cell potential of 0.0 mV. For laboratory use however, the SHE is too fragile to be practical. Other reference electrodes such as Ag/AgCl or saturated calomel electrode (SCE) are commonly used. Moreover, reduction potentials are being measured under standard conditions.

Table 10: standard reduction potentials 298K, volts vs. hydrogen electrode (Schweitzer, 2010).

Redox reaction	Oxidation Reduction Potential	
$\text{Au} \rightleftharpoons \text{Au}^{3+} + 3\text{e}^-$	+ 1.498	↑ Oxidising agents
$\text{O}_2 + 4\text{H}^+ + 4\text{e}^- \rightleftharpoons 2\text{H}_2\text{O}$	+ 1.229	
$\text{Pt} \rightleftharpoons \text{Pt}^{2+} + 2\text{e}^-$	+ 1.2	
$\text{Pd} \rightleftharpoons \text{Pd}^{2+} + 2\text{e}^-$	+ 0.987	
$\text{Ag} \rightleftharpoons \text{Ag}^+ + \text{e}^-$	+ 0.799	
$2\text{Hg} \rightleftharpoons \text{Hg}_2^{2+} + 2\text{e}^-$	+ 0.788	
$\text{Fe}^{3+} + \text{e}^- \rightleftharpoons \text{Fe}^{2+}$	+ 0.771	
$\text{O}_2 + 2\text{H}_2\text{O} + 4\text{e}^- \rightleftharpoons 4\text{OH}^-$	+ 0.401	↑ Reducing agents
$\text{Cu} \rightleftharpoons \text{Cu}^{2+} + 2\text{e}^-$	+ 0.337	
$\text{Sn}^{4+} + 2\text{e}^- \rightleftharpoons \text{Sn}^{2+}$	+ 0.15	
$2\text{H}^+ + 2\text{e}^- \rightleftharpoons \text{H}_2$	0.0000	
$\text{Pb} \rightleftharpoons \text{Pb}^{2+} + 2\text{e}^-$	-0.126	
$\text{Sn} \rightleftharpoons \text{Sn}^{2+} + 2\text{e}^-$	-0.136	
$\text{Ni} \rightleftharpoons \text{Ni}^{2+} + 2\text{e}^-$	-0.250	
$\text{Co} \rightleftharpoons \text{Co}^{2+} + 2\text{e}^-$	-0.277	
$\text{Cd} \rightleftharpoons \text{Cd}^{2+} + 2\text{e}^-$	-0.403	
$\text{Fe} \rightleftharpoons \text{Fe}^{2+} + 2\text{e}^-$	-0.440	
$\text{Cr} \rightleftharpoons \text{Cr}^{3+} + 3\text{e}^-$	-0.744	
$\text{Zn} \rightleftharpoons \text{Zn}^{2+} + 2\text{e}^-$	-0.763	
$\text{Al} \rightleftharpoons \text{Al}^{3+} + 3\text{e}^-$	-1.662	
$\text{Mg} \rightleftharpoons \text{Mg}^{2+} + 2\text{e}^-$	-2.363	
$\text{Na} \rightleftharpoons \text{Na}^+ + \text{e}^-$	-2.714	
$\text{K} \rightleftharpoons \text{K}^+ + \text{e}^-$	-2.925	

2.3.2 The Nernst equation

The relation between energy and its electrical manifestation can be expressed as follows: 1 Joule equals the energy necessary to move an electrical charge of 1 Coulomb against a potential difference of 1 Volt (Edminister, 1995).

$$Q = q\Delta V \quad \text{Eq. 22}$$

Q = electrical energy (J), q = electrical charge (C), ΔV = potential difference (V = JC⁻¹)

$$q = nF \quad \text{Eq. 23}$$

n = number of electrons transferred in the corrosion reaction, F = Faraday constant defined as the electrical charge carried by 1 mol of electrons = 96,485 Cmol⁻¹.

In chemistry ΔV is replaced by E , the measured potential in Volt and Q is replaced by ΔG , the Gibbs energy⁵ (Roberge, 2008).

$$\Delta G = -nFE \quad \text{Eq. 24}$$

The minus sign is necessary because a negative value of ΔG and a positive value of E both indicate a spontaneous reaction.

If products and reactants are in their standard state the equation can be re-written as follows.

$$\Delta G^0 = -nFE^0 \quad \text{Eq. 25}$$

$$-nFE = -nFE^0 + RT \ln Q \quad \text{Eq. 26}$$

$$E = E^0 - \frac{RT}{nF} \ln Q \quad \text{Eq. 27}$$

This equation is known as the **Nernst equation** and is one of the most fundamental equations in corrosion science and engineering, as it gives the useful relation between energy and the potential of a cell to the concentrations of participating ions and other chemical species (Roberge, 2008). Under standard conditions it can be written as:

$$E_{298} = E_{298}^0 - [0.059/n] \log \frac{\text{Concentration of products}}{\text{Concentration of reactants}} \quad \text{Eq. 28}$$

with E_{298}^0 the standard electron potential for a certain concentration (10⁻⁶ mol l⁻¹ in Figure 7). This potential can differ from the standard electron potential (E_{298}^0) given in Table 10, which is based on the activity coefficient. This activity coefficient is a very complex function dependent on multiple variables. For this reason, the concentrations are used as an approximation of the activity coefficient (Roberge, 2008).

⁵ Gibbs free energy can be associated with potential energy, the possibility to do work.
 $\Delta G = \Delta H - T\Delta S$ (Gibbs free energy = enthalpy – entropy)

2.4 Relation Pourbaix diagrams - Nernst equation

E-pH (Electrode potential - pH diagram) or Pourbaix diagrams summarize many thermodynamic data and the behavior of a metal or similar material for specific environmental conditions. The diagrams represent the potential (E) as the ordinate and pH as the abscissa (Roberge, 2000) and give a graphical presentation of the thermodynamic equilibrium states of a metal-electrolyte system. The lines delimiting the different zones are calculated by means of the Nernst equation.

The complete diagram for iron is quite complex, since many equilibria are involved. For this work, a simplified diagram (Figure 7) is used, where an assumed concentration of $[\text{Fe}^{2+}]$, $[\text{Fe}^{3+}]$ and $[\text{HFeO}_2^-]$ of $10^{-6} \text{ mol l}^{-1}$ is present.

E(V)

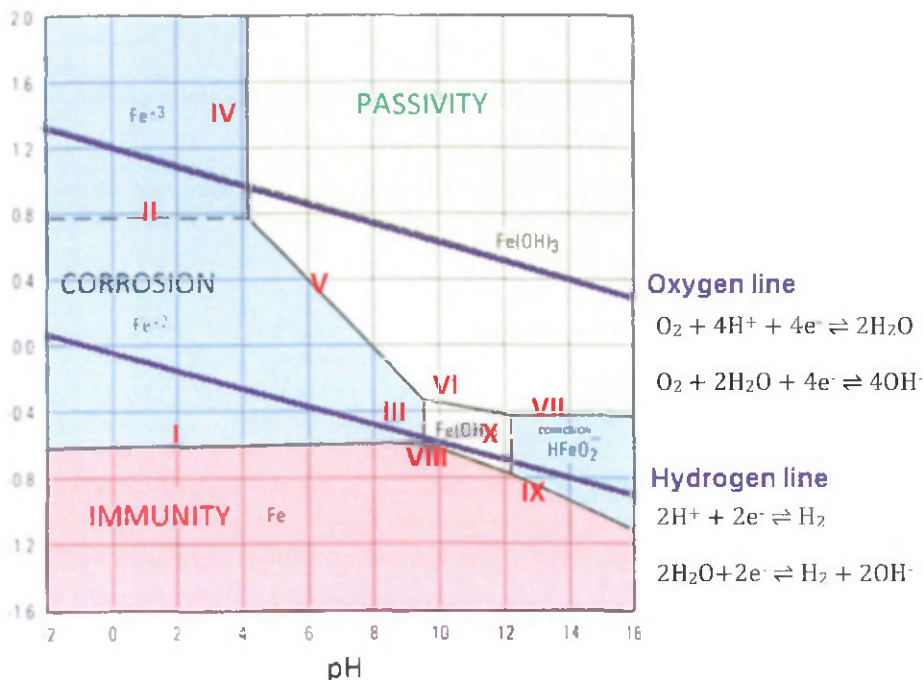


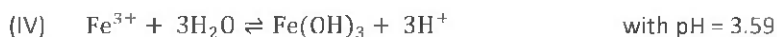
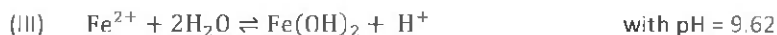
Figure 7: simplified Pourbaix diagram for iron with assumed concentration of $[\text{Fe}^{2+}]$, $[\text{Fe}^{3+}]$ and $[\text{HFeO}_2^-]$ of $10^{-6} \text{ mol l}^{-1}$ (adapted from Bogaerts, 2008, Smet, 2008).

Following equilibria are shown on the diagram:

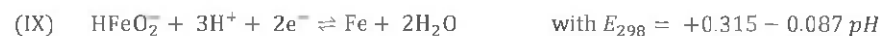
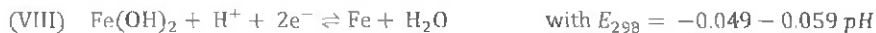
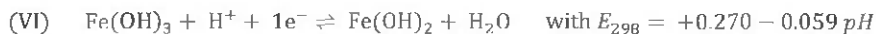
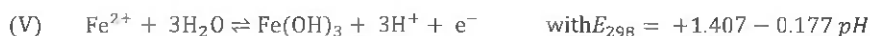
Horizontal lines represent pure electron transfer reactions dependent solely on potential, but independent of pH:



When the pH is high enough, hydroxides can be formed, which reduce the concentration of Fe^{2+} and Fe^{3+} ions. These reactions involve no electron transfer and are solely dependent on the pH. They are given by the vertical lines:



The sloping lines represent equilibria involving both changes in pH as in electron transfer. These reactions are:



On top of these lines of equilibrium the stability diagram for water is plotted (purple lines).

The Pourbaix diagram indicates regions of "Immunity", "Corrosion" and "Passivity". Immunity means that under certain conditions of potential and pH, iron remains in metallic form. In the corrosion zone, iron will rust and Fe^{2+} or Fe^{3+} or FeOOH will be formed. In the passivation zone, protective layers of $\text{Fe}(\text{OH})_3$ or $\text{Fe}(\text{OH})_2$ form on iron and further corrosion of iron does not take place (Schweitzer, 2010).

These diagrams are a useful way to visualize thermodynamic principles and to determine the probability of a corrosion reaction to occur under certain conditions of pressure, temperature and chemical environment. The information in the diagrams can be beneficially used to influence corrosion of pure metals in an aqueous environment. By altering the pH and potential to the regions of immunity and passivation, corrosion can be controlled.

However, there are several limitations of these diagrams. Firstly, the diagram does not give information concerning the reaction rate. Another point is that the diagrams deal with pure metals which are not of much interest to the engineers. For example, influences of alloying elements such as sulfur are not considered. A last assumption that is made is that insoluble products are supposed to be protective. This is not true, as porosity, thickness, and adherence to substrate are important factors, which control the protective ability of insoluble corrosion products. Although the above disadvantages appear to be substantial, the advantages offered by the Pourbaix diagrams far outweigh their limitations (Ahmad, 2006).

2.5 Corrosion kinetics

It can be very misleading to consult only the thermodynamic data concerning a corrosion reaction. When a system has a small thermodynamic potential it does not necessarily mean that the corrosion reaction will be slow. In practice the kinetic factors may render the reaction particularly easy (Bogaerts, 2008). When it comes to corrosion, it is particularly interesting to be able to calculate the amount of mass that will be liberated at the anode in function of the time. Naval architects take this loss in account when they determine the thickness of the ship construction elements. A corrosion allowance is provided on top of the minimum required structural dimensions in respect of the strength of the ship. The main question of corrosion kinetics is the determination of the corrosion rate.

2.5.1 Overpotential or polarization

At the equilibrium potential, both forward and reverse reactions are equal



$|i_c| = |i_a|$ or $i_c + i_a = 0$ and by convention, $i_a > 0$, $i_c < 0$

In the absence of a chemical equilibrium, a net current will flow and the potential will be different from the equilibrium potential E_{eq} . This difference is called overpotential η .

$$\eta = E - E_{eq} \quad \text{Eq. 30}$$

The overpotential represents the extra energy needed (an energy loss that appears as heat) to force the electrode reaction to proceed at a required rate (or its equivalent current density). The polarization is said to be anodic when the operating potential is more positive than its equilibrium potential ($\eta > 0$) or cathodic when the operating

potential is more negative than its equilibrium potential ($\eta < 0$) (Roberge, 2008). The overpotential increases with increasing current density.

$$\eta = iR + \eta_{\text{conc}} + \eta_{\text{act}} \quad \text{Eq. 31}$$

iR is the ohmic drop. It considers the electrolytic resistivity of an environment when the anodic and cathodic elements of a corrosion reaction are separated by this environment while still electrically coupled by a metallic path.

η_{conc} is the concentration overpotential, which describes the mass transport limitations associated with electrochemical processes. η_{conc} is predominant at larger polarization currents or voltages.

η_{act} is the activation overpotential. This is a complex function describing the charge transfer kinetics of an electrochemical reaction. η_{act} is always present and mostly dominant at small polarization currents or voltages.

2.5.2 Ohmic drop: iR

When current is flowing in an electrochemical cell, there is a potential drop between the reference electrode and the working electrode. This voltage drop is caused by the ohmic resistance of the cell. This ohmic resistance is an intrinsic property of an electrochemical cell and depends on the electrolyte conductivity, the distance between the two electrodes and the magnitude of the current. In the literature, ohmic drop and ohmic resistance are sometimes used interchangeably, which may cause confusion.

The ohmic drop is an important factor when studying corrosion phenomena for which there is a clear separation of the anodic and cathodic corrosion sites, e.g. gaps and cracks (crevice corrosion). The ohmic drop is also an important variable in the application of protective methods such as anodic and cathodic protection that force a potential shift of the protected structure by passing a current in the environment (Britz, 1978).

2.5.3 Concentration polarization

2.5.3.1 General

Concentration polarization is the polarization component that is caused by concentration changes in the environment adjacent to the surface of the electrode. When a chemical species participating in a corrosion process is in short supply, the mass transport of that species to the corroding surface can become rate controlling (Roberge,

2000). Concentration polarization is associated with the concentration of ions in solution which shields the metal, thereby causing a decrease in the electrical potential of the cell.

2.5.3.2 Polarity of water

Water consists out of two hydrogen atoms and one oxygen atom. Although it is a neutral molecule, electrons will be positioned closer to the oxygen than to the hydrogen atom because oxygen has a larger electronegativity. A dipole moment is formed. The water molecule has a negative charged side (oxygen) and a positive charged side (hydrogen).

The dipole moment of water is responsible for its behavior in the presence of external electric fields. If a metal electrode is plunged into a suitable electrolyte the metal atoms ionize and go into solution leaving a negative charge on the metal surface caused by the surplus of electrons. This negative charge will attract the positive hydrogen side of the polar water molecule. This ionic structure (layer) will slow down and eventually stop the electron consumption by other ions from the bulk solution. Metal dissolution (corrosion) proceeds until the ionic structure is dense enough to protect and prevent the metal from reacting any further until equilibrium is reached. The ionic structure is known as the electrical double-layer or Helmholtz layer (Figure 8) (Groysman, 2010)

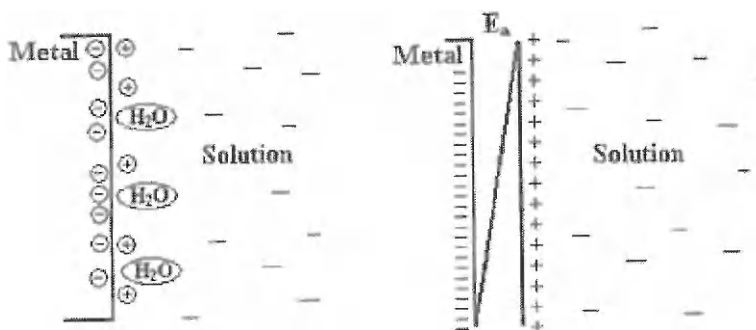


Figure 8: electric double layer formed at the metal surface in water, - = electrons, + = metallic cations, E_a = absolute electric potential (Groysman, 2010).

2.5.3.3 Concentration polarization at the cathode

If an electrolyte is open to the air, gaseous O_2 molecules will first dissolve in the electrolyte and then diffuse throughout the liquid to become uniformly distributed therein. If an electrode is plunged into the electrolyte the O_2 molecules which diffuse to the electrode surface can undergo reduction by the half-cell reaction $O_2 + 2H_2O + 4e^- \rightarrow 4OH^-$ (McCafferty, 2010).

When studying corrosion in an aquatic oxygen containing environment, concentration polarization is a controlling factor when the cathodic processes depend on the reduction of dissolved oxygen since it is usually in low concentration (ppm) (Roberge, 2007). The molecules of O_2 near the surface of the electrode are converted to OH^- ions.

The relation concentration C and distance x from the electrode is very complex but can be simplified considerably using a linear approximation near the metal surface of the electrode (Figure 9).

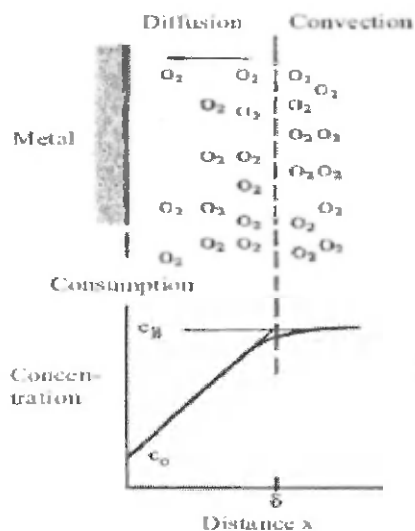


Figure 9: diffusion of O_2 near the electrode surface (Roberge, 2010). Metal surface at ordinate axis, x-axis expresses the distance (x) from the surface, y-axis gives concentration of chemical species being reacted. for well mixed solutions, the concentration is constant for the convection region.

Mass transport to a surface is governed by three forces: diffusion, migration and convection. In the absence of an electrical field, the migration is negligible as there are no charged ionic species. In stagnant conditions, the convection force disappears.

The relative importance of the diffuse layer increases with decreasing concentration. In very dilute solutions it may extend over a distance of several nanometers, whereas the compact layer never exceeds two to three tenths of a nanometer (Marcus, 2002).

2.5.4 Activation polarization

The corrosion rate is determined by the speed at which electrons are transferred between the anode and the cathode here given as a sum of current densities.

$$i = i_a + i_c \quad \text{Eq 32}$$

At the anode electrons are liberated while at the cathode these electrons are consumed. Either the anodic charge transfer or the cathodic charge can control the corrosion rate. By means of a potentiostat, it is possible to study the relation between the changes in potential and the current invoked.

The speed of electrochemical reactions follows the equation of Arrhenius⁶. When a metal electrode is set at its equilibrium potential, the reaction is in balance.

$$i_a = i_0 = nFk e^{\frac{-\Delta G}{RT}} \quad \text{Eq. 33}$$

The total current i of this reaction $i_a + i_c$ results in the following equation:

$$i = i_0 \left(e^{\left(\frac{\alpha nF}{RT}\right)\eta} - e^{\left[-\left(\frac{(1-\alpha)nF}{RT}\right)\eta\right]} \right) \quad \text{Eq. 34}$$

Thus, the translation of Arrhenius for electrochemical reactions is the **Butler-Volmer equation**, which expresses the relation between overpotential η to the net current i and gives both the anodic (forward) and cathodic (backward) reaction.

When the overpotential sufficient high, the reaction is essentially all in one direction and one of the terms in the Butler-Volmer equation is negligible and can be dropped. For a complete anodic equation:

$$i_a = i_0 e^{\left(\frac{\alpha nF}{RT}\right)\eta_a} \quad \text{Eq. 35}$$

$$\ln i_a = \ln i_0 + \frac{\alpha nF}{RT} \eta_a \quad \text{Eq. 36}$$

$$\text{Log} i_a = \text{log} i_0 + \frac{\alpha nF}{2.3RT} \eta_a \quad \text{Eq. 37}$$

$$\eta_a = \beta \log \frac{i_a}{i_0} \quad \text{with} \quad \left(\beta = \frac{2.3RT}{\alpha nF} \right) \quad \text{Eq. 38}$$

Similar, the cathodic equation can be found:

$$\eta_c = \beta \log \frac{i_c}{i_0} \quad \text{with} \quad \left(\beta = -\frac{2.3RT}{(1-\alpha)nF} \right) \quad \text{Eq. 39}$$

A plot of the **Butler-Volmer equation** for the metal dissolution/deposition reaction gives the polarization curves (Figure 10).

⁶ Arrhenius equation: $k = A e^{-E_a/RT}$

with k = rate constant, A = frequency factor specific for each reaction and depending on the probability that the molecules collide in a correct way, E_a the activation energy, R = gas constant and T = temperature in K.

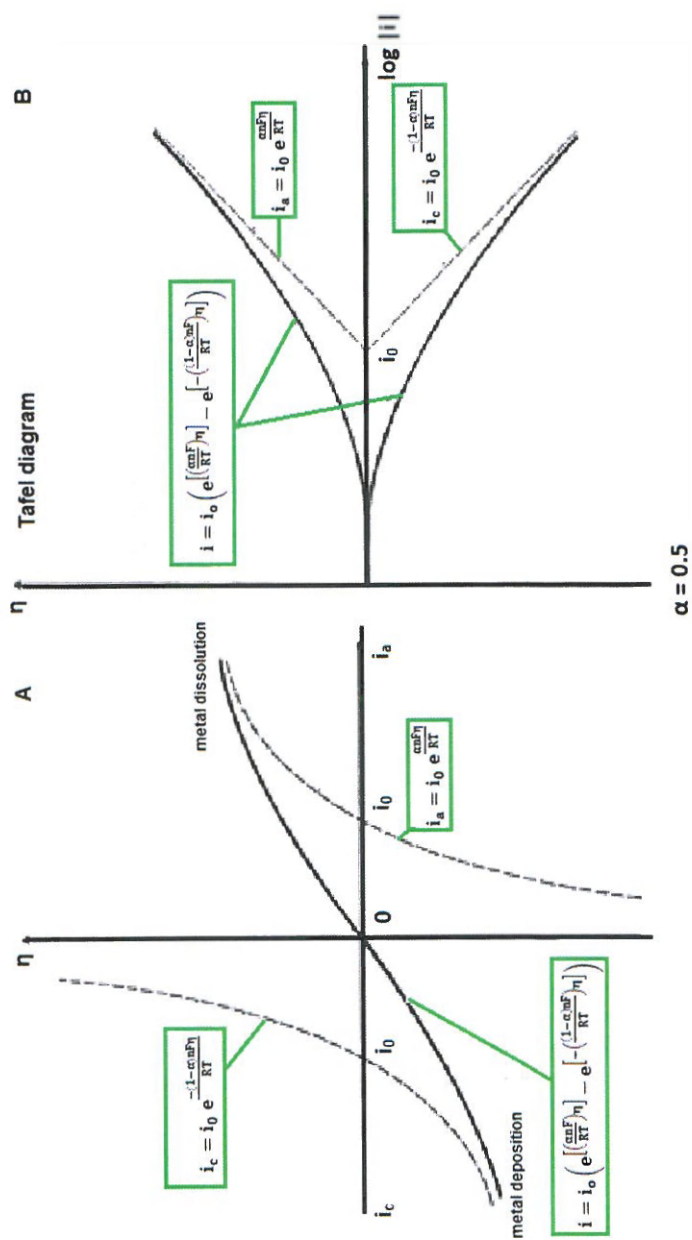


Figure 10: polarization curves, A: overpotential – current density; B: overpotential, logarithmic absolute value current = Tafel diagram (adapted from Smet, 2008).

2.5.5 Linear polarization measurement (LPR)

When the overpotential is very small ($|\eta| < 0.01\text{V}$), the Butler-Volmer equation can be simplified and the relation becomes linear. The linear polarization resistance R_p , given by the slope of the linear part of the curve "potential, external current", is obtained (Figure 11). Around the working electrode corrosion potential (E_{corr}), at a specific moment, a small zone is considered. The LPR measurement starts at a tension of 0.02V below the working electrode potential. Step by step, every second 0.01V is added, the corresponding current is measured and plotted against the potential (Figure 12).

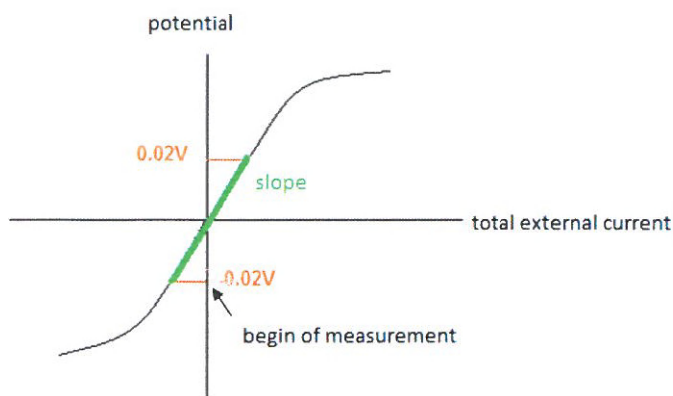


Figure 11: LPR measurement. X axis: external current (i), y-axis: potential (η).

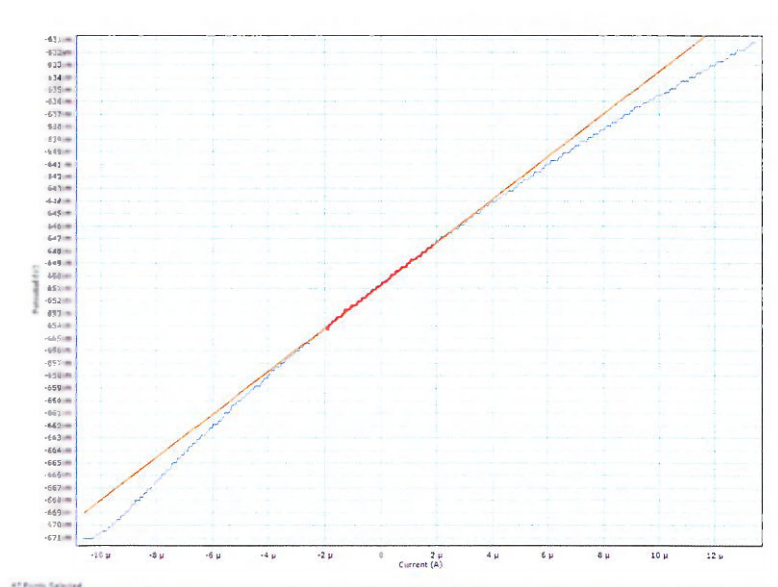


Figure 12: LPR plot. x-axis: current in μA , y-axis potential in mV .

2.5.6 Graphical presentation of kinetic data – E/(log)i diagrams or Evans Diagrams

The anodic- and cathodic reactions in a system cannot be measured and studied individually. If an E/i curve is plotted on the basis of a net current density i as measured with an external ammeter as a function of a varying potential E , then both reactions, reduction as well as oxidation, will be included in the measurement without discrimination, to provide an apparent curve. This curve will cross the vertical at E_{corr} at which the net apparent current is zero. Such a curve is often called an apparent polarization curve and sometimes an electrolysis curve (Figure 13) (Bogaerts, 2008).

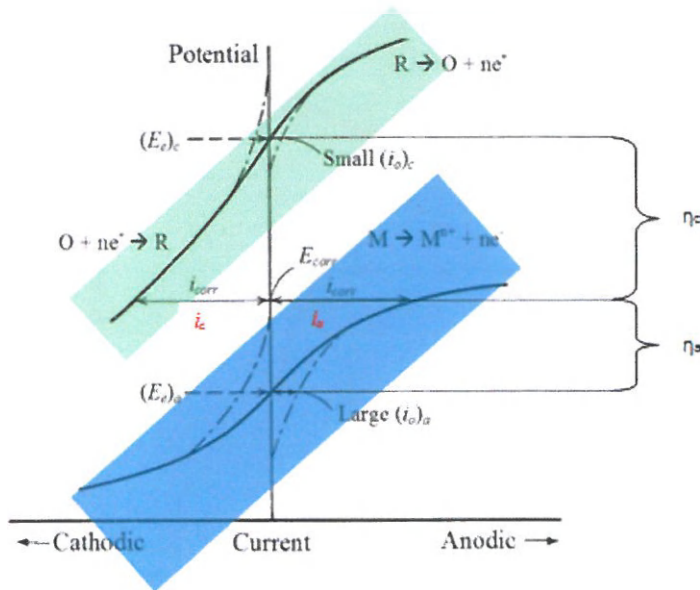


Figure 13: apparent polarization curves (adapted from corrosion center Ohio, 2012). $i_a = i_c = i_{corr}$ at the corrosion potential E_{corr} .

E_{corr} is a mixed potential which lies between $(E_e)_c$ and $(E_e)_a$.

The metal dissolution is driven by the anodic activation overpotential $\eta_a = E_{corr} - (E_e)_a$.

The cathodic reaction is driven by the cathodic activation overpotential $\eta_c = E_{corr} - (E_e)_c$.

The thermodynamic driving force $\Delta E = (E_e)_c - (E_e)_a$.

In practice, a polarization curve becomes linear on a semi- logarithmic plot at approximately 50 mV around the corrosion potential. This region of linearity is called the Tafel region.

2.5.7 Tafel Curve

The Tafel curve represents the total external current (i) (on a logarithmic scale) in function of the potential (E) as $\log i/E$ plots with the negative cathodic current plotted positively, i.e. both the anodic and cathodic current appear in the positive quadrant (Figure 14).

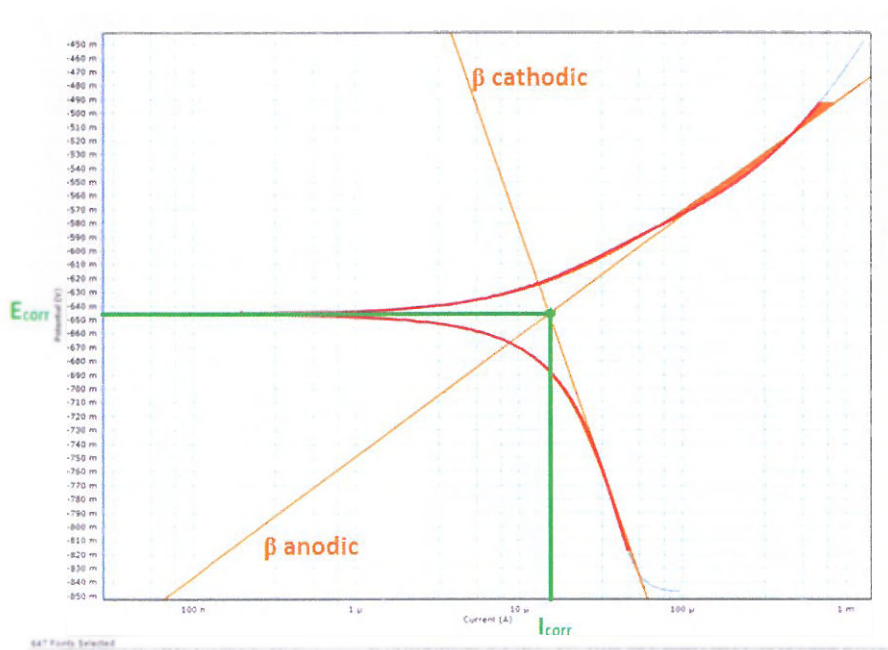


Figure 14: Tafel curve. x-axis: current (μA), Y-axis: potential (mV). Orange lines represent tangents to the curves, red lines are the measured values. E_{corr} is given at the intersection of the tangents.

At the intersection of the tangents $I_a = I_c = I_{corr}$. The corrosion rate is proportional to I_{corr} . The electrons furnished by the corroding iron are consumed by reduction of oxygen and hydrogen ions. At the moment of equilibrium the measured potential of the cell versus a reference electrode equals E_{corr} .

The tangents give the slope of the curve and are defined as the β values.

With the elements from the LPR and Tafel measurement, the corrosion current i_{corr} can be determined, according the Stern-Geary equation (Roberge, 2008):

$$i_{corr} = \frac{1}{2.3 R_p} \frac{\beta_a \beta_c}{\beta_c + \beta_a} \quad \text{Eq. 40}$$

where i_{corr} is the corrosion current (A), R_p the polarization resistance (Ω), and β_a and β_c de slopes of the curves.

2.5.8 Determination of mass loss and corrosion rate

The net current creates or consumes a mass m . The faraday equation states that 96,487 Coulombs (1 Faraday) of charge transfer will oxidize or reduce one gram equivalent weight of material involved in the electrochemical reaction (Roberge, 2008).

$$\frac{\Delta m}{\Delta t} = e \cdot i \quad \text{Eq. 41}$$

$$e = \frac{M}{nF} \quad \text{Eq. 42}$$

Δm = change in mass (g), Δt = time interval (s), e = electrochemical equivalent, n = number of electrons involved, F = Constant of Faraday (Cmol^{-1}), M = Molar mass (gmol^{-1}), i current (A)

so, the mass of the corroded metal is given by (Groysman, 2010):

$$m = \frac{i_{corr} M t}{nF} \quad \text{Eq. 43}$$

m = mass loss (g), t = time(s), i_{corr} corrosion current (A), n = number of electrons involved, F = Constant of Faraday (Cmol^{-1}), M = Molar mass (gmol^{-1}), t = period of current flow (s).

and the corrosion rate, expressed in $\text{mm} \cdot \text{y}^{-1}$ can be calculated from the corrosion current (Groysman, 2010):

$$CR = \frac{i_{corr} M}{nFd} \quad \text{Eq. 44}$$

i_{corr} corrosion current (A), n = number of electrons involved, F = Constant of Faraday (Cmol^{-1}), M = Molar mass (gmol^{-1}) and d the density of the material (gcm^{-3}).

3 Structure of metals

3.1 Crystal structure

Steel in solid condition is composed out of atoms, ordered according a repeating pattern in space, called a crystal structure or lattice. The atoms of diamond, ice and graphite also form crystals, unlike glass and most plastics, which have an amorphous structure (Figure 15) (Atkins, 1992).

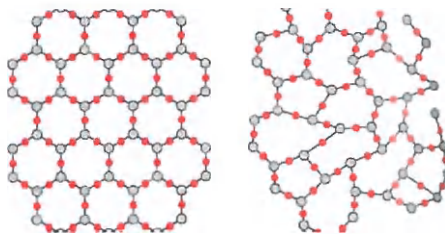


Figure 15: crystal structure and amorphous structure (Atkins, 1992).

In the crystal, iron atoms can easily be replaced by other metal ions and the free space between the iron atoms in the crystal structure can be taken by smaller atoms like carbon or nitrogen (Hermans, 2007).

Similar metal atoms are held together by very strong metallic bonds. This means that in the outer shell of the atoms, also referred to as the valence shell, electrons separate from their atoms. They are present in what is called the Fermi Sea (McCafferty, 2010) around the positive charged ions, which arrange themselves in a very ordered pattern. The atoms are held together because they are all attracted by the negative electron cloud.

The electrons in the cloud can move freely and can carry heat or an electric current through the solid. That is why metal is a good conductor for heat and currents (Lewis, 1997, Neely, 2003).

In nature, seven main lattice structures exist: cubic (simple cubic (SC), body-centered cubic (BCC) and face-centered cubic (FCC)), hexagonal close-packed (HCP), tetragonal (simple tetragonal and body-centered tetragonal), orthorhombic (simple orthorhombic, face-centered orthorhombic, body-centered orthorhombic, base centered orthorhombic), rhombohedral, monoclinic (simple monoclinic and base centered monoclinic) and triclinic. BCC, FCC and HCP are the most common types found in metals. Monoclinic and BCT lattices are encountered in iron oxy-hydroxides and form an important key in rust formation. These lattices are therefore further explained below (Atkins, 1992, Neely, 2003, P. Arnaud, 2007, Massa, 2004).

3.1.1 Body centered cubic (BCC)

The BCC structure (Figure 16) consists of Fe-atoms at each corner of the cube and one in the very center. For each cell, the corner atoms count for $1/8$, the center atom is taken completely. This gives a total of two atoms Fe per cell in the lattice. Iron with a temperature lower than 908°C (α - and β -iron or ferrite) or between $1,401^{\circ}\text{C}$ and $1,538^{\circ}\text{C}$ (δ iron) has this structure, just like chromium, molybdenum, barium and vanadium.

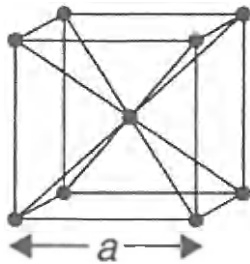


Figure 16: BCC structure (Smallman, 2011).

This is a non-closed packed structure with little space to allow a solution of carbon (max 0.02% at 723°C for α iron and 0.09% at $1,493^{\circ}\text{C}$ for δ iron). It has a lower ductility but a higher strength compared to FCC (Smet, 2008).

3.1.2 Face centered cubic (FCC)

The FCC crystal (Figure 17) consists of a Fe-atom at each corner of the cube and an atom in the center of each cube face. For each cell in the structure, the corner atoms count for $1/8$, the face atoms count for $1/2$. This gives a total of four atoms per cell. FCC is the metallic structure of iron between 908°C and 1401°C (γ -iron or austenite). The austenite phase is the most malleable.

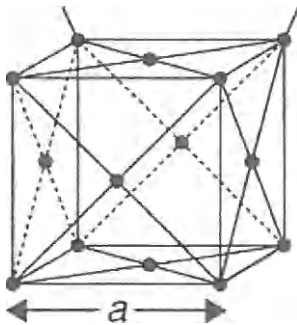


Figure 17: FCC structure (Smallman, 2011).

It has a closed packed structure which allows higher concentration of carbon to be in solution (up to 2.0% at 1144°C).

Aluminum, calcium, copper, lead and nickel also have a FCC structure (Smet, 2008).

3.1.3 Hexagonal close-packed (HCP)

The HCP crystal (Figure 18) consists of a prism with a hexagonal base. Each cell is composed out of six atoms (12 corner points, each atom counting for $1/6$, top and bottom counting for $1/2$ and three center atoms counting completely). This structure can be seen with metals such as beryllium, zinc, cobalt, titanium, magnesium and cadmium.

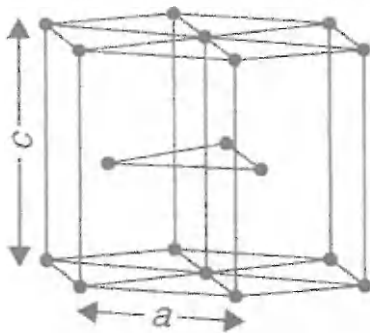


Figure 18: HCP structure (Smallman, 2011).

Also the iron oxy hydroxide ferrihydrite (δ -FeOOH) is composed this way. Due to the structure, the rows do not easily slide over one another, which results in a lower plasticity and ductility than the BCC structure.

3.1.4 Body-centered tetragonal (BCT) and orthorhombic

The BCT and orthorhombic structure (Figure 19) are very similar to the BCC structure. When the cubic lattice is stretched in two directions, this results in a rectangular prism with different lengths for the base sides and the height (BCT structure) or for the three dimensions (orthorhombic). All the sides intersect at right angles.

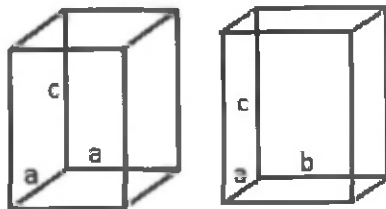
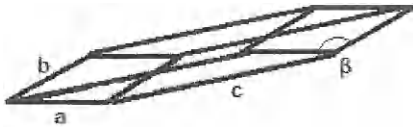


Figure 19: BCT structure, Orthorhombic structure (Smallman, 2011)

BCT structure is formed when γ -iron is cooled rapidly. The carbon atoms in the interstices interfere with the complete transition from FCC to BCC. The BCC structure does not have enough space to contain all the carbon atoms. BCT is an elongated BCC structure and is very hard. The iron oxides goethite (α -FeOOH) and lepidocrocite (γ -FeOOH) have this structure.

3.1.5 Monoclinic

Monoclinic cells (Figure 20) have three axes of different length. Two axes form an oblique angle, the third is perpendicular to these two (Bangert, 2012) resulting in a tunnel-like structure (Kozin, 2012).



The iron oxy-hydroxide akaganeite (β FeOOH), an intermediate form between γ - and α -FeOOH is constituted this way.

Figure 20: monoclinic structure (Smallman, 2011).

3.1.6 Overview

Table 11 gives an overview of the axes and angles of the different crystal structures described above.

Table 11: systems of crystal symmetry (Smallman, 2011).

System	Axes	Angles
Cubic	$a_1 = a_2 = a_3$	All angles = 90°
Hexagonal	$a_1 = a_2 = a_3 \neq c$	All angles = 90° and 120°
Tetragonal	$a_1 = a_2 \neq c$	All angles = 90°
Orthorhombic	$a \neq b \neq c$	All angles = 90°
Monoclinic	$a \neq b \neq c$	Two angles = 90° 1 angle $\neq 90^\circ$

3.2 The Fe-C diagram (iron-carbon) and time temperature transformation (TTT) curve

3.2.1 Introduction

The study of the microstructures of steel is inextricably connected with the binary Fe-C phase diagram. In practice, the diagram Fe-C is most of the time simplified by using Fe_3C instead⁷ of C, as in practice carbide is more relevant for the behavior of most steels. The Fe_3C diagram is *presenting a metastable condition because the formation of Fe_3C is only possible up to 6.67% of carbon*. When carbon is present at a higher concentration, it is found in its elementary, stable form. The diagram is binary because only two elements are involved, in this case Fe and C.

The Fe-C diagram and the TTT curves both describe the occurrence of the different microstructures in a stable system. The TTT diagram takes the time for the transition from one microstructure to another into account, while the Fe-C diagram shows the phase transformation with temperature and carbon content. The solubility of carbon depends on the dimensions of the interstices of the crystal lattice of iron. The number of suitably sized interstices for carbon solution is less in the BCC- than in the FCC lattice. This is because the atomic bonds between the Fe atoms are not flexible enough to accommodate the interstitial atom.

3.2.2 The Fe-C diagram

A phase diagram represents the limits (boundaries and critical points) of stability of the various phases in a chemical system at equilibrium under given conditions. A system is at equilibrium if its free energy is at a minimum under a specified combination of temperature, pressure, and composition. A change in temperature, pressure, and/or composition will result in an increase of free energy and in a possible spontaneous change to another state whereby the free energy is lower.

The lines of equilibrium or phase boundaries, mark conditions under which multiple phases can coexist at equilibrium. Phase transitions occur along lines of equilibrium.

A Fe-C diagram can be roughly divided into 3 parts (Figure 21). The upper part where the Fe-C alloy is 100% liquid, the lower part where the alloy is solid and a central part consisting of a mixture of the solid and liquid physical state.

⁷ Fe_3C is iron carbide or cementite: Chemical compound with 6.67% carbon and 93.33% iron (mass percentages) (R.J. Lewis, 1997).

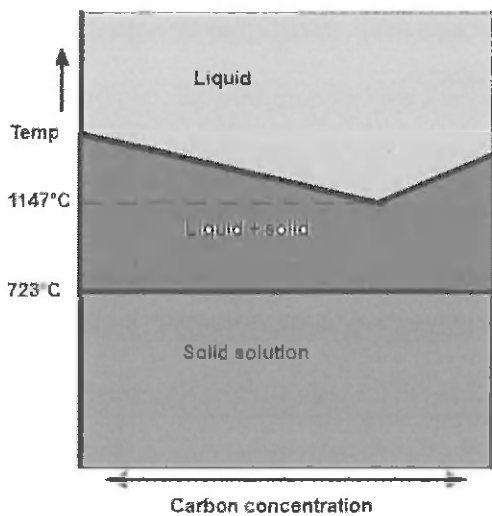
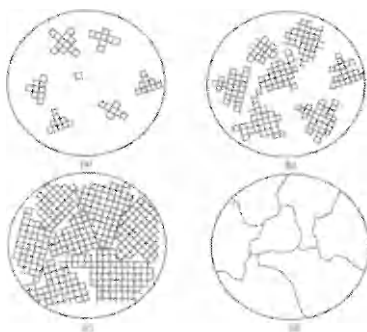


Figure 21: simplified presentation Fe-C diagram.

1,147°C and 723°C are two important temperatures in the Fe-C phase diagram. 1,147°C is the temperature at which austenite has maximum carbon solubility (2.06%). 723°C is the temperature at which ferrite has maximum carbon solubility (0.22%).

During phase transformation, a number of reactions occur, such as crystallization of the liquid phase, segregation of impurities and alloying elements and liberation of the gases dissolved in the melt (Kopeliovich, 2009).

When low carbon steel or mild steel is cooled down below 908°C, ferrite and cementite crystals form in austenite solid solution. Those crystals experience with nucleation and growth stages when temperature is further reduced slowly (equilibrium state at each temperature). The resulted microstructure at room temperature consists of ferrite and cementite crystal grains and their boundaries between them. (Figure 22, Figure 23).



- a) Nucleation of crystals
- b) Crystal growth
- c) Crystals grow together
- d) Grain boundaries as seen under a microscope.

Figure 22: nucleation (NDT- resource center, 2011).

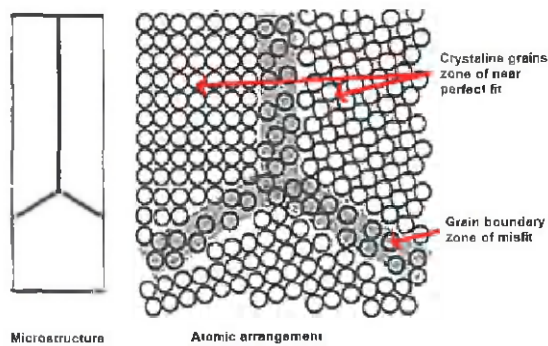


Figure 23: diagram of grain boundaries in a metal (ASM International, 2000).

A grain can be seen as a crystal without smooth faces because its growth was disturbed by contact with another grain or a boundary surface. The interface formed between grains is called a grain boundary. The atoms at the grain boundaries have no crystalline structure and are said to be disordered (NDTResource center – 2011).

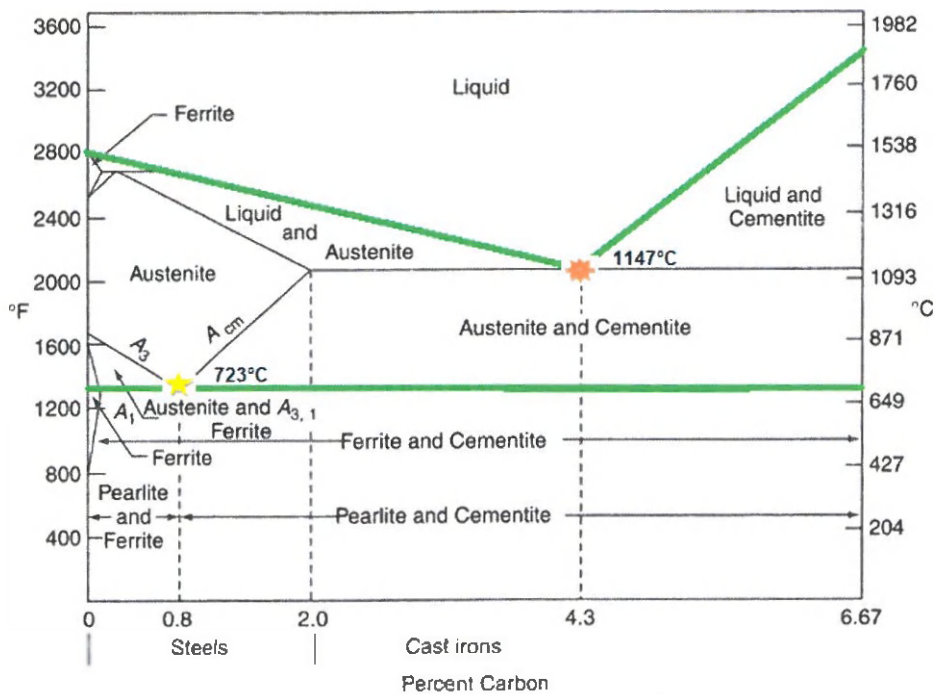



Figure 24: Fe-C diagram (adapted from Neely, 2003).


Figure 24 shows the Fe-C diagram. The vertical axis indicates the temperature in °C on the right hand side and in °F on the left hand side. The horizontal axis represents the

carbon concentration in iron in weight % from 0% carbon to 6.67% carbon. Specific carbon concentrations result in different steel types (Table 12).

Table 12: carbon concentration in different carbon steels (NSW Tafe Commission, 2008).

Carbon Steel	Carbon % (w/w)	Application and properties
Low carbon steel Wrought Iron	<0.1%	Soft, ductile. Easy to shape.
Mild steel	0.1 – 0.25%	Low tensile strength, but it is cheap and malleable; surface hardness can be increased through carburizing.
Medium carbon steel	0.25 – 0.45%	Balances ductility and strength and has good wear resistance; used for large parts, forging and automotive components
High carbon steel	0.45 – 1.0%	Very strong, used for springs and high-strength wires.
Ultra-high carbon steel	1.0 – 2.0%	Very hard –used for knives and punches. Usually anything over 1.2% would be made with powder metallurgy and is considered a high alloy carbon steels.
Cast iron	2.0 – 6.67%	Lower melting point, easy casting, lower toughness and strength than steel.

An important point on the diagram is the Eutectic point () situated at 4.3 wt% of carbon and at a temperature of 1,147°C. At this point, a mixture of two phases of austenite solid and liquid co-exists.

A second important point, the Eutectoid point, is represented by () at a temperature of 723°C and 0.83%wt C. It is the moment where austenite transforms directly to a two-phase solid which is a mixture of ferrite and cementite. At the Eutectoid composition, the mixture forms lamellar structure, called pearlite structure which consists of 88%wt of ferrite and 12%wt of cementite.

Starting from the top left hand corner (Figure 24), going vertically down, following phases are encountered: liquid solution of carbon in iron, δ -iron solid solution of carbon in iron, γ -iron (austenite) solid solution of carbon in iron and α -iron (ferrite) solid solution of carbon in iron.

There are four important lines on the Fe-C phase diagram (Figure 24): A3 is the lower-temperature boundary of the austenite region at low carbon content (< 0.83 %wt C), below which ferrite starts to form γ -iron (austenite). It is boundary of γ -iron (austenite) and γ -iron (austenite) + α -iron (ferrite).

Acm is the lower-temperature boundary of the austenite region at high carbon content ($>0.83\text{wt C}$), below which cementite starts to form in γ -iron (austenite). It is boundary of γ -iron (austenite) and γ -iron (austenite) + cementite.

A1, 723°C , is the so-called eutectoid temperature, which is the minimum temperature for austenite and below which ferrite and cementite start to form in γ -iron (austenite).

A2, 770°C , is magnetic transformation temperature, above α -ferrite becomes paramagnetic⁸.

When looking at the diagram from left to right, microstructures with increasing carbon content are encountered. Alloys containing less than 2% carbon are called steel. Steel must be malleable; this means that it should completely return into the austenite phase when it is heated. Carbon content under 2wt C is called steel, above 2wt C it is called cast iron. In practice, the maximum carbon concentration is set at about than 1.5% (Smet, 2008). When cooling austenite with a carbon concentration of 0.01%, ferrite grains are formed. The maximum solubility of carbon into the ferrite microstructure at 723°C is limited to about 0.02%. Austenite with a higher carbon content forms ferrite up to this concentration and the remaining transforms into pearlite. Up to the eutectoid concentration of 0.83%, only ferrite and pearlite are encountered. As said before, at a concentration of exactly 0.83% carbon, the steel is solely composed out of pearlite. Above this concentration, the first cementite (also called carbon carbide) is introduced. Alloys, containing from 2% to 4.3% of carbon are called cast iron. They experience transformation at the eutectoid temperature and form a combination of austenite and cementite. When cooling below 723°C , this results into ferrite, pearlite and cementite. Content of carbon higher than 4.3% are not used in practice, as it is too hard and brittle. Pure cementite at room temperature is represented by the bottom right hand corner, having a carbon concentration of 6.67%.

Iron is an allotropic element, which means that it can exist in different structures. Its preference for a specific structure is temperature dependent (Lewis, 1997; Neely, 2003; Hermans, 2007). Pure iron has 4 allotropic structures, from α to δ iron (Figure 25). In literature, the β structure of iron is often not mentioned, as both α - and β -iron have a BCC structure. β -iron is ferromagnetic⁹ below the Curie temperature.

The horizontal lines in Figure 25 represent the phase changes during cooling, when latent heat is released or absorbed. As can be seen on the curve, the transformation from β - to α -iron is not an isothermal process as at the Curie temperature; there is a sudden change in specific heat of Fe, explaining the drop.

⁸ Paramagnetic material is only attracted when in the presence of an externally applied magnetic field.

⁹ Ferromagnetic material can be strongly magnetized in the direction of the magnetizing field when placed in magnetic field.

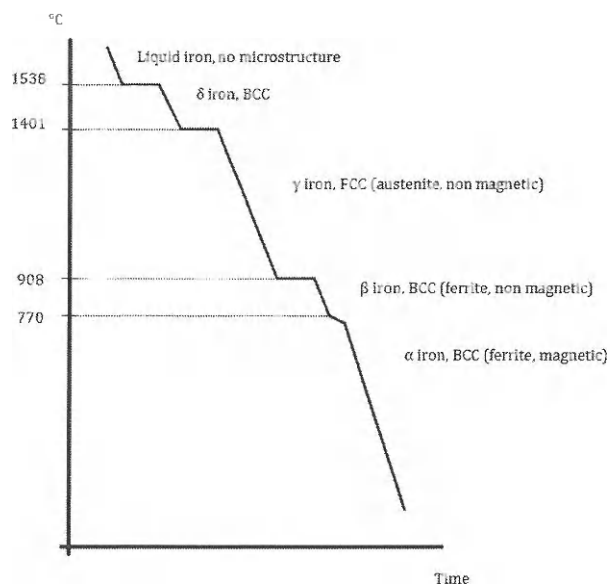


Figure 25: time temperature (°C) curve pure iron.

The mixture of two or more metals is called an alloy. The metal which has the largest concentration is called the solvent; the other is called the solute. In solids, the rate of movement of the atoms is rather limited. The rate of diffusion is temperature dependent.

Two major types of solid metal solutions exist: the substitutional and the interstitial solution. A substitutional solution is a combination of atoms with more or less the same size. The alloying element replaces some atoms in the lattice structure (Figure 26 A), while in interstitial solutions, the atom sizes differ greatly and the small atoms position themselves in the space between the base atoms (Figure 26 B). Iron-carbon is an example of such a solution where the small carbon atoms fill the space between the iron atoms (Roberge, 2006, Neely, 2003).

There is also the possibility that there are empty spaces in the crystal structure. These are called vacancies (Figure 26 C). Around the melting point, about 0.01 to 0.1% of the places in the lattice are unoccupied. These vacancies change their position extremely fast at higher temperatures (up to 10^{12} times a second). This explains how material transport through a metal is possible (Hermans, 2007).

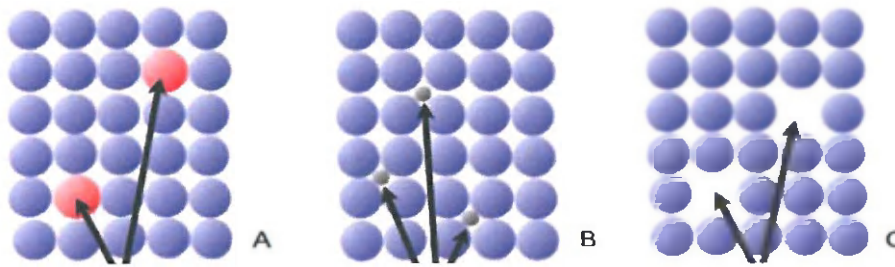


Figure 26: lattice representation of an alloy. (A) Substitutional; (B) Interstitial; (C) Vacancies (Hermans, 2007).

3.2.3 The TTT diagram

The Fe-Fe₃C diagram only applies in a situation of thermodynamic balance, without the influence of the transformation rate. The TTT (Time Temperature Transformation) diagram (Figure 27), also called CT (Continuous Transformation) diagram describes the microstructure changes versus the rate of temperature drop. The driving force for phase transformations is the reduction of free energy (Pieters, 2007).

Steel at temperatures above A₃ or A_{cm} line is austenitic and stable. To keep this stability, cooling takes infinite time (red dotted line). If the temperature drops below this temperature the austenitic stability disappears. Crucial is the speed of this process. The left red colored curve (M_s) indicates the start of a transformation and the right red colored curve (M_f) represents the finish of a transformation. This is a logarithmic scale, so a faster reaction time moves the curve to the left. At a certain temperature, the carbon in the lattice can no longer move freely and will slow down the reaction speed, pushing the curve back to the right. If the movement of the carbon stops, we obtain a fixed temperature. The area between the two curves indicates the transformation of austenite to different types of crystal structures. Once the transformation is completed, the microstructure is fixed and will not change further during cooling.

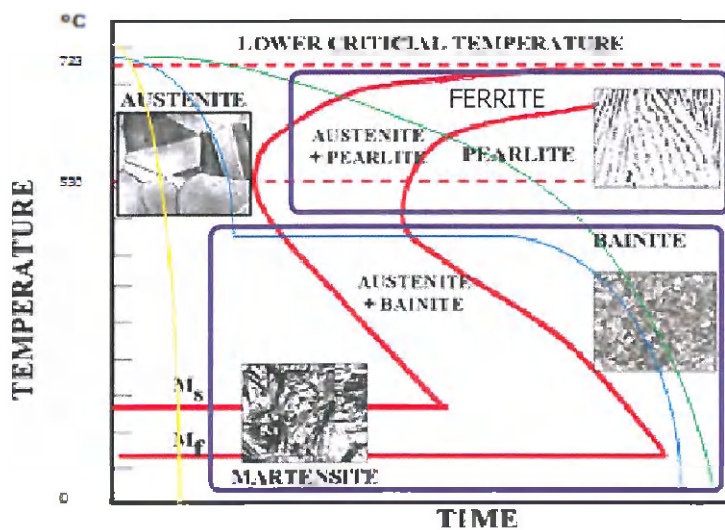


Figure 27: TTT diagram, logarithmic scale on X axis. M_s : starting of transformation; M_f : finish of transformation, (adapted from S. Z. Elgun, 1999).

When cooling takes place at a very slow rate (green line), all the austenite can transform into ferrite and pearlite. The cooling curve is rather horizontal.

The transformation into ferrite (Figure 28) is only possible for very low carbon concentrations. There is no composition change, only a change in structure from FCC to BCC.

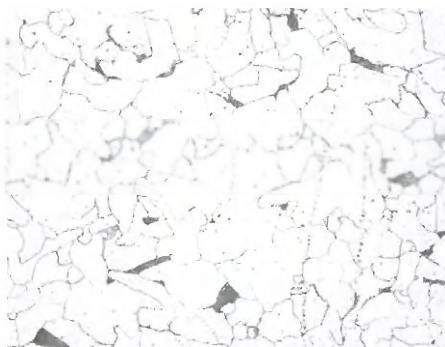


Figure 28: SEM image, magnification 500x, ferrite structure. clear grains, no cementite present.

Pearlite is a mixture of ferrite and cementite (Figure 29). The 3 dimensional shape of pearlite can easily be compared with a cabbage (Figure 30) (Bhadeshia, 2008). If the cabbage leaves are the ferrite, the cementite is the space between them. The chemical composition of pearlite is identical of austenite. Therefore, complete transformation is possible.

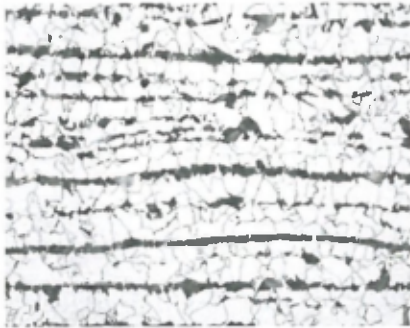


Figure 29: SEM image, magnification 500x, pearlite: white zones ferrite and dark zones cementite.

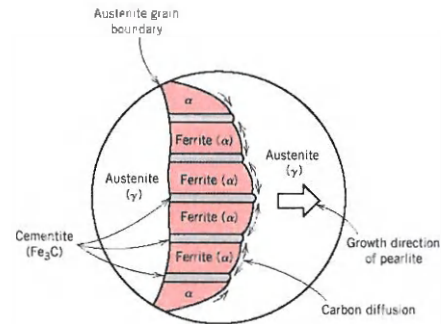


Figure 30: cross section of pearlite (University of Tennessee, 2012).

In case of a rapid cooling (yellow line), martensite is formed within the grain boundaries (Figure 31). It is the hardest structure formed out of austenite. It has a BCT structure and is very hard and brittle. The carbon in the austenite does not participate in the transformation and therefore, to limit the strain within the martensite, it forms as thin plates. During transformation, the unwanted impurities are absorbed by the original austenite boundaries and can make this structure susceptible for impurity embrittlement.

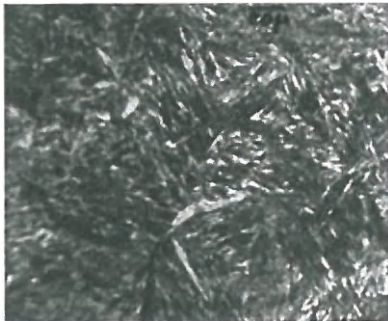


Figure 31: SEM image, magnification unknown, of martensite. Thin plates are visible (Olson, 1992).

Bainite (Figure 32), a combination of ferrite and cementite is formed when rapid cooling is interrupted by immersing the metal into a salt bath¹⁰ at constant temperature (blue line). This is followed by another cooling phase. It is not as hard as martensite, but is more stable and has less internal stress, as the carbon particles participate in the transformation and thus the plates grow to limited sizes. It is harder, stronger and tougher than pearlite at lower temperatures.

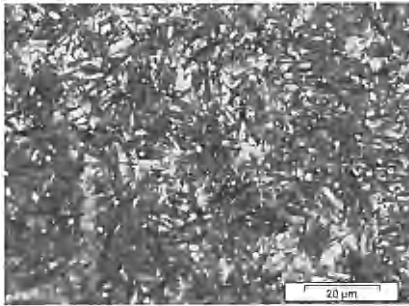


Figure 32: SEM image, magnification unknown, of bainite. plates with limited size are visible, resulting in strong and stable combination of ferrite and cementite, less internal stress than martensite (Luzginova, 2012).

Slow cooling promotes the formation of large grains, fast cooling results in small grains (Neely, 2003). Grain size has an important effect on physical properties.

At ambient temperature, it is generally considered that fine grained steels give a better combination of strength and toughness, whereas coarse-grained steels have better machinability (Roberge, 2008). The purple rectangles drawn on Figure 27 show both fast and slow transformation zones.

¹⁰ The rate of cooling is relatively rapid during quenching in brine, somewhat less rapid in water, and slow in oil.

3.3 Alloy elements

Ordinary grade A ship construction steel is mainly composed out of iron with certain alloy elements, as defined by class societies (Table 13).

Table 13: chemical requirements ordinary strength hull structural steel (ABS, 2012).

Grade A	
	Chemical Composition, % max. unless specified otherwise
C	0.21 ⁽¹⁾
Mn	min 2.5 x C
Si	0.50
P	0.035
S	0.035
N	See note 2
Cr	See note 2
Mo	See note 2
Cu	See note 2
C + Mn/6	0.40

1 A maximum carbon content of 0.23% is acceptable for Grade A sections.

2 The contents of nickel, chromium, molybdenum and copper are to be determined and reported. When the amount does not exceed 0.02%, these elements may be reported as $\leq 0.02\%$.

The purpose of alloying a metal is to improve its properties compared to ordinary carbon steel (Kopeliovich, 2011). Table 14 gives an overview of different influences of alloying elements on steel properties.

Table 14: influence of the alloying elements on the properties of steel (ODS metals, 2007).
↑ increase ↓ decrease, = constant, - unknown

Alloying element	Mechanical properties												
	Hardness	Tensile strength	Yield point	Elongation	Reduction of area	Notch Toughness	Elasticity	High temperature stability	Cooling rate	Carbide formation	Wear resistance	Forgeability	Machinability
Silicon	↑	↑	↑↑	↓	=	↓	↑↑↑	↓	↓	↓	↑↑↑	↓	↓
Manganese at pearlitic steels	↑	↑	↑	=	=	=	↑	=	↓	=	↓↑	↑	↓
Manganese at austenitic steels	↓↓↓	↑	↓	↑↑↑	=	=	=	=	↓↓	=	=	↓↓↓	↓↓↓
Chromium	↑↑	↑↑	↑↑	↓	↓	↓	↑	↑	↑↑↑	↑↑	↑	↓	↓
Nickel at pearlitic steels	↑	↑	↑	=	=	=	=	↑	↓↑	=	↓↑	↓	↓
Nickel at austenitic steels	↓↓	↑	↓	↑↑↑	↑↑	↑↑↑	=	↑↑↑	↓	=	=	↓↓↓	↓↓↓
Aluminium	=	=	=	↓	↓	↓	=	↑↑↑	↓	↑↑	↑↑↑	↓	↓
Tungsten	↑	↑	↑	↓	↓	↓	=	↑↑↑	↓	↑↑	↑↑↑	↓	↓
Vanadium	↑	↑	↑	=	=	↑	↑	↑↑	↓	↑↑↑	↑↑	↑	↓
Cobalt	↑	↑	↑	↓	↓	↓	=	↑↑	↑↑	↑↑	↑↑↑	↓	↓
Molybdenum	↑	↑	↑	↓	↓	↓	=	↑↑	↓	↑↑↑	↑↑	↓	↓
Copper	↑	↑	↑↑	=	=	↓	=	↑	=	=	=	↓	↓
Sulphur	=	=	↓	↓	↓	↓↓↓	=	=	=	=	=	↑↑↑	↑↑↑
Phosphorus	↑	↑	↑	↓	↓	↓↓↓	=	=	=	=	=	↓	↓

Alloy elements have a large influence on the corrosion process (Penning, 2004). A number of theories exist, but they are often unclear and contradicting each other (Melchers, 2003). It must be noted that the influence of a specific alloy can be altered by another alloy element (ASM international, 1990). Certain is that Al, Si, Mo and Cr passivate the substrate by forming a thin and strong oxide film on the steel surface, protecting it from chemical attacks such as seawater (Weidmann, 1990).

Some of the alloy elements have an influence on the formation of the microstructure (Kopeliovich, 2011). The change in chemical composition influences the size and shape of the austenite area on the iron-carbon phase diagram. A four type classification can be given: open, expanded, closed or contracted (Figure 33) (Maalekian, 2007).

Open field: Alloying elements such as Ni, Mn and Co widen the temperature range for stable austenite. Austenitic stainless steel (called Hadfield steel), with 1%C, 13%Mn and 1.2%Cr is an example. Ni and Mn, when added in sufficient large concentrations, can eliminate the BCC structure down to room temperature in favor of the FCC structure.

Closed field: This type of alloying elements creates the opposite effect as type 1, as the formation of BCC is encouraged in favor of FCC. The normal cooling process through the γ -phase is skipped when adding alloy elements such as Al, Si, V, Mo and Cr. They also decrease the solubility of carbon in the austenite, increasing the amount of carbides in the steel.

Expanded field: This group is represented by C, N, Cu, Zn and Au. The γ -phase field is expanded compared to the basic Fe-Fe₃C diagram, but its range of existence is cut short by compound formation. The expansion of the γ -phase by carbon and nitrogen, allows the formation of a homogenous solid solution (austenite).

Contracted field: Mainly B, but also Ta, Zr and Nb have the effect of contracting the γ -phase on the diagram.

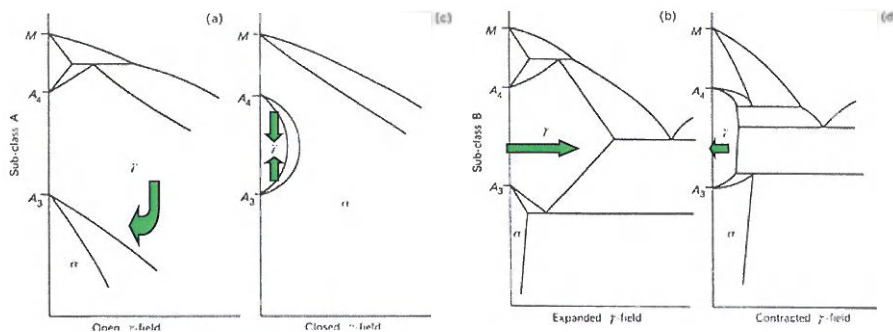


Figure 33: classification alloy types: (a) open field; (b) closed field; (c) expanded field; (d) contracted field (adapted from Maalekian, 2007).

The influence of the above mentioned elements can be seen at the eutectoid temperature of the Fe-C diagram. Ferrite formers (closed field formers) such as Cr and Mo increase this temperature, limiting the formation of austenite. Austenite stabilizers (open field formers) such as Ni, Mn and C act in the opposite way (Figure 34).

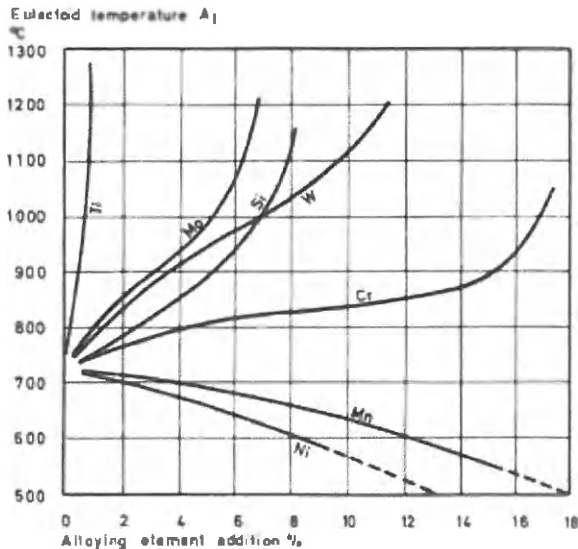


Figure 34: effect of alloy addition on eutectoid temperature of 723°C at 0.83%wt carbon concentration (Maalekian, 2007).

When analyzing the steel composition, the alloy elements can be found in different forms:

- In free state
- As inter metallic compound with each other or with iron
- As non-metal inclusions (oxides, sulfides...)
- As interstitial compounds such as carbides¹¹ and nitrides
- As solid solution

The formation of carbides is crucial. If no carbides can be formed the alloying elements reside in the steel as solid solutions. Cu and N are special since they are soluble in iron to a certain extend. In case of high Cu and N concentrations they reappear as metal inclusions (Cu) or nitrides (N). Elements which have a greater affinity with oxygen than with iron form non-metallic inclusions. These are discussed under the next heading.

Alloying elements creating stable carbides in steel appear as chemical compounds with carbon and iron or are retrieved in the solid solution. All this depends on the carbon-

¹¹ A carbide is a chemical composition of carbon with an less electronegative element, such as iron (Fe₃C) or silicon (SiC) or calcium (CaC₂) (Oxforddictionaries.com, 2012)

alloy ratio. With low carbon content and high alloy content, carbide is formed and the excess of the alloying elements are found in solid solution. On the other hand, if the amount of carbon is large enough, all of these elements will be transformed into carbides.

Silicon, nickel, cobalt and aluminum decrease the stability of the carbides, helping them to break down in free graphite reducing the strength of the steel.

The majority of elements, such as Ni, Si, Cu and Al, that dissolve only in ferrite and cementite without the formation of special carbides slow down the transformation processes. Cobalt is an exception and speeds up the transformation (Figure 35). Cr, W, V and Mo are alloying elements that dissolve mainly into basic phases (ferrite, austenite, cementite) of iron-carbon alloys or form carbides, increasing steel toughness and strength. This last group affects the TTT curves, but not in a uniform way.

- At 700-500 °C (pearlite formation), they slow the transformation
- At 500-400 °C, they dramatically slow the transformation
- At 400-300 °C (bainite formation), they speed up the transformation (Figure 35)

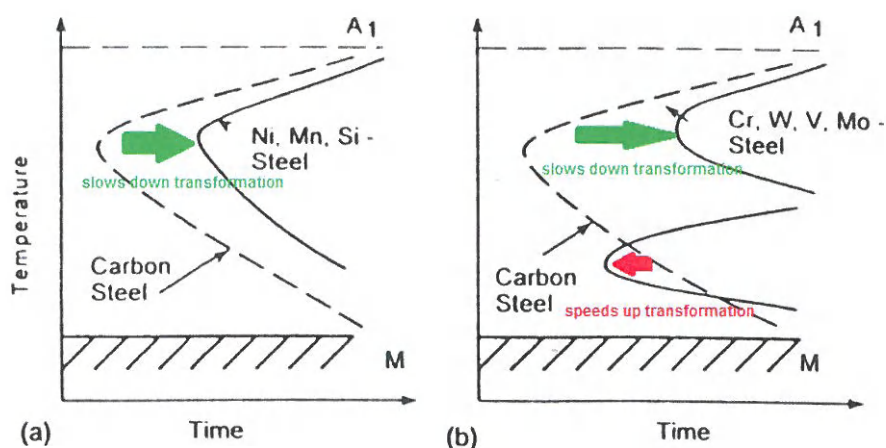


Figure 35: diagrams of isothermal transformation. (a) Carbon steel and steel alloyed with non-carbide-forming elements; (b) carbon steel and steel alloyed with carbide-forming elements (ASM, 1991).

At the bottom part of the TTT curves, where martensite is formed, most alloying elements (except Co and Al) lower the temperature at which this transformation start. Figure 36 shows this effect for C. Adding more than 0.7% C lowers the martensite finish temperature below ambient temperature. As a result, higher C steels cooled at a very rapid rate will contain larger amounts of austenite.

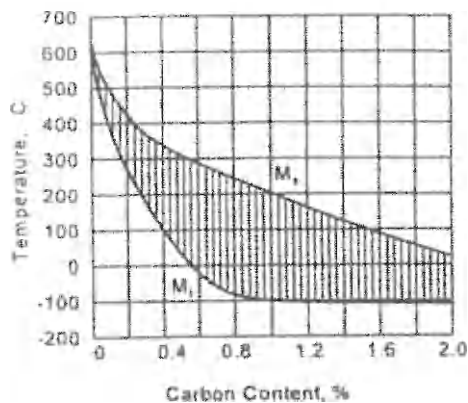


Figure 36: influence of carbon content on the martensite transformation. M_s : start of transformation; M_f : finish of transformation (Abbaschian, 2009).

3.4 Inclusions

The word inclusions refers to “non-metallic” inclusions. Inclusions can be defined as foreign material in a metallic matrix. The particles are usually compounds (such as oxides, sulfides) but can be of any substance that is foreign to and essentially insoluble in the matrix (ASM, 2000). They are also classified as undesired elements in the steel. Elements such as Al, Si, C and Ti added during steel melting deoxidize the steel by taking oxygen from the iron, transforming it into oxides such as Al_2O_3 . As these deoxidizers are only added at the end of the melting process, most of them do not have the time to pass to slag¹² and remain as inclusions in the solid metal.

The amount of impurities in the metal defines its cleanliness. The term steel cleanliness is a relative one, since even steel with only 1 ppm of oxygen and sulfide still contains 10^9 to 10^{12} non-metallic inclusions per ton (Herring, 2009).

Despite of small content of non-metallic inclusions in steel (0.01-0.02%) they have a significant influence on mechanical properties such as tensile strength, ductility, fatigue strength, weldability, machinability and corrosion resistance.

¹² Slag is a byproduct of the metal melting process. It represents undesired impurities that float to the top during the melting process. Above this, slag forms after oxidation of the metal as a protective crust of oxides on the top of the metal being melted protecting the liquid metal underneath.

Chemically, five main types can be distinguished:

- Sulfides such as FeS, MnS, Al_2S_3 , CaS, MgS, Zr_2S_3 , FeS-FeO and MnS-MnO
- Oxides such as FeO, MnO, Cr_2O_3 , SiO_2 , Al_2O_3 , TiO_2 , FeO-Fe₂O₃, FeO-Al₂O₃, FeO-Cr₂O₃, MgO-Al₂O₃ and 2FeO-SiO₂
- Silicates such as SiO₂
- Nitrides such as ZrN, TiN, AlN and CeN
- Phosphides such as Fe₃P and Fe₂P (Herring, 2009).

Another possible subdivision for these inclusions is to divide them as per origin: indigenous and exogenous. Indigenous or endemic inclusions result from chemical reactions in the molten or solidifying steel. Exogenous inclusions have a foreign origin such as slag or refractories. The last ones are usually larger than the first and therefore another subdivision is possible: macro-inclusions and micro-inclusions (Juvonen, 2004).


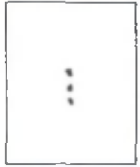

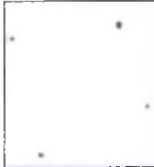
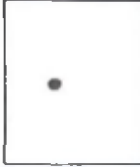
Nonmetallic inclusions have detrimental effects on ductility parameters such as elongation. Larger inclusions disrupt the homogeneity of the metal structure, so their influence can be considerable. They result in negative properties such as higher fatigue and can initiate ductile fractures. Small inclusions can be both detrimental and beneficial for the metal, for example improve the machinability of steel (Kiessling, 1978).

ASTM developed two standards for the determination and classification of inclusions. These are ASTM E45-11: Standard Test Method for Determining the Inclusion Content of Steel, and ASTM E2142-08: Standard Test Methods for rating and classifying Inclusions in Steel Using the Scanning Electron Microscope (ASTM International, 2011). In addition ISO published a norm for the determination of these inclusions: ISO4967, Steel Determination of Content of Nonmetallic Inclusions—Micrographic Methods Using Standard Diagrams. It gives a methodology to distinguish in a uniform way the quantity of inclusions in a steel sample and consequently assess the suitability of that type of steel for a given use.

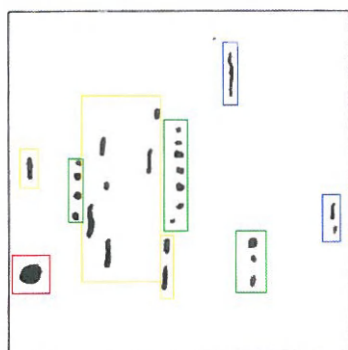
ISO 4967 defines five different groups representing the most common inclusion types. Other, nontraditional inclusions can be compared with the five mentioned above. Every of the five groups is subdivided into two sub-groups to give an impression of the thickness of the inclusion (fine or thick). ISO 4967 gives a series of pictures as a reference for each group.

Identification is done by inclusion form, distribution and dimension. A specific inclusion length refers to a defined index (Table 15).

Table 15: overview inclusions types and appearance (based on ISO 4967, 1998).

Index	Inclusion type				
	A	B	C	D	DS
	sulfate type	aluminate type	silicate type	globular oxide type	single globular type
	Total length μm	Total length μm	Total length μm	Number	Diameter μm
0.5	37	17	18	1	13
1	127	77	76	4	19
1.5	261	184	176	9	27
2	436	342	320	16	38
2.5	649	555	510	25	53
3	898 (<1181)	822 (<1147)	746 (<1029)	36 (49)	76 (<107)
					
	highly malleable, individual grey particles with a wide range of aspect ratios (length/width) and generally rounded ends	numerous non-deformable, angular, low aspect ratio (generally < 3), black or bluish particles (at least three) aligned in the deformation direction	highly malleable, individual black or dark grey particles with a wide range of aspect ratios (generally > 3) and generally sharp ends	non-deformable, angular or circular, low aspect ratio (generally < 3), black or bluish, randomly distributed particles	circular, or nearly circular, single particle with a diameter > 13 mm

When combining all these elements together, for any given sample, the inclusions can be determined in a uniform way (Figure 37).



- : Single Globular type
- : Silicate type
- : Aluminate type
- : Sulfite type

After comparison with the standard figures, following result is obtained for this example: A2,B2,C1,DS2,5.

Figure 37: example determination inclusions,

(Adapted from ISO 4967, 1998).

This can be of use for chemical or statistical description.

4 Metallographic sample testing

4.1 Introduction

The theory explained in the previous chapter is transferred to practical experiments. The samples, used in the experimental set up, described in chapter 5 are analyzed through various methods in order to determine the chemical and metallurgical characteristics. Chemical composition, microstructure and the inclusions of metals can be determined through particular instruments such as a microscope and spectroscope. The samples have to undergo a specific preparation before examination can take place. The methodology and an introduction to the theory behind the measurements is given in this chapter.

4.2 Chemical composition

4.2.1 Atomic emission spectroscopy (AES)

Every element in the steel has its specific use and its presence or absence defines the physical properties of the steel such as tensile strength, ductility or corrosion resistance. It is therefore important to know the exact composition of the studied samples.

To determine the elemental composition of the metal sample, the ARL 4460 Metals analyzer (OCAS, 2011) was used, which is based on Optical Emission Spectroscopy (OES), also called Atomic Emission Spectroscopy (AES). It requires sputtering of the surface and is therefore a destructive method.

Before measurements can take place, all corrosion and other impurities have to be removed from the metal surface by grinding (Figure 38).



Figure 38: sample preparation: A: grinding; B: sample before and after grinding.

In the AES instrument, the sample is positioned close to a metallic pin (often tungsten). High energy sparks are created across an argon-filled void, (Van Lierop, 2007) between

the electrode and the prepared sample's surface. Argon of the highest purity is used because of its inert character. The evaporated and vaporized atoms form a gas cloud.

When (spark) energy is applied on atoms, electrons are promoted to a higher energy level. This energy is re-emitted as electromagnetic radiation, when the electrons return from the higher energy level to a lower one, in the guise of photons¹³. They have an energy content that is equal to the difference between the excited and the ground state of the electron. A prism can be used for the separation of the electromagnetic radiation in its different wavelengths, similar to the diffraction of light into a rainbow. These wavelength bands are also called spectral- or emission lines and they form a defined pattern depending of the atom that produced it. When presented along an increasing frequency line, the atomic emission spectrum is formed (Figure 39).

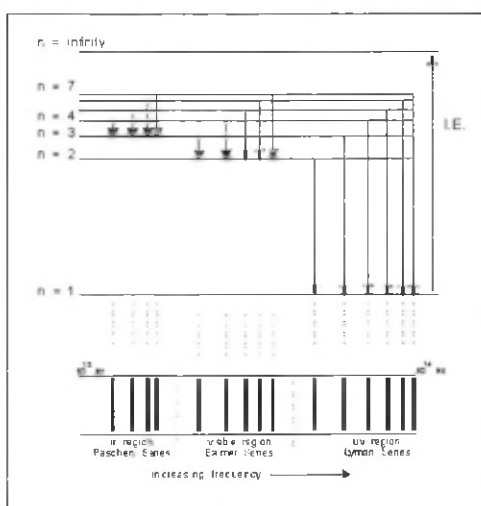


Figure 39: atomic emission spectrum. Electrons promoted to higher energy level (n levels) return to lower level (arrows pointing down), I.E = internal energy. Under: different emission lines shown with increasing frequencies (www.avogadro.co.uk, 2012).

The more intense the emission lines are, the higher the concentration of a specific atom in the sample. The intensity of the line can be compared with standard lines. Thus, the AES can both determine the presence of different atoms in the sample as well as their concentration (Walsh, 1955, Dulski, T.R., 1996).

The resulting spectra contain separate analytical lines with different amounts of light. To separate these lines and to measure the intensities, a set of mirrors, a monochromator (Figure 40) (which separates the different wavelengths through a diffracting grating so

¹³ A photon is the basic unit for electromagnetic radiation.

that each wavelength can be measured by means of one detector) and photomultiplier tubes (to detect the different spectra) are used.

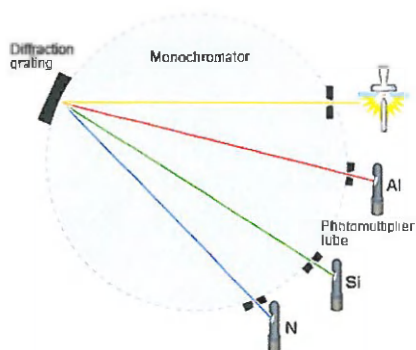


Figure 40: monochromator. Separation of the different wavelengths through diffraction. (Shimadzu, 2012).

The measurement electrode has to be cleaned very thoroughly to avoid contamination with previous samples (Figure 41).

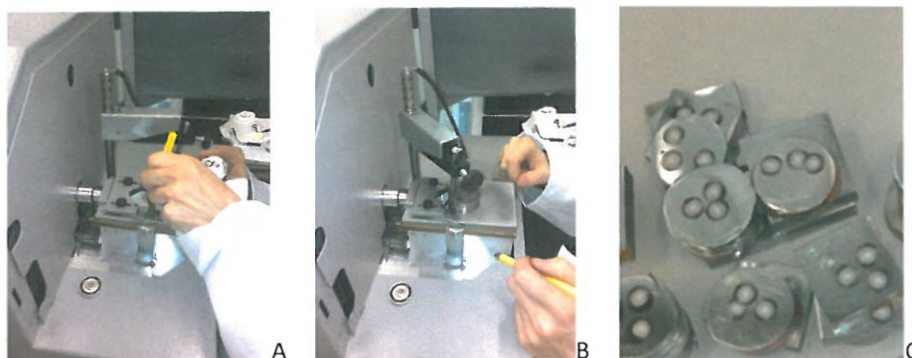


Figure 41: electrode. A: cleaning; B: positioning; C: samples after test

Every sample is analyzed 3 times and the results are averaged. This measurement is destructive, so every time, the position of the sample has to be changed. The ARL 4460 can determine the concentrations of following elements in the steel sample: S, Si, Mn, P, S, Cr, Mo, Ni, V, Al, Cu, Ti, Nb, As, Sn, Co, Pb, B, Sb, Zr, Bi, Ca, Zn, Ce, Fe and Cd.

The complete results are added in Table 18.

4.2.2 Glow discharge optical emission spectroscopy (GD-OES)

For the correct interpretation of the corrosion formation of the CRS steel, additional tests were performed on the specific samples. These included an analysis with the Specturama GDA 750, a glow discharge optical emission spectroscopy (GD-OES) (Figure 42), which is a precise chemical characterization technique for quantitative composition analysis, with element precision in the range of ppm. GD-OES uses glow discharge plasma (ionized gas) to give an impression of the distribution of the elements in the corrosion film or coatings on metallic material. It is possible to analyze the quantitative composition and thickness of coatings or corrosion layers. Depth profiling by GD-OES are obtained by measuring emission intensities during glow discharging without ultra-high vacuum (Suzuki, 2005). Emission intensities are given for constituent elements as a function of sputtering time. The quantitative relationship between the composition and thickness can then be estimated. As with the AES, sputtering is used.

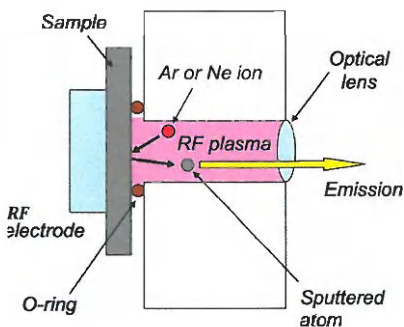


Figure 42: GD-OES principle. Plasma used on sample to obtain emission and identification of the atoms (Hatano, 2012).

4.3 Nonmetallic inclusions

4.3.1 ASTM E45-05

The word inclusions refers to “nonmetallic” inclusions. Inclusions can be defined as foreign material precipitated from the metallic matrix. The particles are usually compounds (such as oxides, sulfides) but can be of any substance that is foreign to and essentially insoluble in the matrix (ASM, 2000). They are also classified as undesired elements in the steel. Elements such as Al, Si, C and T added during steel melting deoxidize the steel by taking oxygen from the iron, transforming it into oxides such as Al_2O_3 . The oxygen is reduced in order to prevent the oxidizing of the steel. As these deoxidizers are only added at the end of the melting process, most of them do not have the time to pass to slag and remain as inclusions in the solid metal. Categorized as an

intruder, they disrupt the homogeneity of structure, so their influence on the mechanical and other properties of the steel can be considerable.

According to the ASTM standard E45-05, determination of inclusions can be done by macroscopic and microscopic methods.

Macroscopic methods (fracture, macro-etch) evaluate larger surface areas than microscopic test methods and because examination is visual or at low magnifications, these methods are best suited for detecting larger inclusions. Macroscopic methods are not suitable for detecting inclusions smaller than about 0.40mm in length and the methods do not discriminate inclusions by type.

Microscopic test methods give a more detailed impression of the size, number and distribution of the inclusions and are applied on a polished surface under a microscope. To allow uniform reporting of the samples, standard reference charts are developed for comparison. Microscopic determination is used to identify (very small) individual inclusions. An important disadvantage of these microscopic methods is that the small investigated surface is supposed to be representative for a much larger surface area. For large structures, it is necessary to repeat these tests in order to have a realistic and scientific correct result, as the inclusions are not necessarily uniformly distributed throughout the steel. The possibility of a sample at the edges of the Gauss curve cannot be ignored.

4.3.2 Scanning electron microscope (SEM)

Electron microscopy uses electrons instead of light to visualize the surface of a sample. The electrons have a smaller wavelength than light photons and so the resolution of an electron microscope can be much higher than that of a light microscope (0.1µm to 200nm).

Thermal energy is applied to a filament (usually made of tungsten, which has a high melting point) to "shoot" electrons away from the "electron gun" toward the specimen under examination (Figure 43). As the electron beam traces over the object, it interacts with the surface of the object, dislodging secondary electrons from the surface, reflecting electrons on the surface (backscattered electrons) and emitting X-rays. Dot by dot, row by row, an image of the original object is "scanned" onto a monitor for viewing.

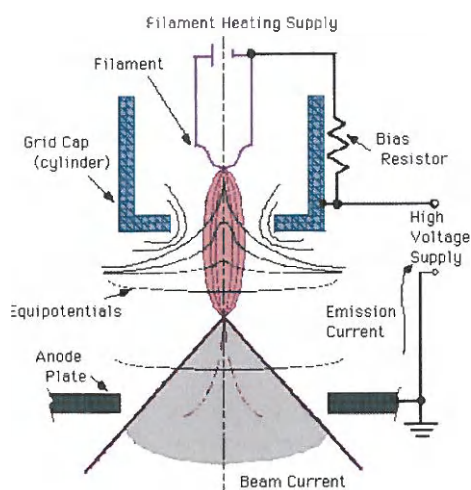


Figure 43: Electron microscope source. Specimen is scanned with thermal energy (Iowa State University, 2012).

The electron beam passes through a vacuum to maintain its stability. If not, gases can hinder the electrons or react with them, causing random discharge. The gas molecules can condensate on the sample, lowering the contrast and obscure detail in the image.

An EDX (Energy-dispersive X-ray) detector is used to separate the X-rays of different elements into an energy spectrum. When the specimen is bombarded with an electron beam inside the SEM, the atoms are excited. As they relax to their stable ground states, they emit their characteristic patterns of X-rays. Every element releases X-rays with unique amounts of energy during the transfer process. Thus, by measuring the amounts of energy present in the X-rays being released by a specimen during electron beam bombardment, the identity of the atom from which the X-ray was emitted can be established (Brown, 2009). X-ray energies are directly related to the atomic structure of the substances that emit them. EDX can be used to determine the elemental or oxide composition of the material.

4.3.3 Testing

Before inclusions in the metal can be determined, a lot of pre-processing is compulsory. Only very small samples are needed. At OCAS, the samples are machined with a Servocut A 300 and subsequently embedded in grey and pink Durofast using the Struers Citopress 20. To avoid mixing-up the samples are engraved with a unique sample number. Further the specimens are ground to a roughness of 100 μm and subsequently 50 μm . Afterwards they are cleaned with water and pressurized air.

The last step to make the inclusions visible is a three step polishing (Largo, DAC and NAP) of the sample with the Rotoforce-4. The metal is cleaned with methanol and special cloths, to avoid scratching and contamination of the surface.

The small inclusions are studied with a Jeol JSM6490LV Scanning Electron microscope (SEM) and identified with an Energy dispersive X-ray (EDX) detector.

Every sample was 100 times enlarged. Only when interpretation of the inclusions was difficult, a larger scale was used. Two types of inclusions were discovered in the samples investigated: globular (ex. aluminum oxide) and elongated (ex. manganese sulfide), both single and in line. An indication letter was given to each type of inclusion. Figure 44 shows an example of each type of inclusion encountered during this study.

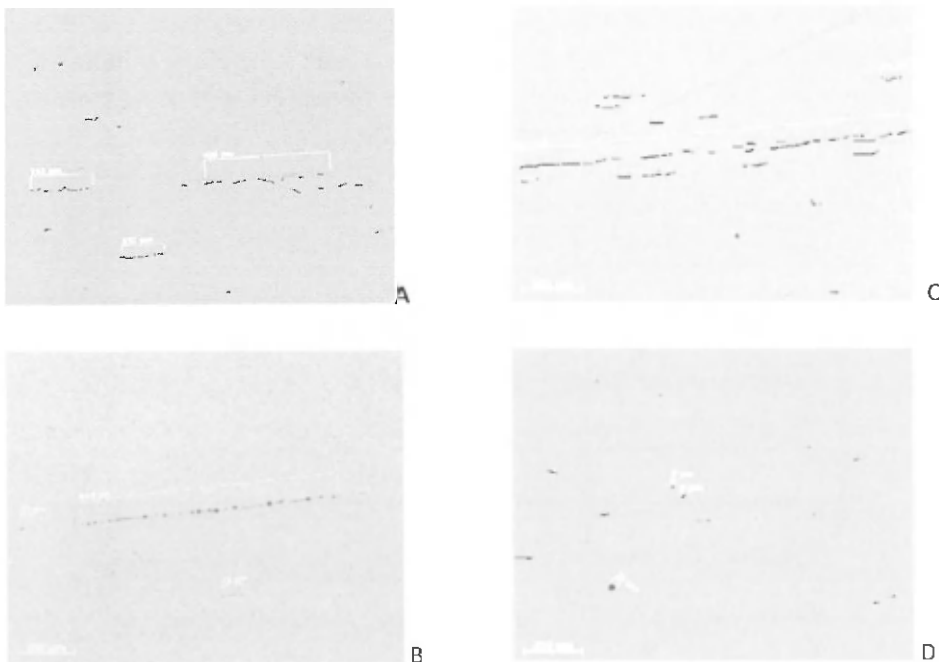


Figure 44: different types of inclusions found in studied steel samples: A = _____ = manganese sulfide, single; B = = aluminum oxides, line; C = _____ = manganese sulfide, line; D = . = aluminum oxide, single.

To have an idea of the amount of inclusions in the steel, for each sample, the most contaminated area was visually selected and measured. For every type of inclusion, the largest 3 were considered. The amount of the specific inclusions was noted, as well as the maximum dimension, measured in μm . Then, these figures were multiplied and added to each other. The result gives an impression of the purity of the sample. Large variations between the different samples were noted.

4.4 Phase analysis

X-Ray powder Diffraction (XRD) is a method to identify the crystalline compounds or phases in the sample. This technique is complementary to EDX. EDX can show us the amount of FeOOH in the sample, but the XRD gives extra information and discriminates between α -FeOOH (goethite), β -FeOOH (akaganeite), γ -FeOOH (lepidocrocite), and δ -FeOOH (feroxyhyte). For the extra measurements on the CRS steel, the Bruker D8 Discover was used.

XRD uses x-rays of one single wavelength. The x-rays are reflected on the sample surface by the very small crystals in the sample. The single wavelength is split on the sample into several beams under different angles to the sample. The detector is placed around the sample and while the sample rotates, it registers the position and strength of these beams. The data is plotted as strength (intensity) vs. position (angle Θ) and results in a diffraction pattern. As each chemical compound has a unique diffraction pattern, which is compared to a database of patterns to find the corresponding phases (Kamimura, 2005) (Figure 45).

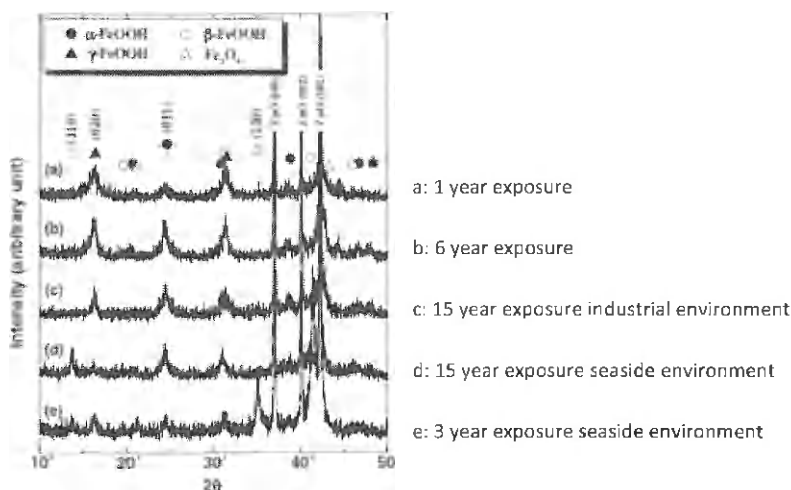


Figure 45: XRD diffraction pattern on weathering steel after different exposure periods (1, 3, 6 and 15 years) (Kamimura, 2005).

4.5 Microstructure

The microstructure of steel is the key to its behavior, because the crystal structure, size, carbon content and arrangement of the micro constituents (BCC ferrite, FCC austenite, orthorhombic cementite, etc.) determine its properties (Langford, 2005). To reveal the microstructure the sample is polished again (NAP) and etched with Nital 4% (4% nitric acid in methanol) during 15 seconds and dried with compressed air. An inverted optical microscope for metallography, enlarging 100 and 500 times gives clear indication of ferrite, pearlite and bainite grains in the metal, as with the etching, the grain boundaries become visible.

Four pictures are taken from every sample: Center and side of the sample, both 100 times and 500 times enlarged (Figure 46).

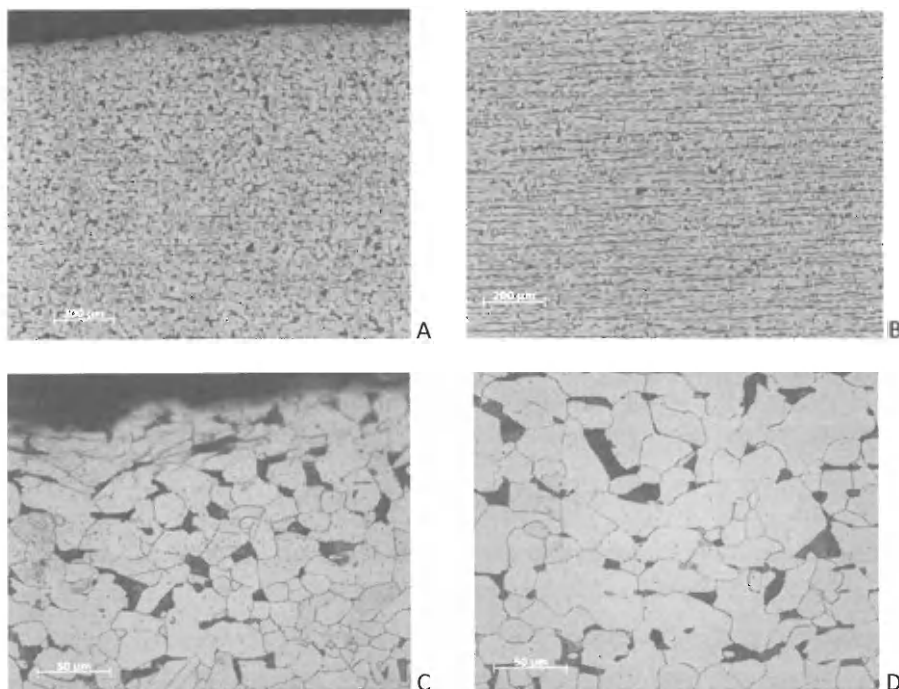


Figure 46: SEM microstructure steel sample images. A: side, 100 enlarged; B: Center, 100 times enlarged; C: Side, 500 times enlarged; D: Center, 500 times enlarged.

The interpretation of the microstructure was done by a metal specialist of OCAS, Zelzate. Digital Image Processing Software program Axiovision of Zeiss determined the concentrations of the different phases, such as ferrite and pearlite, visible on the pictures hereunder.



Figure 47: SEM image 100% ferrite.

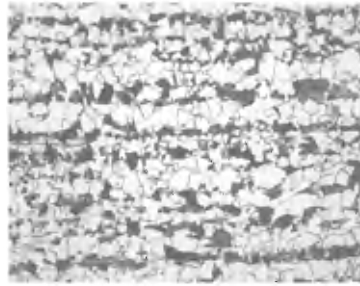
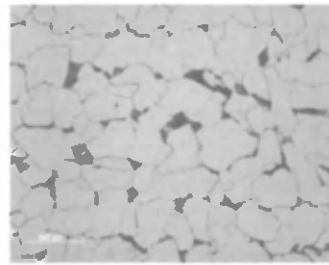


Figure 48: SEM image ferrite-pearlite structure.

Figure 47 shows a 100% ferrite structure, no black grains are visible. Figure 48 gives an impression of a ferrite-pearlite structure, this specific example having 21% of pearlite (black parts). Pearlite is composed out of subsequent layers of ferrite and cementite and this is reflected as dark grains under the microscope. A number of samples have a layered structure. Figure 49 A shows a layered structure, B has no layers.



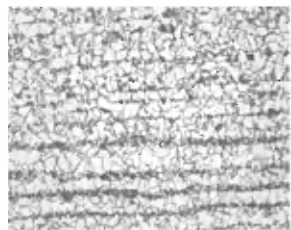
A



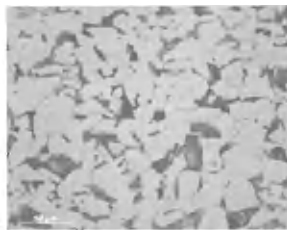
B

Figure 49: SEM images showing microstructure: A: layered structure; B: non layered structure.

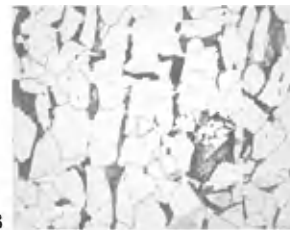
The size of the grains was also determined through visual interpretation of the pictures at first sight. This means that the most occurring grain size is considered. It was decided to generate three categories: small, medium and large grains (Figure 50).



A



B



C

Figure 50: SEM images showing grain size: A: small grain size $<20\mu\text{m}$; B: medium grain size between $20\mu\text{m}$ and $30\mu\text{m}$; C: large grain size $>30\mu\text{m}$.

Small grains are grains $<20\mu\text{m}$, large grains are $>30\mu\text{m}$ and medium are consequently those in between. The results of this interpretation are also incorporated in Table 18.

5 Experimental set up at the Antwerp Maritime Academy

5.1 Introduction

Many laboratory studies examine the corrosion rate of steel, also ship construction steel. One of the major disadvantages of these studies is the theoretical way all these experiments are performed, using new, clean, perfect steel plates. Our experiments start from reality: steel plates collected out of the hull plating of existing ships resulting in “what is” and not in “what could be”.

5.2 Sample collection

For these experiments, 40 steel plates (approx. 30 x 50cm) out of the ballast tank construction were collected from ships performing steel repair work in dry dock. No selection criteria were set and the samples were gathered upon arising opportunities. Experimental corrosion resistant steel was received from Korean steel mill POSCO. It was decided to add this CRS steel 2 times into the test set-up, to allow comparison.

5.3 Sample preparation

Every steel plate had to be cut into small pieces. At first, Antwerp Ship Repair promised its cooperation and cut square samples (side length 5 cm) out of the plates. This was too time consuming and interfering with commercial activities, so after a few samples, an alternative had to be found. Dredging company DEME was so kind to open up their workshop and tools at Zeebrugge for the remaining work, resulting in round samples with a diameter of 5cm. Out of every steel plate, 13 samples were cut, serving for different measurements (see 5.4). A unique code (steel plate name-sample number), was hammered into the metal and written on the side (Figure 51). Samples were sandblasted to SA 2.5 and degreased with methanol.

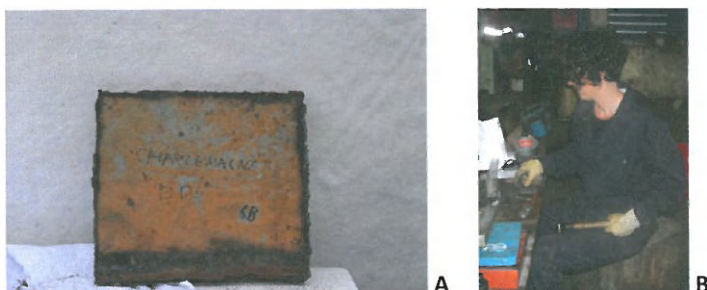


Figure 51: A: steel plate example approximately 50x60cm, B: sample preparation DEME Zeebrugge.

Steel plate identification: number from 1 to 32, in some occasions, a letter was added, when several plates were collected out of the same ship (ex 29A, 29B).

5.4 Sample number

A first set of four samples (1.1-1.4) was prepared for electrochemical measurement (see 5.6) at different time intervals: at the beginning, after 6, 12 and 18 months exposure to seawater.

Next, one sample (2.1) was destined for metallurgic tests, performed at OCAS, following the procedures explained in Chapter 4.

A second set of four samples (3.1- 3.4) was used for weight loss measurement (see 5.7) at different time intervals: 6 months, 10 months, 20 months, 24 months complete immersion. Samples that were weight-measured after 6 months immersion were then put into the spray tank (4/24) and weighted again after 6 months.

A third set of four samples (4.1-4.4) was destined for photographic analysis (see 5.9) and ultrasonic thickness measurement (see 5.8). To allow for ultrasonic thickness measurement, the samples were painted at 1 side. Photos were taken daily during the first month and for 3 different conditions: dry environment, wet-dry condition (spray tank with 4 hours spray each day) and wet condition (continuous immersion in seawater).

The samples were arranged per number and per purpose in separate permeable cases and placed in the cube tanks 1, 2 and 3 of the test facility (Figure 52).

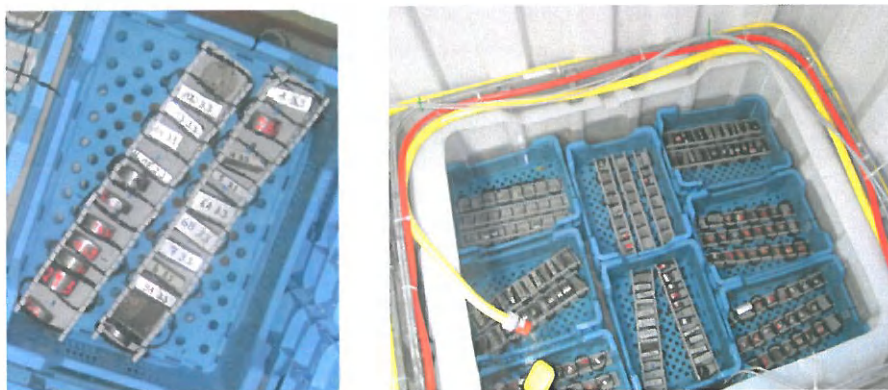


Figure 52: experimental set-up: sample numbering and positioning in cube container.

5.5 Test facility

A test facility was built from scratch at the Antwerp Maritime Academy, starting from a standard 20 feet freight container. Inside this container, two compartments were constructed. The first served as a laboratory; the second part contained the samples in three cube tanks (Figure 53).

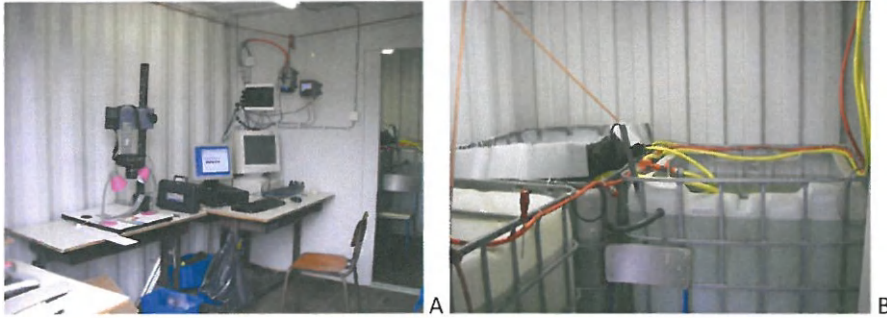


Figure 53: test facility at Antwerp Maritime Academy. A: laboratory, B: compartment with cube containers.

A large 25m^3 tank was filled with natural North Sea water, pumped out of the fore peak tank of a dredging vessel (Figure 54). This water had a salinity of 34 promille (MUMM, 2011).

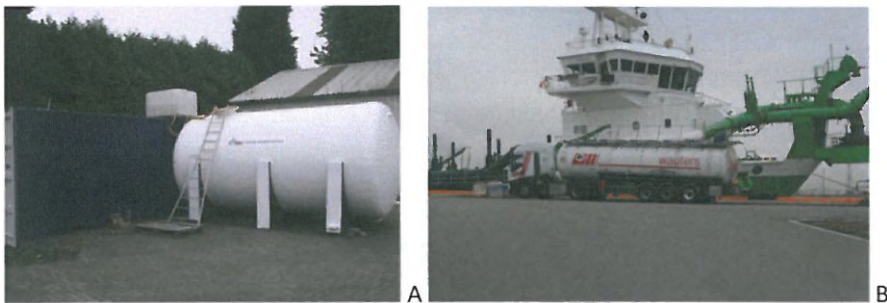


Figure 54: test facility at Antwerp Maritime Academy. A: 25m^3 tank with seawater, B: collecting seawater at vessel (8/3/2010).

From the 25m^3 seawater tank, the seawater circulated into the three cube containers. Two containers held samples that are always submerged. The third one was equipped with a spray installation for the simulation of a wet/dry tank condition (Figure 55).



GENERAL ARRANGEMENT

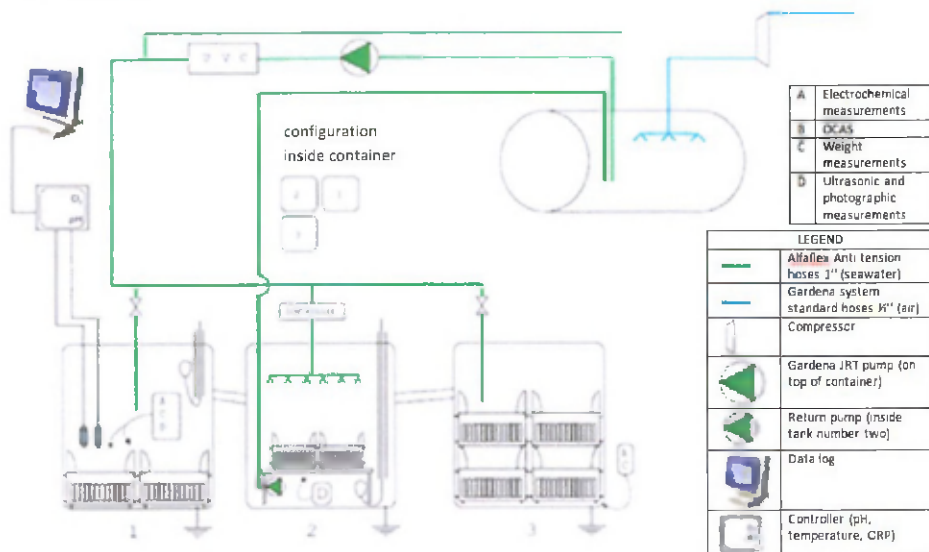


Figure 55: schematic overview of the test facility with 25m² seawater tank, 1 and 3 are cube container with permanent immersion, 2 is a cube container with spray system. Water circulating, passing through UVC lamp to kill organisms. Constant measurement of pH, oxygen concentration in ppm and temperature in °C.

In container nr 1, the dissolved oxygen (DO) content was measured continuously with a Hach Lange 5740 DOB.99 sensor (Germany) and maintained at approximately 10ppm (variations between 7.08ppm and 12.8ppm) by means of an air pump. Temperature and pH were monitored as well, with a Hach Lange DPD 1R1.99 sensor (Germany). The temperature is dependent to seasonal changes, as it is on board. Throughout the experiment, the temperature of the water varied between -1°C and +24.4°C. The pH is not artificially altered and varied between 7.8 and 9. All data originating from those sensors were checked on a regular basis and are kept for future reference.

After passage in the cube containers, the water was returned to the sea water storage tank. To prevent unwanted growth of micro-organisms and algae, a UVC filter was installed within the water flow.

The experimental set up encountered some problems in the start-up period. After a few days immersion, the samples showed some bluish areas, which were later identified as traces of cutting oil, influencing the corrosion pattern. All preparatory work had to be repeated, resulting in a delay of a month.

5.6 Electrochemical measurements

Electrochemical methods are only suitable for reactions of electrochemical nature, thus for corrosion of metals in an electrolyte. The main characteristics of corrosion are electrode potential, electric current and electric resistance. This was explained in chapter 2.

Electrochemical methods allow for real time measurement, and so changes in the environment and corrosion rate can be followed. Several electrochemical measurement techniques are used in laboratories and in the industry. Amongst them are the measurement of REDOX potentials (ORP) and the linear polarization resistance (LPR). Also frequently used is the electrochemical impedance spectroscopy (EIS). For our experiments, LPR and the Tafel method were selected. The results were used as a reference value to benchmark the results from the weight loss method.

Before testing, sample preparation was necessary. Corrosion was removed from the surface and the samples were hand dried. An Ag/AgCl electrode in saturated KCl-AgCl solution was used as a reference electrode. The counter electrode was composed out of platinum. The seawater solution had a pH of 7.8. A VersaSTAT 3 potentiostat (Princeton Applies Research, USA) was connected to the computer and controlled by software VersaStudio (Figure 56).

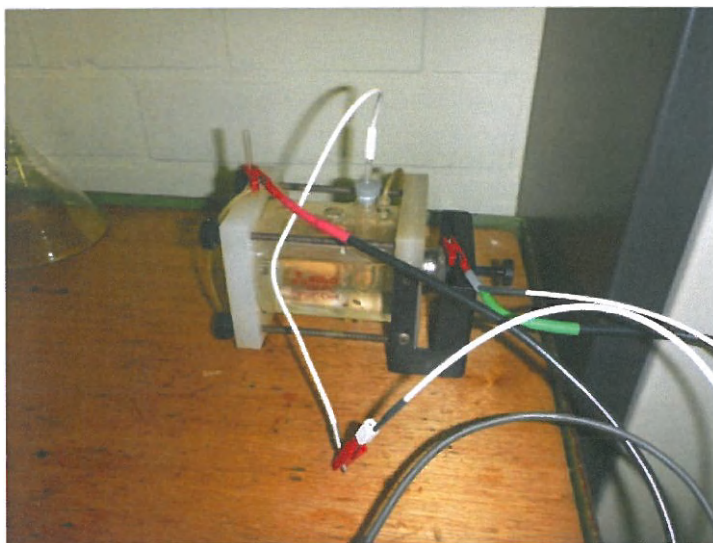


Figure 56: electrochemical measurement set up. Green is working electrode (sample), red is counter electrode (platinum), white is reference electrode (Ag/AgCl).

5.6.1 Determination of the equilibrium potential E_{eq}

Initially, the equilibrium potential (E_{eq}) (also referred to as the open circuit potential OCP) of the working electrode (our steel sample after grinding) was measured during a period of two hours and plotted on a graph. This equilibrium potential was found by adding the measured potential to the potential of the reference electrode (Ag/AgCl with E_{eq} of 197mV) (Figure 57, Figure 58):

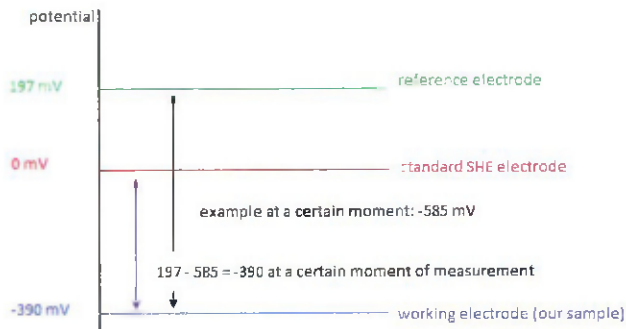


Figure 57: potential measurement principle at certain time. Potential of working electrode related to reference electrode (197mV)

During the measurement (Figure 57, Figure 58), the measured potential drops towards -617 mV as a thin corrosion layer is formed. The objective, the equilibrium potential (E_{eq}) is never reached with ordinary steel, as the corrosion continues.

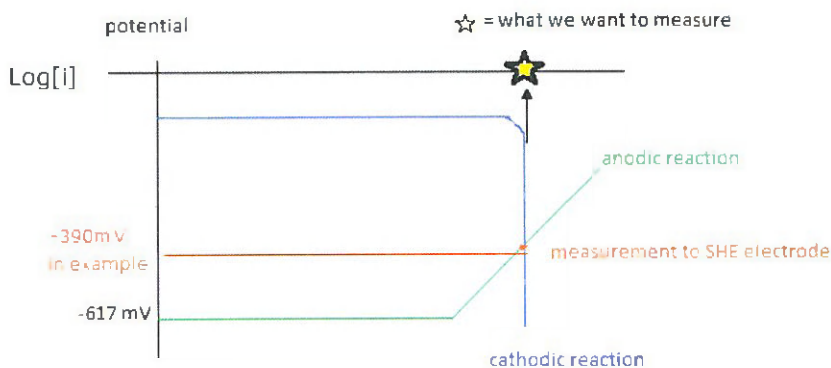


Figure 58: potential measurement principle. Current related to potential.

-617mV is the equilibrium potential for the reaction $\text{Fe} \Rightarrow \text{Fe}^{2+} + 2\text{e}^-$.

The corrosion rate is proportional to the difference between the measured potential (V) and the potential at equilibrium (E_{eq}). The following graph represents the measured potential (V) at a given moment in function of the elapsed time (s). Attention must be given to the very small scale on the Y-axis (Figure 59). This enlargement is only given to demonstrate the descending curve. At larger scale, the line would appear horizontal.

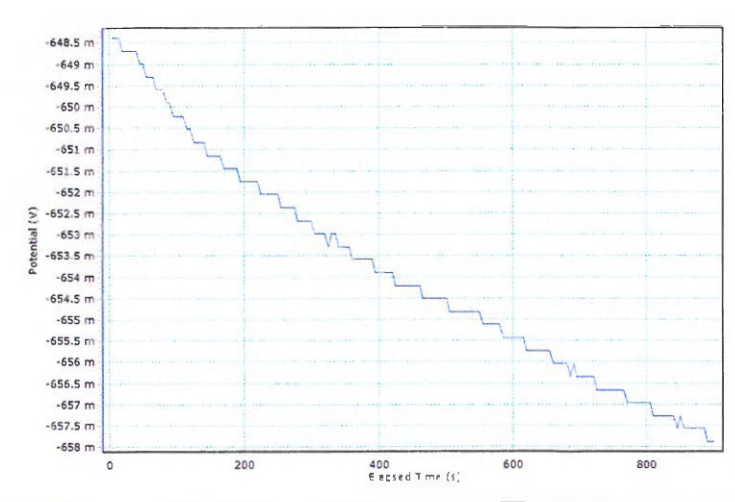


Figure 59: potential measurement (mV) at a given time with respect to reference electrode (197mV).

LPR and Tafel were determined according the methodology explained in chapter 2.

5.7 Weight loss method

This method is very simple. A sample is weighed before it comes into contact with its environment. After a defined immersion period T , depending on the steel type and the environmental conditions the corrosion products are removed with an etching agent and the bare steel is weighed again. The weight loss is an indication of the corrosion rate, usually expressed in mm/year (Groysman, 2010).

The weight loss is related to the exposed surface area. To allow comparison of the steel samples, the weight loss has to be divided by the exposed surface area.

$$k = \frac{M_i - M_f}{A \cdot T} \quad \text{Eq. 45}$$

where k is the corrosion rate in $\text{g}/(\text{cm}^2 \cdot \text{hours})$, M_i and M_f the initial and the final mass in (gram), A the surface in cm^2 and T the immersion period, hours.

Using this equation, the corrosion rate for a given period can be calculated into thickness loss.

$$k_p = \frac{k \cdot 10 \cdot 8760}{d} \quad \text{Eq. 46}$$

K_p is the metal loss in mm year^{-1} , d the density of the metal in kg m^{-3} , 10 is the conversion from cm into mm, 8760 is the conversion from days into years.

Although being a very simple method, some limitations can be found. A considerable time is needed for accurate measurement. On-line, real time monitoring is not possible. This method gives a general indication concerning the corrosion rate and does not reflect eventual change in environmental conditions during the test period.

At the beginning of the experiment, the samples were sandblasted to SA2.5 to remove all corrosion traces. Then, the initial weight was measured with a precision of 0.01g (Kern, PLE3100-2W, Germany). As the corrosion rate is function of the exposed surface, the precise dimensions were set with a caliper.

The samples were completely immersed in the seawater container and lifted after 6, 10, 20 and 24 months. Another set was put in a spray tank (4 hours spray per day) and taken out after 6 months.

They were etched for minimum 10 minutes with a mixture of 20 g Sb_2O_3 and 60 g Sn_2Cl in 1L 37% HCl. This method removes all of the corrosion products and allows an accurate mass loss measurement solely based on the weight of the remaining steel. After drying, the new weight and dimensions were noted (Figure 60).

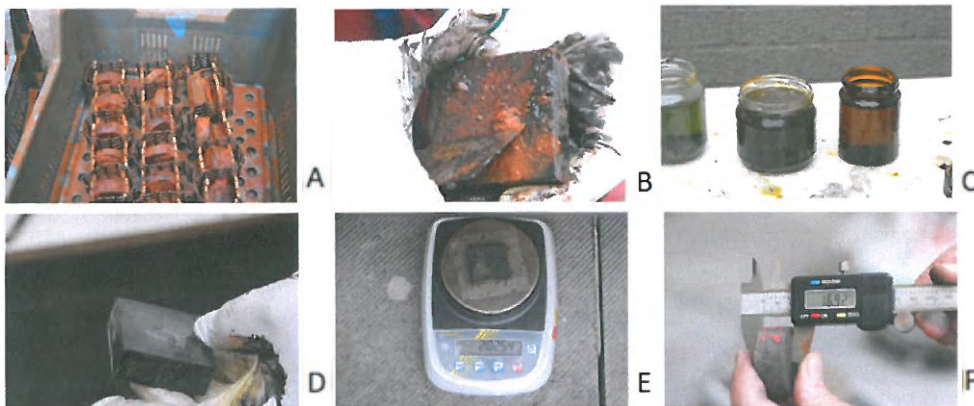


Figure 60: weight measurement procedure. A: samples after 2 years immersion; B: rust scraping; C: etching of samples; D: sample after etching; E: weight measurement; F: measurement of dimensions with caliper.

These various time intervals allow for multiple interpretations. It is possible to evaluate whether corrosion occurs in a linear way or whether passivation starts after a defined time interval. The results of these measurements can be found in chapter 6.

5.8 Ultrasonic measurement

Ultrasonic thickness measurement is a simple non-destructive test, commonly used for the investigation of the structural integrity of ships (IMO, 1993). During ultrasonic measurement, high frequency energy is used on materials such as metal, ceramics and hard plastics to gather information such as the plate thickness. The energy is produced as a wave and travels through the material as it vibrates the individual atoms and can be reflected, diffracted and focused as can be with light waves.

Attempts were made to measure the loss of sample thickness with an Electroline TI-25M Ultrasonic Thickness Gauge (United Kingdom). Practical experience learned that the obtained values were highly influenced by the exact position of the transducer due to the surface roughness of the material, leading to an overall sample variation which was too large to allow any significant relation. No other parameters were found useful to supplement the assessments made of corrosion rates made through thickness measurements. This method was considered to be inappropriate for the objectives put forward in this research and the obtained results were discarded.

5.9 Photographical measurement

Corrosion at the metal surface is composed out of different oxides and hydroxides, all with their specific color. We assumed that the color change at the surface of the metal in function of the time would be a measure for the change in chemical composition of the corroded surface and would give an insight into the evolution of the corrosion at the initial phase. New, non-corroded steel has a grey, silver like color. As soon as corrosion starts, brown, black, red and orange colors appear at the surface. Every corrosion product has its own specific color, from almost black for FeO to red for Fe_2O_3 .

For this experiment, a set of samples was placed in the seawater container and lifted every day for 2 weeks (Figure 61). Each time, a RAW, 12 bits photo was taken with a Nikon D200, an AF Micro Nikkor 60mm 1/2.8 lens and software "Nikon Capture 4". This was done under standardized conditions (Exposure mode: aperture priority F29 shutter time 1/1.3, sensitivity ISO 100, white balance preset, SRGB color mode, auto tone composition & saturation sharpening, Hue adjustment 0°).

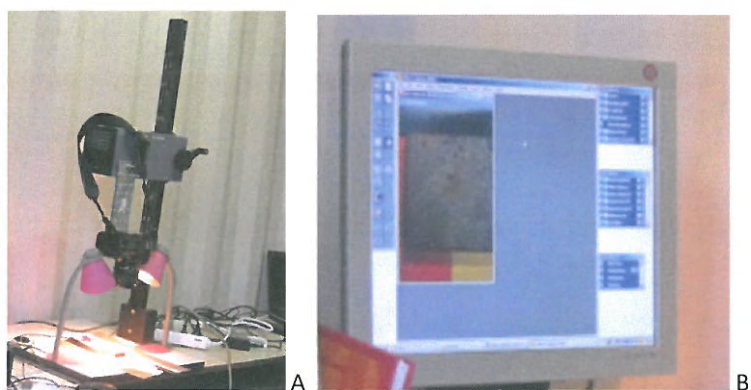


Figure 61: photographic measurement set up at Antwerp Maritime Academy.

After 2 weeks, the frequency of recording dropped to 2 times a week and after a month, the test was stopped as no further changes to the surface were apparent (Figure 62).

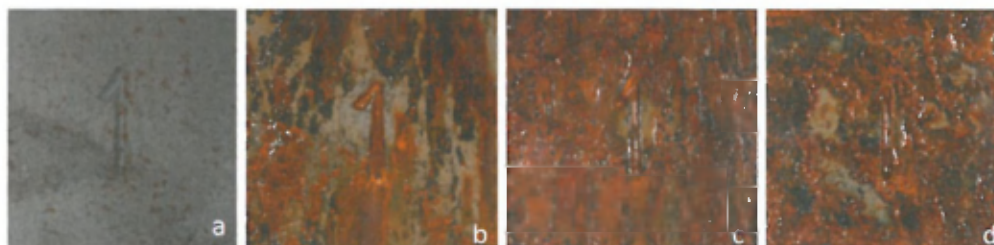


Figure 62: photos of same sample after different periods of immersion; a: start of experiment, b: 1 day, c: 7 days, d: 31 days.

The results of these experiments are not incorporated in this work.

6 Impact of ship construction steel properties on ballast tank corrosion rate

6.1 Introduction

One of the major parameters that define the useful lifetime of a ship is the condition of the ballast tanks. Understanding the complex combination of factors that determine the progression of corrosion in these crucial compartments of a ship's hull is therefore paramount to the prolongation of the life of a merchant vessel, and to an improved return on investment for the ship owner.

Therefore, different corrosion models, based on laboratory experiments as well as on in situ observations (Paik, 2004, Qin, 2003, Verstraelen, 2009, De Baere, 2010), study the relationship between corrosion and age of the vessel (Verstraelen, 2009, Paik, 2002), cathodic protection (Pedferri, 1996, Roberge, 2000) and many other parameters (De Baere, 2010, Gardiner, 2003, Soares, 2009). Up until now, however, only little attention was given to chemical, physical and mechanical properties of ship construction steel and its relation to the corrosion process.

As in many other regards, classification societies play a key role in the construction of ships when it comes to steel. In their "Rules and regulations" the class societies put forward a minimum set of requirements for the ship construction steel to be used (DNV, 2012, ABS, 2012). The steel may only be produced in class approved facilities and during production an analysis of the material and prescribed tests of the rolled metal are required.

Ship classification societies have varying specifications for steel. In 1959, the major societies agreed to standardize their requirements. There are now five different grades of steel (grades A to E) which are employed in merchant ship construction and referred to as International Association of Classification Societies (IACS) steels. Grade A steel consists of the ordinary mild steel as defined in the Lloyds Register requirements, which is commonly used in ship building. Grade B is a better quality mild steel than grade A and specified for use in locations where thicker plates are required, in more critical regions. Grade C, D and E possess increasing notch-tough characteristics (Eyres, 2007).

Table 16 provides a cross reference between the abbreviations used by the class societies and the ASTM A 131 standard (ASTM, 2008).

sacrificial anodes. Coating maintenance in ballast tanks is very difficult and the use of corrosion resistant material could reduce the need for expensive initial coating application, maintenance and reapplication. This would reduce construction time and dry-dock time significantly, entailing an important economic advantage (De Baere, 2012).

The most obvious material selection for use in ballast tanks would be Corten steel. However, the chlorides in the seawater destroy the protective passivation layer.

The seawater corrosion resistance was improved by increasing the concentration of Mn, Cr, Ni and Al. Examples of such an alloy are the Marin 400, 490 & 490Y produced by JFE Steel Cooperation (JFE, 2012). With the help of ABS, American Bureau of Shipping we obtained a sample of experimental Korean corrosion resistant steel (CRS) especially developed for use in ballast tanks. The chemical analysis of the corrosion resistant steel sample in our possession (Table 18) indicated that this steel has been developed in the same line of thinking.

The existence of the ASTM A 131 & IACS standards should imply that the steel used at the different ship construction yards all over the world is uniform and of the same composition. Although the steel plates are verified by the class societies from the furnace till the effective use and every steel plate needs a certificate before it can be used for shipbuilding, non-conform steel is still employed (Van Der Stichelen, 2012).

There is more to steel quality and corrosion resistance than just the composition of the steel. For example, the corrosion rate of carbon steels can be influenced by its microstructure (Perez, 1996, Videm, 1996, Asahi, 1999, Lopez, 2003). Indeed, the compositional and micro structural properties can vary significantly between products of the same grade from different manufacturers and these variations may lead to substantial differences in the corrosion resistance of the steel (Clover, 2005).

It is therefore the aim of this chapter to develop a new strategy to analyze the impact of steel composition and structure on the rate of corrosion. By starting from effectively used plates cut out of ballast tanks of merchant vessels, we try to cover at least part of the variability encountered in the real merchant fleet. This variability requires to be analyzed with multivariate statistical techniques. In addition, test conditions were created similar or close to those encountered at sea (eg, through the use of natural sea water, or by simulating the alternation of wet and dry periods in a ballast tank). As such, it is our aim to provide a set of results which is complementary with more conventional lab results. Therefore, a set of tests were performed at the AMA as described in chapter 5.

6.2 Results & discussion

6.2.1 Exploratory data analysis

The data on the composition of the steel samples show a large variability. The presence of outliers in almost all components requires the use of robust methods in order to avoid a bias due to the extreme values of the composition components. The known division into grades of steel samples is recovered by a cluster analysis using the Manhattan distance (Perlibakas, 2004) between the composition components. This distance is better protected against outliers than the Euclidean distance.

A robust principal component analysis based on an algorithm of Croux (Croux, 2005) is used in order to incorporate the principal parts of the variations in composition into two independent components. The main idea is to use the median instead of the mean as a location parameter. The median is the common name for the 1/2 quantile. In order to be consistent in the data analysis we used quantile regression (Koenker, 2001) to relate the weight loss with the composition. We performed this analysis using at most two independent PCA components. The calculations are done using the statistical computing language R (R development Core Team, 2011) (and its three packages 'cluster' (Rousseeuw, 2012) 'pcaPP' (Filzmoser, 2012) and 'quantreg' (Koenker, 2012)).

6.2.2 Statistical interpretation

The database used for statistical interpretation consisted of the chemical composition per sample, the quantity of enclosures, an evaluation of the extent of the ferrite, pearlite or bainite structure, and finally the corrosion rate in $\text{g m}^{-2} \text{year}^{-1}$, determined by way of the weight loss method, after 6 months of exposure to the conditions in the tank. An overview per sample is presented in Table 18.

Table 18: Overview of the steel composition and structure in the different steel samples.
Division in three cluster. Average per cluster given, as well as standard deviation per element.

Cluster	Nr.	Chemical Analysis										Layers		Weight Loss g m ⁻² year ⁻¹	Grain size in µ
		C	Si	Mn	P	S	Cr	Mo	Ni	Al	Cu	Layers	% 2 nd ph.		
1	7	0.07	0.21	0.88	0.01	0.00	2.11	0.59	0.00	0.99	0.00	Yes	21.00	351.30	25
	32	0.03	0.21	0.89	0.01	0.00	2.09	0.59	0.00	1.02	0.00	Yes	24.00	401.48	15
	average	0.05	0.21	0.885	0.01	0	2.10	0.590	0	1.005	0	Yes	22.5	376	20
	SD ±	0.02	0.00	0.005	0.00	0	0.01	0.00	0	0.015	0		1.5	25	5
2	12	0.13	0.37	1.36	0.01	0.00	0.01	0.00	0.01	0.03	0.01	Yes	24.00	443.60	5
	28A	0.10	0.45	1.49	0.01	0.00	0.02	0.00	0.03	0.04	0.02	Yes	20.00	451.67	5
	20	0.14	0.41	1.41	0.02	0.02	0.01	0.01	0.01	0.02	0.01	Yes	24.00	468.63	5
	21	0.11	0.30	1.29	0.02	0.01	0.02	0.01	0.06	0.00	0.19	Yes	19.00	471.84	40
	17	0.19	0.36	1.25	0.02	0.03	0.07	0.01	0.08	0.00	0.25	Yes	34.00	493.59	10
	29B	0.13	0.37	1.28	0.01	0.01	0.08	0.02	0.06	0.03	0.08	Yes	21.00	583.74	10
	28B	0.09	0.44	1.49	0.01	0.00	0.02	0.00	0.03	0.03	0.02	Yes	20.00	590.27	5
	30	0.17	0.44	1.26	0.01	0.01	0.06	0.03	0.14	0.03	0.28	Yes	20.00	607.33	10
	23	0.19	0.46	1.31	0.02	0.03	0.04	0.00	0.04	0.03	0.06	Yes	30.00	612.38	10
	18	0.15	0.44	1.33	0.01	0.00	0.05	0.01	0.05	0.02	0.16	Yes	22.00	621.76	10
	average	0.140	0.404	1.347	0.014	0.011	0.036	0.009	0.051	0.023	0.11	Yes	23.4	534	11
	SD ±	0.011	0.016	0.028	0.002	0.003	0.008	0.003	0.012	0.004	0.03		1.6	23	3
3	1	0.13	0.22	0.59	0.02	0.02	0.02	0.00	0.01	0.01	0.01	Yes	12.00	396.44	50
	2	0.14	0.24	0.67	0.01	0.01	0.04	0.00	0.02	0.03	0.04	Yes	16.00	463.16	15
	3	0.16	0.07	0.82	0.02	0.01	0.03	0.00	0.02	0.00	0.02	No	21.00	509.30	25
	4	0.08	0.25	0.94	0.03	0.02	0.04	0.00	0.06	0.04	0.08	No	7.00	454.72	50
	5	0.10	0.22	0.58	0.03	0.02	0.03	0.00	0.02	0.04	0.03	No	6.00	380.92	50
	8	0.19	0.25	0.57	0.01	0.02	0.03	0.00	0.03	0.03	0.03	Yes	17.00	584.85	30
	10	0.15	0.13	0.67	0.02	0.01	0.01	0.00	0.01	0.05	0.01	Yes	13.00	592.96	25
	11	0.06	0.26	0.43	0.01	0.01	0.06	0.04	0.14	0.00	0.17	No	4.00	557.03	20
	13	0.13	0.18	0.83	0.01	0.00	0.02	0.00	0.03	0.03	0.01	Yes	12.00	461.07	30
	14	0.15	0.22	1.06	0.03	0.00	0.03	0.00	0.01	0.03	0.02	Yes	23.00	425.34	10
	15	0.05	0.25	0.42	0.01	0.01	0.07	0.03	0.13	0.00	0.30	No	1.00	572.06	25
	16	0.19	0.02	0.82	0.03	0.01	0.02	0.00	0.01	0.00	0.01	Yes	14.00	570.44	40
	19	0.18	0.05	0.77	0.02	0.01	0.03	0.00	0.02	0.00	0.02	Yes	20.00	421.87	50
	22	0.07	0.26	0.92	0.02	0.01	0.02	0.00	0.04	0.01	0.02	No	0.00	447.85	5
	24	0.08	0.21	0.87	0.01	0.01	0.04	0.01	0.04	0.03	0.04	Yes	9.00	598.60	25
	31	0.15	0.20	0.74	0.01	0.01	0.02	0.01	0.03	0.03	0.01	No	21.00	579.28	40
	25A	0.19	0.34	0.80	0.01	0.01	0.02	0.00	0.02	0.03	0.01	Yes	18.00	549.52	15
	25B	0.15	0.29	0.79	0.01	0.01	0.02	0.00	0.02	0.00	0.01	Yes	19.00	581.03	20
	25C	0.14	0.24	0.79	0.02	0.01	0.03	0.01	0.02	0.02	0.01	Yes	16.00	580.66	10

Cluster	Nr.	Chemical Analysis										Layers		Weight Loss	Grains
3	26A	0.09	0.26	0.58	0.03	0.02	0.01	0.00	0.01	0.00	0.02	No	11.00	560.16	25
	26B	0.11	0.14	0.86	0.02	0.01	0.01	0.00	0.01	0.00	0.01	Yes	12.00	570.32	30
	26C	0.09	0.26	0.57	0.02	0.02	0.01	0.00	0.01	0.00	0.02	No	7.00	490.31	30
	27B	0.19	0.20	0.82	0.02	0.01	0.02	0.00	0.01	0.02	0.01	Yes	21.00	585.19	30
	27C	0.18	0.19	0.70	0.01	0.01	0.02	0.00	0.02	0.05	0.01	No	21.00	620.96	25
	28C	0.10	0.21	1.06	0.01	0.00	0.03	0.00	0.02	0.04	0.01	Yes	17.00	676.30	20
	29A	0.15	0.23	0.78	0.02	0.01	0.02	0.00	0.02	0.04	0.03	Yes	23.00	501.98	25
	29C	0.16	0.24	0.78	0.02	0.01	0.02	0.00	0.02	0.04	0.03	Yes	14.00	405.12	25
	29D	0.16	0.22	0.52	0.01	0.03	0.02	0.00	0.08	0.00	0.04	Yes	12.00	539.03	30
	29E	0.16	0.22	0.52	0.01	0.03	0.02	0.00	0.08	0.00	0.04	No	16.00	477.14	30
	29F	0.16	0.20	0.50	0.01	0.02	0.02	0.00	0.09	0.00	0.05	Yes	14.00	542.52	20
	6A	0.16	0.20	1.13	0.01	0.00	0.02	0.01	0.02	0.04	0.02	Yes	20.00	474.67	10
	6B	0.16	0.20	1.13	0.01	0.00	0.03	0.01	0.02	0.04	0.02	Yes	16.00	476.19	5
	9A	0.12	0.23	0.89	0.01	0.01	0.03	0.01	0.02	0.02	0.02	Yes	18.00	526.52	20
	9B	0.12	0.23	0.89	0.01	0.01	0.03	0.00	0.02	0.02	0.03	Yes	13.00	557.09	20
average		0.135	0.210	0.77	0.016	0.012	0.026	0.004	0.033	0.020	0.036	Y/n	14.2	521	25
SD ±		0.007	0.011	0.03	0.001	0.001	0.002	0.002	0.006	0.003	0.009		1.0	12	2.1

Robust principal component analysis explains 85% of the variability by one single component (Comp 1) which is a linear combination of the chemical elements Mn, C and Fe:

$$\text{Comp 1} = -0.109C + 0.812Mn - 0.563Fe \quad \text{Eq. 47}$$

Figure 63A shows the results of the quantile regression, with Comp 1 serving as the explanatory variable for the corrosion rate: the black line represents the median regression and the two red lines represent the regression of the first and third quantile. On the plot, three clusters of observations appear. Moreover, the introduction of a second component (Comp 2, shown on Figure 63B), which is a linear combination of Mn, C, Fe, Si, Ni and Cu, enhances the differences between the three clusters, as well as raises the explained variability to more than 95%.

$$\text{Comp2} = -0.163C - 0.31Si + 0.425Mn - 0.162Ni - 0.355Cu + 0.729Fe \quad \text{Eq. 48}$$

The shaded plane on Figure 63 represents the average corrosion rate. Additionally, the ordination results were confirmed by an independent cluster analysis, which resulted in three distinct clusters, which correspond completely with those found on the quantile regression plot (Figure 63A) and the three-dimensional PCA (Figure 63B).

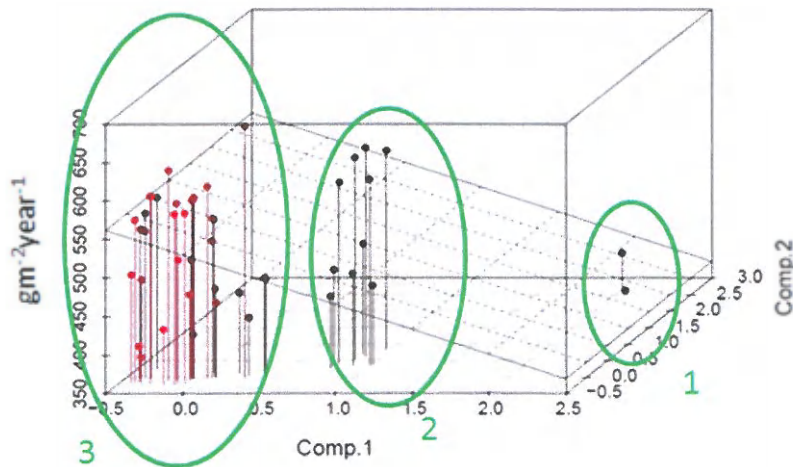
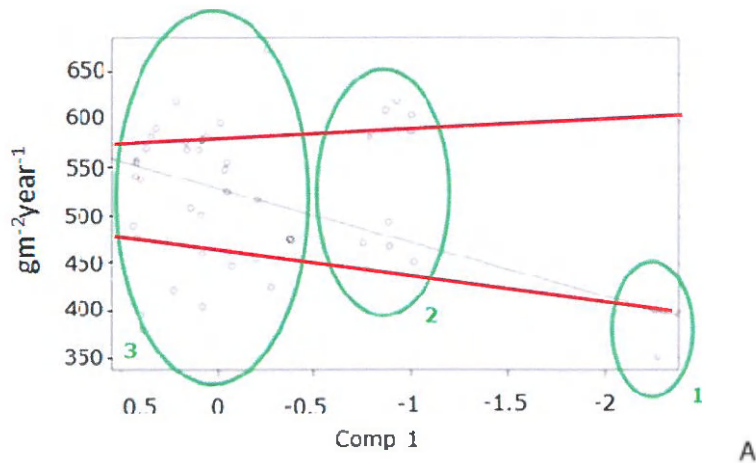


Figure 63: quantile regression of weight loss ($\text{g m}^{-2} \text{ year}^{-1}$) on comp 1 and comp 2, with indication of three clusters 1: CRS steel, 2: High tensile steel, 3: Grade A steel.

A: 2 dimensional: comp 1. The black line represents the median regression and the two red lines represent the regression of the first and third quantile

B: 3 dimensional: comp 1 and 2.

On Figure 63 and Figure 64, one observes that the 2-element cluster 1 differs greatly from the other 2 clusters.

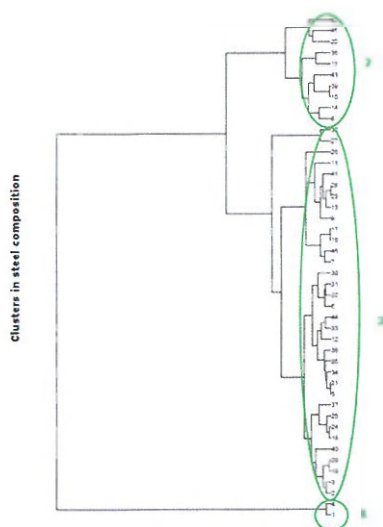


Figure 64: clusters based on steel composition. The first division is given by the C content, the second by the Mn concentration. Further divisions are related to Si, Ni and Cu concentrations.

Cluster 1 is easily explained. The chemical composition of these specimen (nr. 7 & 32 table 18) is fundamentally different from the other grades, as well as the corrosion rate (on average $376 \text{ g m}^{-2} \text{ year}^{-1}$). In terms of the steel composition, these two samples possess a very high concentration of Cr, Mo and Al, low concentrations of C and no Si, Ni or Cu.

From the quantile regression on the data from clusters 2 and 3 it was revealed that the corrosion rate of these two clusters is not significantly different: quantile regression on clusters 2 and 3 yields a slope of -41.47 with 90% CI [-74.87; 59.85] (data not shown). However, the chemical composition and microstructure of these two clusters are different. The samples of cluster 2 have a lower concentration of both Fe and C in favor of an increased concentration of Mn, Si, Ni and Cu. All these samples had small grains compared to the average grain size and all had a layered structure with a high concentration of the second phase. Mn and Si are known to refine the grain size of the metal and this is desirable since the refined structure increased both strength and toughness (Gardiner, 2003). These samples could be identified as being high tensile steel (HTS).

HTS is stronger than ordinary mild steel and, as a result, thinner scantlings are allowed. However, it is important to remember that the allowance for corrosion applied to the minimum plating thickness during new construction is based on a percentage of the plate's original thickness. Typically, a figure of 20% to 30% is applied (The Standard Club, 2004). This type of steel allows for slimmer ship constructions increasing the cargo carrying capacity for the same displacement.

Cluster 3 collects the ordinary grade A steel samples. Their chemical composition is certainly not uniform and a wide range of microstructures was encountered with various grain sizes and compositions. Unfortunately, the data presented in this dissertation did not provide a uniform correlation between the corrosion rate and the chemical composition in combination with microstructure of these Grade A alloys. Based on these observations, HTS ($534\text{gm}^{-2}\text{year}^{-1}$) steel is found to corrode at the same rate as ordinary grade A steel ($521\text{gm}^{-2}\text{year}^{-1}$).

The results after 10, 20 and 24 months of permanent immersion and the outcome of the test after 6 months wet/dry condition can confirm the outcome of the first tests and give even more explicit figures and larger discrepancies between the corrosion rate of the A + AH and the CRS. No significant differences could be found in the corrosion rate between A and AH steel. The results for the permanent immersion tests are given in Table 19. Note that for the 6 months permanent immersion two values are given. The value in italic is the corrosion rate calculated with a density based on the chemical composition of the elements. The second value gives the corrosion rate for the density based on the volume measurement of the samples. The first value corresponds with the value given in Table 18.

Table 19: overview corrosion rates for the 6, 10, 20 and 24 months permanent immersion. % gain of CRS to A and AH steel. Corrosion rates based on calculated density (weight/volume).

	CRS corrosion rate in $\text{gm}^{-2}\text{year}^{-1}$	A + AH corrosion rate in $\text{gm}^{-2}\text{year}^{-1}$	% gain	CRS corrosion rate per year % m/m	A + AH corrosion rate per year % m/m	% gain
6 months permanent immersion	376 ± 25 <i>378.66</i> ± 18.97	530.56 ± 11.66 <i>535.20</i> ± 10.84	29%	1.05	1.84	43%
10 months permanent immersion	NN	NN	NN	0.97	1.61	40%
20 months permanent immersion	229.16 ± 5.57	383.57 ± 9.43	40%	0.61	1.35	55%
24 months permanent immersion	232.16 ± 27.11	360.59 ± 11.16	36%	0.65	1.24	51%

Besides the permanent immersion, weight measurements were also carried out after 6 months of wet/dry situation. Again, this test resulted in a considerable gain for the CRS (table 20).

Table 20: corrosion rate after 6 months wet/dry situation. % gain of CRS to A and AH steel. Corrosion rates based on calculated density (weight/volume).

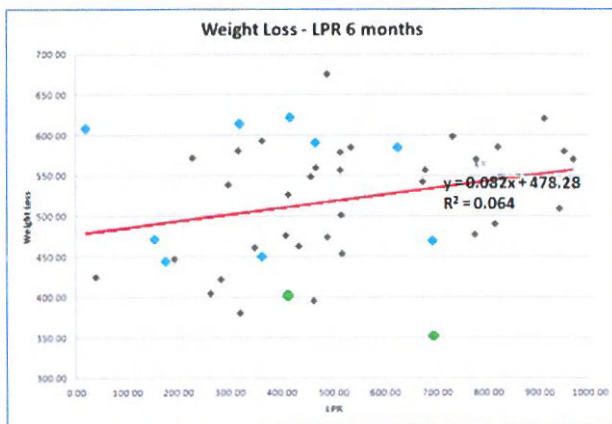
	CRS corrosion rate in $\text{gm}^{-2}\text{year}^{-1}$	A + AH corrosion rate in $\text{gm}^{-2}\text{year}^{-1}$	% gain	CRS corrosion rate per year % m/m	A + AH corrosion rate per year % m/m	% gain
6 months spray tank	692.93 ± 74.01	962.07 ± 16.15	28%	1.95	3.37	42%

6.2.3 Use of electrochemical measurements

In addition to the weight loss measurements, attempts were made to quantify the corrosion rate as a function of the electrochemical properties of the different materials. To this end, the weight losses were correlated with two specific parameters obtained from electrochemical measurements, viz. the Tafel and LPR (Figure 65A, B).



A



B

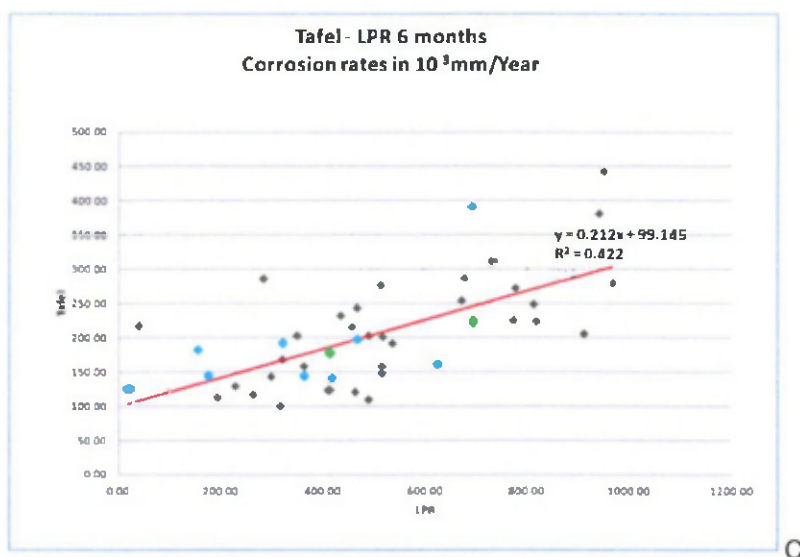


Figure 65: scatter plot of the weight loss measurement in function of respectively Tafel & LPR values. Green dots representing CRS, blue dots grade AH and grey dots grade A steel.

A: Tafel 6 months; B: LPR 6 months; C: Corrosion rate 6 months. Tafel & LPR are expressed in 10^{-3} mm year⁻¹ and the weight loss in g m⁻² year⁻¹. C: Scatter plot of the Tafel in function of the LPR measurement after 6 months of immersion of the steel samples. Both parameters are expressed in 10^{-3} mm year⁻¹. A linear regression line was added.

In neither of the cases a significant regression could be recorded. Also, no correlation could be found between the two parameters of the curve themselves (Figure 65C), given a R^2 value of barely 0.422. The clusters obtained through PCA analysis of the weight loss measurements could not be reproduced on these graphs. After these tests, we were informed that the instrumentation had broken down and that there were irregularities in the results. It was decided to reject the results as it was not clear whether they were reliable or not. Later, after the purchase of new equipment, the mass loss results were confirmed by electrochemical measurements performed at KdG University College in Antwerp. The corrosion rate of the CRS in mmpy was calculated and compared with the average value obtained from a batch of A & AH samples (Table 21). The electrolyte was the same natural seawater used for the mass loss experiments.

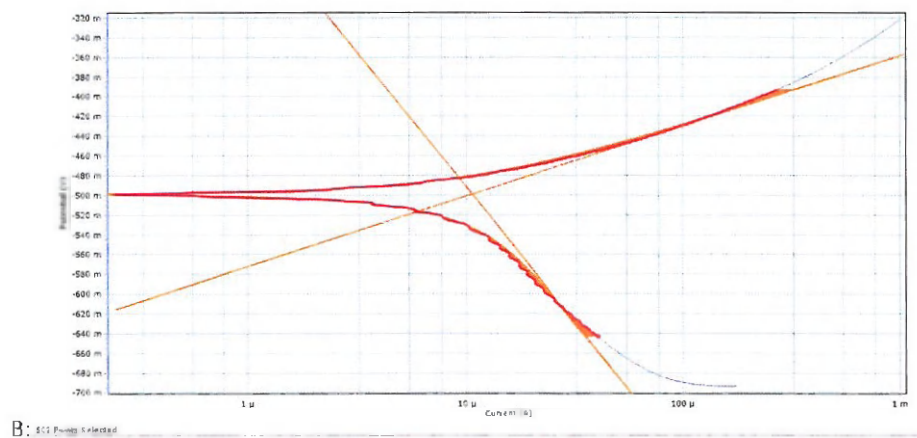
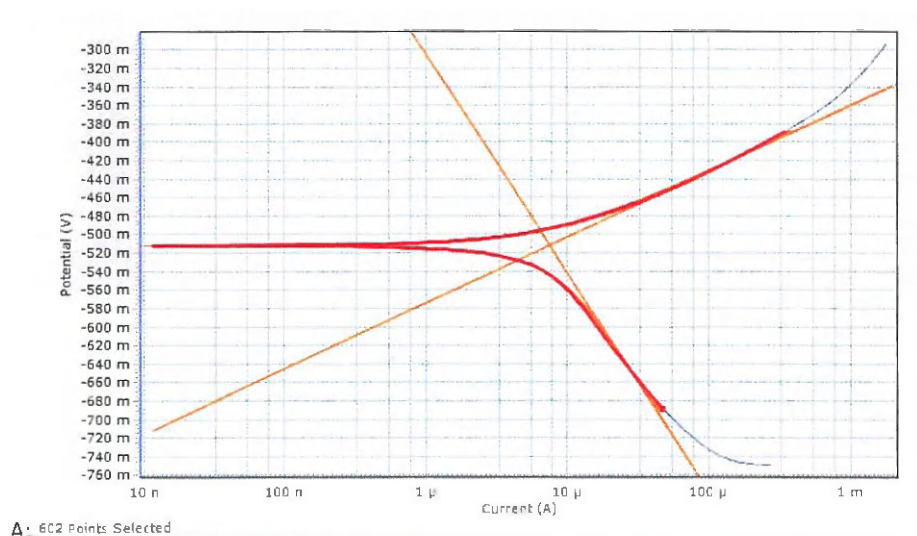
Table 21: Electrochemical determination of the corrosion rate. LPR and Tafel, expressed in $\text{mmy} \cdot 10^{-3}$.

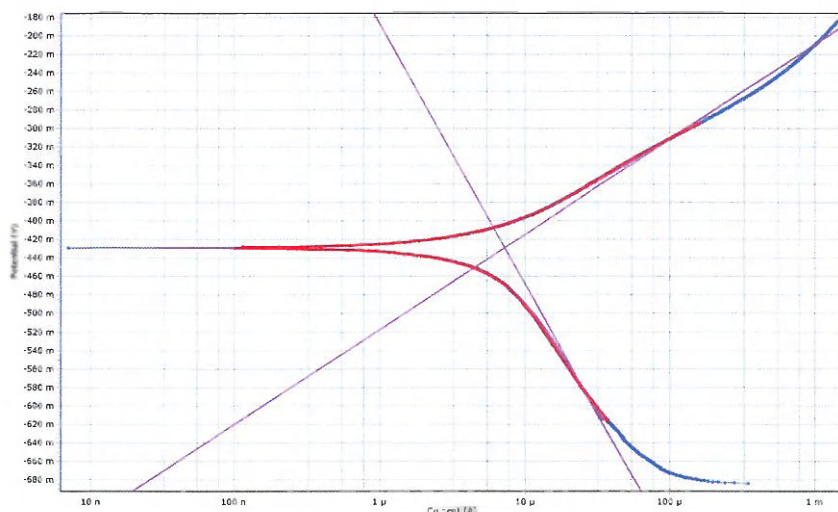
	A + AH after 2 hours in $\text{mmy} \cdot 10^{-3}$	CRS after 2 hours in $\text{mmy} \cdot 10^{-3}$
Number samples	41	1
LPR	325.84	71.73
Tafel	268.20	47.53

Also, prolonged electrochemical tests (145 hours) were done on one grade A, AH and CRS samples. The Tafel curves after 145 hours are given in Table 22 and Figure 66. Table 23 shows the results of the LPR calculations.

Table 22: β values as per Tafel curve of A, AH and CRS steel after 145 hours, expressed in volt.

β (V)	β_a	β_c
A	0.072	-0.225
AH	0.071	-0.275
CRS	0.103	-0.280





C: 645.8 mV/Seliger

Figure 66: Tafel curves A: grade A, B: grade AH and C: CRS steel after 145 hours. Tangents to the slopes are the β values.

The Stern-Geary equation, described in chapter 2, gives the inversely proportional relation between the polarization resistance R_p and the corrosion current i_{corr} . The CRS has higher values of R_p and corresponding lower i_{corr} measurements. The corrosion speed of the CRS is significantly lower than A and AH steel, although the result of the 121 hours shows an increased corrosion rate.

Table 23: prolonged electrochemical measurements for 20, 44, 68, 121 and 145 hours. R_p , i_{corr} and corrosion speed are given for A, AH and CRS steel.

R_p (Ω)	20h	44h	68h	121h	145h
A	1240	1197	1424	1640	1754
AH	1527	1700	1449	1225	1634
CRS	3835	3177	3787	2632	2804
i_{corr} ($\mu A cm^{-2}$)	20h	44h	68h	121h	145h
A	19.12	19.81	16.649	14.452	13.516
AH	16.064	14.428	16.927	14.218	15.014
CRS	8.535	10.305	8.643	12.434	11.146
Corrosion speed ($mm y^{-1}$)	20h	44h	68h	121h	145h
A	0.224	0.232	0.194	0.169	0.151
AH	0.188	0.169	0.198	0.166	0.176
CRS	0.100	0.121	0.101	0.146	0.137

We concluded that the electrochemical measurements support the reduced corrosion rate of the Korean steel assessed by weight loss measurement. If the absolute values of the weight loss method are compared with the electrochemically obtained corrosion

rates the difference is rather large. This is not abnormal. As described by Y. Zou (2011), electrochemical reactions under rust are not simple reactions anymore, including metal anodic dissolution and oxygen cathodic reduction, but complex corrosion processes composed of multiple sub-processes involving rust redox reactions, mass transportation through rust, electric charges movement between interfaces, microorganism propagation in porous rust and some other complex corrosion processes, which make metrical corrosion rates different between electrochemical and weight-loss measurements (Zou, 2011).

6.2.4 Applicability of the different steel types in corrosion prevention

We already mentioned that the use of stronger high tensile steel allows lighter, more flexible structures (see 6.1). This flexibility causes however fatigue and corrosion problems (Paik, 2002, Løseth, 1994). The reduction in the scantlings due to high-tensile steel has in some cases given higher repair costs due to an increased number of fatigue cracks and steel replacement due to corrosion (Løseth, 1994).

Figure 63 shows that the corrosion rate of high tensile steels (cluster 2) is matching the corrosion rate of ordinary grade A steel (cluster 3).

Pricewise the difference in price between high tensile steel and mild steel will support the use of mild steel at the building stage, also when including the cost of steel replacement and fatigue repairs (The Standard Club, 2004).

Already back in 1994 Løseth et al. pointed towards an increased corrosion problem due to a double hull construction (only four years after OPA₉₀) and emphasized the necessity of a good coating system and maintenance policy (IMO PSPC was adopted December 2008).

If the CRS shows a yield stress and tensile strength satisfying the high tensile steel requirements, the observed reduced corrosion rate would smooth away the above mentioned disadvantage of recent high tensile steel grades. This is discussed in chapter 7.

An improved corrosion resistance might make less stringent coating requirements feasible without endangering the safety of ship and crew and maybe making coating totally unnecessary.

Coating ships' tanks is troublesome mainly because of the preparatory works such as substrate treatment, edge rounding and climate conditioning. A coating is only satisfying when 100% intact. Paint damages caused by external impact create small anodes

besides the huge intact area acting as cathode resulting in terrifying local corrosion rates of 4 to 5mm per year (own in situ observations during tank inspections).

6.3 Conclusions

The average corrosion rate of grade A steel is comparable with the corrosion rate of HTS steel (Roberge, 2000), which is supported by the statistical analysis of the observations in our sample. Since HTS allows the construction of lighter ships the impact of the corrosion losses becomes relatively more important and may endanger the safety and the lifetime expectancy of ships.

The optimization of structural design and the use of high tensile steels have led to a reduction in the stiffness of the ship's structural members. The result is an increased degree of fatigue which contributes to the shedding of scale on vertical and inverted surfaces. The newly exposed steel presents a renewed opportunity for general corrosion to occur at an accelerated rate (OCIMF, 1997).

Many tankers have been built with a high percentage of HTS, some in the region of 80 to 90 percent. The high percentage of HTS has been reduced in recent years to somewhere around 30 % due to corrosion and fatigue considerations (Intertanko, 2002).

The average corrosion rate of cluster 2 and 3 after 6 months permanent immersion is $535 \text{ gm}^{-2}\text{y}^{-1}$. The Korean CRS is corroding at a rate of $376 \text{ gm}^{-2}\text{y}^{-1}$. The results after 10, 20 and 24 months are even more explicit at give a gain of more than 30%. The corrosion rate in a wet/dry situation is significantly higher, but also there, a reduced corrosion rate of about 30% is obtained.

This CRS might trigger a reduction of the corrosion allowance, reducing the weight and increasing the cargo carrying capacity. This is elaborated in the next chapter.

7 The chemical, mechanical and physical properties of the Korean Corrosion Resistant Steel (CRS)

7.1 Introduction

The use of corrosion resistant material on board ships is not new. The Norwegian M/T Lind delivered in 1960 was the first ship to be equipped with stainless steel cargo tanks and ever since stainless steel is used commonly in the tanks of chemical tankers (IMO, 2000).

In April 2011 the Japanese classification society ClassNK approved NSGP-1 steel manufactured by Nippon Steel Corporation's Oita Works as complying with the IMO's new performance standard for corrosion resistant steels for application on the inner top and bottom of the cargo tanks of crude oil tankers. NSGP-1 shows a more than five times higher corrosion resistance compared with conventional steel plates. Because of their optimized alloy composition, NSGP-1 can still be welded and processed in the same way as conventional steel plate (Japanese Metal Bulletin, 2011).

A large body of literature has been studied and does not show many examples of the corrosion resistant material suitable for ballast tank construction. The Japanese steel mill JFE introduced such a steel grade some years ago, but this was withdrawn for unknown reasons. Consequently the experimental alloy in our possession of which the supplier pretends it is specially developed for use in ballast tanks is interesting and merits our full attention.

Chapter 6 proves the improved corrosion resistance of this CRS. Two supplementary research questions should be asked: first, is this CRS suitable as ship construction material and secondly, why is this CRS corroding substantially less fast? Most probably the answers will be found in the chemical and mechanical properties of this steel.

Chemical composition, inclusions and microstructure define the physicochemical characteristics. Mechanical properties include tensile strength, hardness, notch toughness and weldability.

7.2 Overview of the performed tests

Tests were performed at OCAS in Zelzate, Karel de Grote University College in Antwerp, and VUB in Brussels.

7.2.1 Chemical properties

7.2.1.1 Chemical composition

Ships are commonly constructed out of grade A steel, which is usually aluminum or silicon killed steel. Sometimes, high tensile steel (AH) is used, which is produced as fully killed, grain-refined material (ArcelorMittal 2001). The chemical composition of grade A and AH steel as specified by Lloyd's Rules (2001) including the major components is given in Table 24.

Table 24: chemical composition as specified by Lloyd's Rules (2001). Elements are given in %wt.

Grade	C _{max}	Mn	P _{max}	S _{max}	Si	Al ¹	Nb
A	0.21	¹	0.035	0.035	0.50 max	-	-
AH36 ²	0.18	0.70 – 1.60 ³	0.035	0.035	0.50 max	0.020 min	0.020-0.050

¹. % manganese not less than 2.5 times % carbon.

². Residual elements are restricted to the following maximum: copper ≤ 0,35%; chromium ≤ 0.20%; nickel ≤ 0.40%; molybdenum ≤ 0.08%

³. 0.90% - 1.60% manganese for t ≥ 12.5mm

The chemical composition of the CRS was determined at OCAS, by an optical emission spectrometer, ASR 4460 Metals analyzer (see 4.2).

7.2.1.2 Density

The density of the CRS has been calculated based on the chemical analysis obtained by the optical emission spectroscopy. The mass % of each component was multiplied with the density of the pure substance.

7.2.1.3 Grain size

Ship construction steel is hot rolled. During the hot rolling process the steel is heated till well above the eutectoid temperature of 723°C, where austenite begins to appear. Each island of austenite grows until it intersects with its neighbor. With a further increase in temperature, these grains grow. The final grain size depends on the maximum temperature to which the metal is heated (Neely, 2003).

The microstructure of the samples was studied through a Zeiss bright field microscope using two different magnifications (10x10 and 10x50) (see 4.5). The composing elements (ferrite, pearlite and bainite) were identified and for each sample was defined whether or not it had a layered structure. Based on the average observed grain size, the samples were subdivided into three categories: small, intermediate and large grain size. Small grains measured <20µm and large granulates had dimensions in excess of >30 µm.

7.2.1.4 Inclusions

Manganese sulfides (MnS) and aluminum oxides (Al₂O₃) were studied according the ISO4967 procedure, by means of a scanning electron microscope (SEM). Subsequently, they were identified with an energy dispersive X-ray (EDX) detector (see 4.3).

7.2.2 Mechanical properties

7.2.2.1 ASTM A 131M

ASTM A 131M (2008), "Specification for Structural Steel for Ships", itemizes different steel grades with specific mechanical properties and applications. Every classification society describes the minimum requirements in their classification rules and regulations. Table 25 gives the mechanical properties for hull steels according IACS, the International Association of Classification Societies.

Table 25: Mechanical properties for hull steels (Common Structural Rules for Bulk Carriers, IACS). ReH : minimum yield stress, in MPa, of the material, Rm : ultimate minimum tensile strength, in MPa, of the material, t : thickness in mm.

Steel grades for plates with t ≤ 100 mm	Minimum yield stress R _{eH} , in MPa	Ultimate tensile strength R _m , in MPa
A-B-D-E	235	400 – 520
AH32-DH32-EH32-FH32	315	440-570
AH36-DH36-EH36-FH36	355	490-630
AH40-DH40-EH40-FH40	390	510-560

The same ASTM A 131M regulation prescribes a tensile and toughness test for steel less and more than 50mm thick and a test for rivet steel and rivets. Since this research examines shell plating samples, only the test for material less than 50mm is considered. Unless a specific orientation is requested, tension test specimens may be taken parallel or transverse to the final direction of rolling.

7.2.2.2 Hardness

The hardness of steel is determined by testing its resistance to deformation. A number of methods can be employed, such as the Brinell, Vickers (HV) and Rockwell (HRB or HRC) test. The steel to be tested is indented by a hardened steel ball or diamond under a given load and the size of the impression is then measured. For steel an empirical relationship exists between hardness and tensile strength. The hardness is often used as an indication of the tensile strength.

HV hardness has been measured using a properly calibrated Zwick 3212 hardness tester at Karel de Grote University College (2012).

7.2.2.3 Notch toughness

The Charpy test measures the energy absorbed by a standard notched specimen while breaking under an impact load. It is used as an economical quality control method to determine the notch sensitivity and impact toughness of engineering materials (ASTM E23, 2007).

Samples of approximately 100x10x10mm were prepared and a Charpy V notch of 2mm depth was applied. The test on the CRS was executed according DIN EN 10045 T1 with a calibrated pendulum ram at room temperature, 0°C and -20°C.

Toughness tests are not required for ordinary grade A steel. Charpy V-notch tests must be made on grade B material over 25 mm in thickness and on material of grades D, E, AH32, AH36, DH32, DH36, EH32, and EH36. Some exceptions, where no test is required exist.

7.2.2.4 Tensile strength and yield stress

The yield stress is a material strength variable used to determine the ship's hull girder strength. Once the yield point is passed some of the deformations become plastically. The ultimate tensile strength (UTS), often shortened to tensile strength (TS) or ultimate strength, is the maximum stress that a material can withstand while being stretched or pulled before necking occurs. This is when the specimen's cross section starts to contract significantly (Degarmo, 2003, Smith, 2006) (Figure 67).

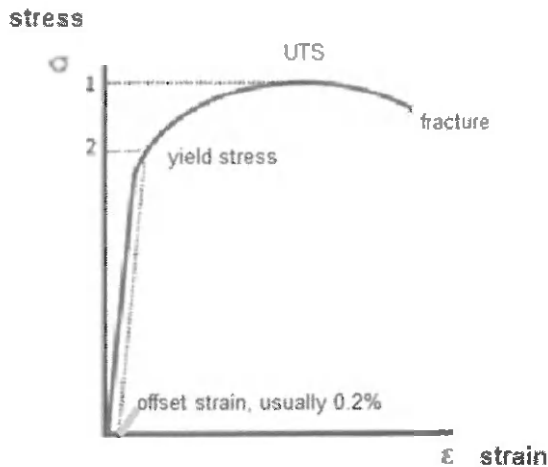
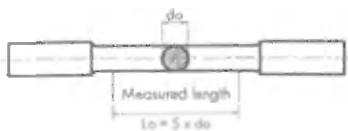


Figure 67: stress-strain diagram, in MPa function of elongation in %.

A stress-strain diagram is determined by a tensile test and expresses the relationship between a load applied to a material and the resulting deformation. The specimen deformation (strain) is function of the increase in gauge length. Stress is the ratio of the tensile load F applied to its original cross-sectional area and is expressed in MPa or N/mm^2 . The elongation (A_5) is a measure of the general ability of the material to be plastically deformed and is a good parameter for the ductility of a material (Shackleford, 2005). Elongation can be calculated as follows:

$$A_5 = (L_u - L_0) / L_0 \times 100\%$$

Eq. 49



with:

L_0 : defined length before the tensile test

d_0 : shaft diameter before the tensile test

L_u : length after fracture.

The measurements on the CRS material were done with a tensile strength tester Amsler 300 kN, type 1 (measuring error on force read out < 1%) and an Extensometer MFA 2, both calibrated every two years. Tensile speed was set at 15 MPa/s.

Back in 2011, the American Bureau of Shipping (ABS) published an extensive statistical study on the material properties of shipbuilding material (Vanderhorn and Wang 2011). This study uses a statistical analysis of shipbuilding steels from five manufacturers in the USA and Asia, and includes over 140,000 samples. The results of this study were used to benchmark the outcome of toughness and tensile strength tests.

7.2.3 Weldability

7.2.3.1 Practical test

A practical welding test, following an undefined procedure and using arc welding with standard ship welding rods for A and AH grades was done at Antwerp Ship Repair by a certified welder.

7.2.3.2 Suitability for welding test

A simple welding test has been done at Karel de Grote University College (October 2012). The basic material consisted out of CRS and measured 15.5x70x180mm. The test was done at a temperature of 20°C, with a welding current $I_t = 112A$, an arc voltage $U_b = 26.2V$ and a welding speed of 16.4cm/min. The welding sample was transversally cut and etched with a methanol + 5% HNO_3 solution for 20 seconds.

Vickers hardness of the weld was measured with a calibrated Zwick type 3212 hardness tester along a measuring line parallel with the surface of the basic material crossing the fusion zone just beneath the weld zone.

7.2.3.3 Carbon equivalent

The carbon equivalent (CE) is an indicator expressing the critical cooling time required for a steel material to change into 100% martensite (Kasuya, 2007). This cooling time can be related directly to cold cracking and is commonly used to judge the weldability of the steel. The carbon equivalent was calculated by means of two formulas.

The first equation is given by the American Welding Society (AWS)

$$C.E. = \%C + \frac{(\%Mn + \%Si)}{6} + \frac{(\%Cr + \%Mo + \%V)}{5} + \frac{(\%Ni + \%Cu)}{15} \quad \text{Eq. 50}$$

The second equation was developed by the Japanese Welding Engineering society and is based on the work from Ito en Bessyo (The Japanese welding Engineering Society, 2011). This carbon equivalent is considered to allow a more realistic assessment of the weldability of low carbon steels (steel qualities that contain less than 0.25% of C) (ASM International, 1997).

$$P_{cm} = \%C + \frac{\%Si}{30} + \frac{(\%Mn + \%Cu + \%Cr)}{20} + \frac{\%Ni}{60} + \frac{\%Mo}{15} + \frac{\%V}{10} + 5B \quad \text{Eq. 51}$$

7.3 Results & discussion

7.3.1 Chemical properties

7.3.1.1 Chemical composition

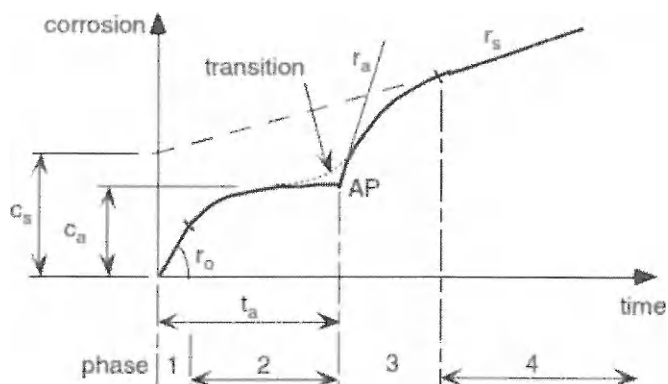
The chemical composition of traditional steel Grade A, corrosion resistant steel types developed for use in sea water (JFE-Marin 400), CRS and weathering Corten A steel are given in Table 26.

Table 26: chemical composition traditional steel compared with JFE-Marin 400, experimental POSCO CRS and Corten A steel (ASTM, JFE, POSCO, 2012).

Element	Grade A	JFE-Marin 400	Corten A	CRS
C	0.13	<0.15	0.12	0.025
Si	0.24	<1	0.25-0.75	0.207
Mn	0.66	<1.4	0.20-0.50	0.89
P	0.015	<0.030	0.07-0.15	0.012
S	0.016	<0.02	0.03	0.004
Cr	<0.02	0.50-1.50	0.50-1.25	2.08
Ni	<0.02	<0.50	0.65	0.001
Mo	<0.005			0.59
Al	0.006	<0.55		1.015
V	<0.005			0.001
Nb	<0.005			0.006
Cu	<0.02	0.20-0.60	0.25-0.55	0.001
Ti	<0.005			0.005

The concentration of five chemical components of CRS deviates significantly from ordinary grade A steel. CRS has a much higher concentration of Cr and Al, a higher concentration of Mo and a far lower concentration of C and Cu. The major differences with Corten steel involve the same elements.

In 2004, Melchers made a comparative analysis of previously reported observations, where the relation of the concentration of certain alloying elements to the corrosion rate was studied. He developed an interesting complex time dependent model subdividing the corrosion process in 4 phases (Figure 68).



r_o [mm/yr]: Initial corrosion rate, r_a [mm/yr]: corrosion rate at the beginning of the anaerobic phase, r_s [mm/yr]: linear corrosion rate of the anaerobic phase (after > 5 years), AP: start of the anaerobic phase, c_s : Corrosion depth in mm at t_a , c_a : corrosion depth in mm at the start of phase 4.

Figure 68: corrosion time dependent model (Melchers, 2004).

The first phase is defined as being initial corrosion, kinetic controlled. Phase two consist out of corrosion controlled by oxygen diffusion. These two phases together comprise approximately three years. Phase three and four are respectively the initial and linear anaerobic phase.

CRS can be classified as high alloyed low carbon steel. Bleckenhorst (1986) collected an impressive corrosion rate dataset on a considerable range of steel compositions after immersion in North Sea water at different depths (45 and 90m) for 1.5, 4 and 7.2 years. The higher described model by Melchers (2004) was used during the interpretation of the data. It is particularly interesting to note that one of the steel grades studied, H16, has a chemical composition very similar to the CRS steel (Table 27).

Table 27: composition H16 (Melchers, 2003) and CRS, expressed in %wt.

Element	H16	CRS
C	0.01-0.02	0.025
Cr	1.5	2.08
Al	1.5	1.015
Mo	0.5	0.59
Ni	Very small	Very small
Cu	Very small	Very small

A comparison of the corrosion rates of CRS with steel grade H16 (Table 28) should be treated cautiously, as the environmental test conditions were not the same. CRS was tested in aerated, circulating seawater with an oxygen concentration varying between 7.08 and 12.8 ml/l at ambient temperature while the samples of Beckenhorst were

stored 45 respectively 90 meters below the surface. For metals such as iron the corrosion rate increases linearly with a rising oxygen concentration (Baboian, 2005).

Table 28: corrosion rate of H16 (Melchers, 2003) and CRS, expressed in mm y^{-1} .

Corrosion rates	H16	CRS Own test results
R_0	0.018 mm y^{-1}	0.049 mm y^{-1}
R_a	0.011 mm y^{-1}	0.030 mm y^{-1}

The influence of the different important alloying elements of the CRS are further developed hereunder.

Carbon

The influence of the carbon concentration on the corrosion rate is contested. As illustrated by Figure 69 Pleshivtse (2009) supposes a directly proportional relation between corrosion rate and carbon content.

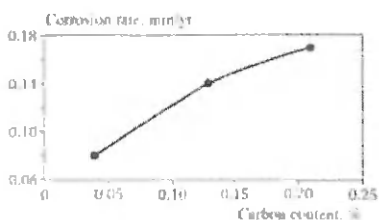


Figure 69: relation corrosion rate in mm y^{-1} to carbon content in %wt (Pleshivtse, 2009).

A low carbon content implicates the presence of very little iron carbide (Fe_3C). The presence of iron carbide in the surface film is considered to increase the corrosion reaction by selectively increasing the cathodic reaction rate (Nesic, 1993).

In his study, Melchers (2003) however states: “carbon content for the kinetic controlled phase and the oxygen-diffusion phase has no significant influence. However, when anaerobic bacteria control corrosion the corrosion rate increases with carbon content.”

Formation of a rust layer

Rusting process consists out of the formation of Fe-oxides, Fe-hydroxides and Fe-oxy-hydroxides. Ferrous hydroxide $\text{Fe}(\text{OH})_2$ and hydrated ferrous oxide $\text{FeO} \cdot n\text{H}_2\text{O}$ are elements of the first diffusion barrier layer formed on the surface. Air-oxidation (aerobe) of $\text{Fe}(\text{OH})_2$ results in $\gamma\text{-FeOOH}$ (lepidocrocite) when the reaction is fast and in Fe_3O_4 (magnetite) in case of a slow reaction (Nagayama, 1962). Finally both transform into γ -

Fe_2O_3 (maghemite) (Tamura, 2012). Hydrolysis of Fe^{3+} results in the formation of $\alpha\text{-FeOOH}$ (goethite) or/and $\alpha\text{-Fe}_2\text{O}_3$ (hematite). The latter is loose, flaky and porous and does not shield the substrate from the environment. It will come off easily and the steel surface will be exposed again, restarting the corrosion process.

Tamura (2008) and Saha (2012) state that rust on exposed steel is composed out of different layers (Figure 70). The outer layer is dark and consists of $\alpha\text{-FeOOH}$. The layer closest to the Fe-substrate, which is formed in a lean oxygen environment is Fe_3O_4 ($\text{Fe}_2\text{O}_3\cdot\text{FeO}$, magnetite) which is stable and protective with self-maintaining properties (Tamura, 2008, corrosion doctors, 2012, Saha, 2012). In case of damage to the Fe_3O_4 layer the base metal is exposed, and the Fe^{2+} ions go into solution and react with water and oxygen to form $\text{Fe}(\text{OH})_3$. The aging of $\text{Fe}(\text{OH})_3$ leads to dehydration even in the presence of water and forms $\alpha\text{-FeOOH}$ (Tamura, 2008).

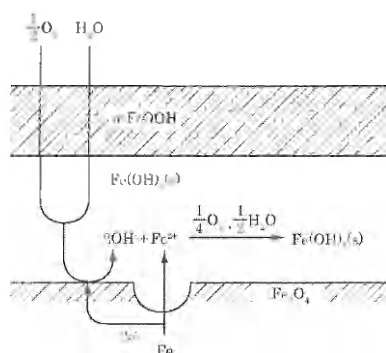


Figure 70: overview of rust film formed in the initial stage of corrosion (Tamura, 2008).

After exposure, initially iron oxides and iron oxy-hydroxides such as $\gamma\text{-FeOOH}$ develop. Amorphous rust ($\delta\text{-FeOOH}$) is considered to be an intermediate phase. (Yamashita, 2004)

Alloy elements such as chromium, facilitates the formation of stable and strong $\alpha\text{-FeOOH}$ or goethite (Saha, 2012). With the progress of corrosion, the corrosion rate decreases due to the increase in the thickness of the $\alpha\text{-FeOOH}$ solid. $\beta\text{-FeOOH}$ is believed to form in a marine environment as a porous layer, negatively affecting the corrosion rate (Dunn, 2000).

This theory is confirmed by Kimura (2005) employing spectroscopy analysis. He discovered that in the initial stage of the corrosion process $\text{Fe}(\text{O},\text{OH})_6$ nuclei, corresponding the $\gamma\text{-FeOOH}$ phase are formed. An $\text{Fe}(\text{O},\text{OH})_6$ unit nucleus is the smallest unit of structure wherein six oxygen atoms (some of which being $-\text{OH}$) surround an Fe atom. Under repeated cycles of wetting and drying $\gamma\text{-FeOOH}$ transforms into $\alpha\text{-FeOOH}$ (Figure 71). From bottom to top, four layers can be distinguished: (1) the colloidal rust

formed on Fe with 5% Cr (m/m) immersed in artificial seawater for two weeks (wet), (2) the dried powder of it (dry), (3) the rust formed on Fe with 5% Cr (m/m) exposed to atmosphere for 15 years, and (4) powder of α -FeOOH. The corresponding atomic structures (network structures) are shown to the right.

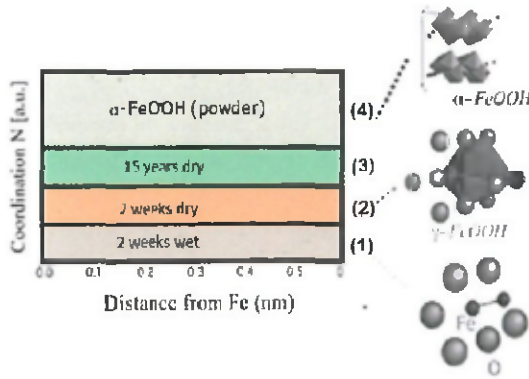


Figure 71: formation of FeOOH layers after exposure (adapted from Kimura, 2005).

Shuichi Hara (2007) sets a relationship between the corrosion rate of steel and the composition of the rust layers. These corrosion rates can be classified by the protective ability index (PAI). Figure 72 gives a visual projection of this relationship by:

$$PAI = \frac{\alpha}{\gamma - FeOOH + \beta - FeOOH + S} \text{ in an industrial environment Eq. 52}$$

$$PAI = \frac{\beta - FeOOH + S}{\gamma - FeOOH + \beta - FeOOH + S} \text{ in a seaside environment Eq. 53}$$

α , γ^* , β and s are the mass ratio of: $\alpha = \alpha - FeOOH$, γ^* = the total of $\gamma - FeOOH$, $\beta - FeOOH$ and the spinel-type iron oxide, $\beta = \beta - FeOOH$, S = Spinel-type iron oxide (mainly Fe_3O_4).

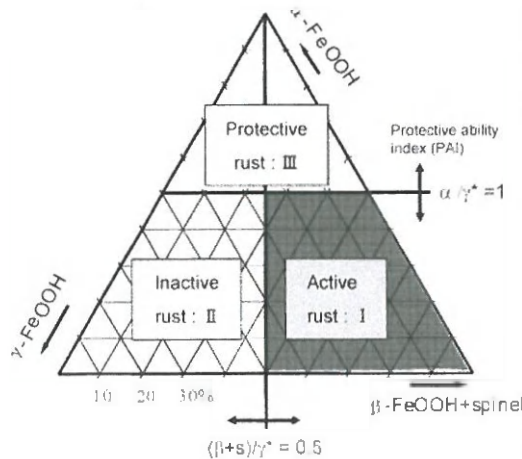


Figure 72: relation corrosion rate, composition rust layer (Shuichi, 2007).

With this knowledge, it is now possible to relate to the influences of the alloying elements Cr, Mo, Al and Cu.

Chromium

Morcillo (1999) points out the importance of chromium and other alloy elements. Chromium in Cr-goethite prevents the penetration of water, oxygen and aggressive corrosive anions such as chloride ions (Miyuki, 1998, Saha, 2012). Increasing the chromium concentration in the goethite decreases the crystal size and provides a stronger and more protective layer against atmospheric corrosion (Yamashita, 1996). Chromium is very prominently present in our sample (2.08%).

Melchers (2003) states that the influence of chromium ($\leq 2.5\%$) on the initial corrosion rate in the absence of other critical elements is negligible. However, if small quantities of molybdenum and aluminum are added as well (as in our sample), the corrosion rate is reduced considerably and this effect increases with an increased chromium concentration. This effect continues in time, certainly in the anaerobic phases.

However, scientists do not agree about the way chromium is distributed in the oxide layer. Yamashita (2000) and Zhang (2002) state that when the steel substrate corrodes, the element chromium has to be redistributed in the layer, because it has a different solubility in metal compared to rust. Some Fe are replaced by Cr in the oxy-hydroxides to form $\alpha\text{-Fe}_x\text{Cr}_{1-x}\text{OOH}$. The other Cr ions precipitate on defects and grain boundaries. $\text{Cr}(\text{O},\text{OH})_6$ is here described as Cr-substituted goethite.

In 2004, Yamashita described another theory. A goethite crystal is formed by a $\text{FeO}_3(\text{OH})_3$ octahedron. Here, Fe^{3+} is surrounded by three O^{2-} ions and three OH^- ions. The network of these octahedrons form the goethite structure. Smaller and larger vacancies can be noticed. The larger ones are formed by double chains of oxygen atoms, leading to the orthorhombic (chapter 3) structure, which can be seen as an elongated octahedron. XAFS (X-ray absorption fine structure) spectra indicated that Cr^{3+} in the rust layer is coordinated with O_2 to make a complex anion which settles in the vacant sites, in between the double chains of the ultrafine $\alpha\text{-FeOOH}$ crystal as a surface-adsorbed and/or inter-granular ion (Figure 73). As such, the Cr complex fills the gaps and prevents the passage of other corrosion accelerating substances such as chloride ions or oxygen molecules. The structure also becomes denser and therefore stronger.

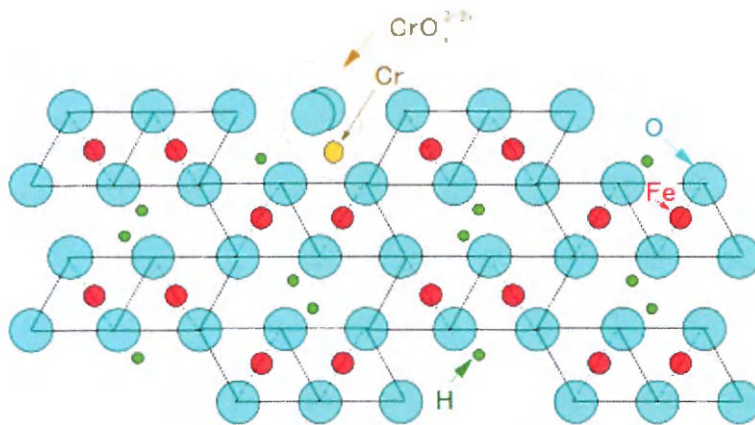


Figure 73: schematic illustration of goethite crystal, where $\text{CrO}_{x^{3-2x}}$ complex ion adsorbs at the surface (Yamashita, 2004).

Molybdenum

Molybdenum reduces the intensity of the oxidizing effect required to ensure passivity and decrease the tendency of previously formed passive films to break down (Euro-inox, 2004).

Research by Olefjord and Marcus (1987) pointed out that molybdenum is present in the passive film in the Mo^{6+} oxidation state. The surface enrichment of molybdenum is believed to facilitate the passivation process. Besides this, the susceptibility of steels to inter-granular attack decreases with increased Mo concentration. Cr and Mo also increase the resistance to pitting and crevice corrosion (Ahmad, 2006), especially in chloride-rich environments (Asphahani, 1987). Also, alloys containing Ni or Mo are less susceptible to hydrogen embrittlement (Schweitzer, 2007).

Melchers (2003) states that the addition of molybdenum is beneficial to corrosion solely in case of small quantities ($<0.5\%$). Larger concentrations do not yield an influence. Also, he mentions that the combination of molybdenum (0.5-1.5%) and 1.5% chromium lowers the corrosion rate in the initial phase while the combination with aluminum (1.5%) gives the opposite effect.

Finally, Mo imparts strength for high-temperature service (Roberge, 2000). According to MacDougall (2002), however, the role of Mo is still under discussion.

Aluminum

During steel making process, oxygen is used to lower the carbon content during the conversion of pig iron into steel. When the temperature drops, the solubility of oxygen in steel decreases and iron oxide is formed. This can be prevented by adding deoxidizing agents (Campbell, 2008). Aluminum is a common deoxidizer (ASM, 2000) and together with Cr, Si, Ti, V, Mo and W, it is added as a ferrite stabilizing element. Ferrite has small grains which reduces the possibility of stress corrosion cracking (ASM, 1993, Ralston, 2010). Besides this, the solubility of carbon in ferrite is very small, resulting in an improved corrosion resistance.

Carbon or alloy steel heated to a temperature just above the upper critical temperature transforms to austenite. Heating the steel to progressively higher temperatures will eventually result in coarsening of the austenite grains. The temperature at which this occurs depends to some extent on the composition of the steel (chapter 3), but is influenced primarily by the type and degree of deoxidation used in the steelmaking process. Deoxidizers such as aluminum inhibit grain growth, thereby increasing the temperature at which coarsening of the austenitic grains occurs. Aluminum is most commonly used for grain size control because of its low cost and dependability (Akron steel treating company, 1987).

The grain size of Fe-crystal is an important parameter in the strength of the steel. The relation between yield strength to grain size is given by the following equation:

$$F_y = F_0 + \frac{K}{\sqrt{d}} \quad \text{Eq. 54}$$

with F_y = yield strength (MPa), F_0 = yield strength of very large isolated crystals (for mild steel 5MPa), K = constant, which for mild steel is $38 \text{ Nmm}^{-3/2}$, d = grain size

The formula shows that decreasing the grain size will enhance the yield strength (Kumar, 2012). This idea is generally accepted by the scientific world although, according our literature study, an exact scientific explanation is not obvious.

An important characteristic of a successful alloy is its ability to form and maintain a stable, protective oxide film. Aluminum and silicon alloying additions can contribute positively to this requirement. However XRD, GD-OES & SEM analysis were not able to indicate the accumulation of aluminum in the oxide layer of the CRS sample. The Al concentration increases gradually throughout the corrosion layer (Figure 74). Zhang (2002) performed an XRD analysis on 'Cor-Ten' steel and was also not able to prove the presence of Cu and P in the compact rust layer. It can thus be suggested that the absence of aluminum in the oxide layer does not necessarily mean that there is no positive effect.

According to Melchers (2003), an aluminum concentration between 0% and 1.5% reduces the corrosion rate in the initial corrosion phase. The presence of molybdenum seems to counteract the positive influence of aluminum in the initial phase as well as during the anaerobic phase.

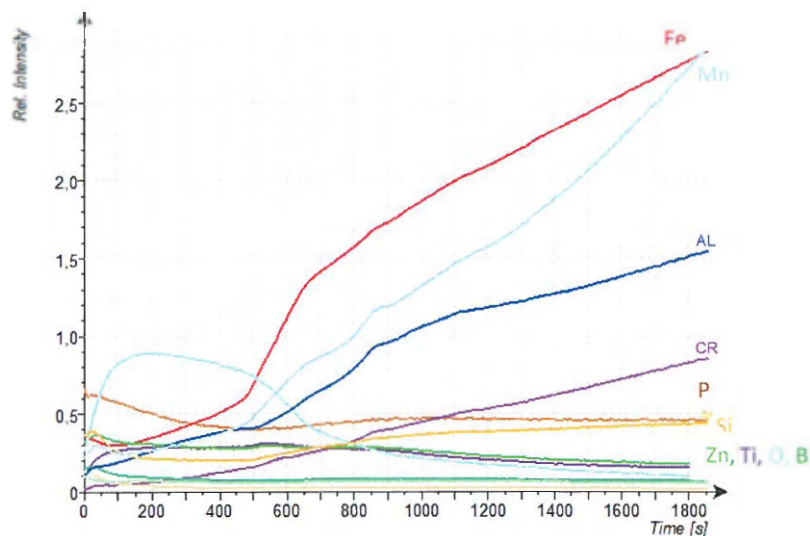


Figure 74: GD-OES analysis of CRS steel oxide layer: Dark blue line is Al line. An almost linear increase in Al concentration is visible.

More research such as but not limited to XPS and EIS on this topic needs to be undertaken before the relation between aluminum concentration in the alloy and corrosion resistance of the steel in a saline environments is explained.

Copper

Cohen (1961) and Stockbridge (1996) studied the distribution of alloying elements during the formation of the compact rust layer on weathering steel and have attributed important characteristics to the presence of Cu in the alloy. It has been found that the presence of Cu retards the growth of rust and suppresses the supply of oxygen to the steel surface. It reduces the conductivity of the rust, retards the crystallization of rust and contributes to a uniform dissolution of the steel and a formation of a rust layer at the initial stage.

However, in our corrosion resistant sample the concentration of copper is very low while the concentration of aluminum is high. The corrosion resistance of 'Cor-Ten' steel is based on a protective oxide layer, called patina that builds up when the steel is exposed to atmospheric conditions. When immersed in sea water 'Cor-Ten' does not perform

significantly better than mild steel, as the patina does not stabilize in the presence of chlorine (Key to metals, 2010). Its use is therefore not recommended in such conditions (NACE Resource Center, 2012). The Korean CRS is specially developed for use in ship's ballast tanks where salinity is inevitable.

7.3.1.2 Density

The calculated density of CRS is 7.646tm^{-3} . The average density of ship construction steel varies between 7.75 and 8.05tm^{-3} (Elert, 2009). CRS is between 1.4 and 5% lighter, which can, amongst others, be explained by the higher concentration of aluminum and the lower concentration of copper.

7.3.1.3 Grain size

The Korean corrosion resistant steel shows equiaxed grains with an average size between 20 and $30\mu\text{m}$ (Figure 75). The structure is layered ferrite/pearlite/bainite with a 2nd phase of approximately 22%. The average grain sizes of all the samples are incorporated in chapter 6 (Table 18).

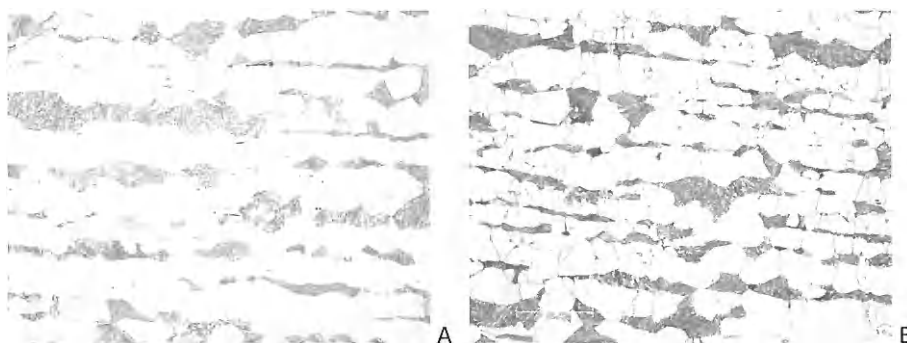


Figure 75: microstructure CRS. A: sample 7 B: sample 32 through optical microscope at (10x50) magnification. Bainite structure (OCAS, 2011)

Grain refinement is an effective means for improving the strength and lowering the ductile-brittle transition of structural alloys (Morris, 2001). Fine grains improve many properties of steels. When only considering the grain size, steels with finer grain size have better notch toughness than coarser-grained steels as a result of lower transition temperatures. Also, a small grain size improves bendability and ductility and it improves yield strength in quenched and tempered steel. There is also less distortion, less quench cracking and lower internal stress in heat-treated products. Austenitic-grain growth can be controlled by adding aluminum, titanium, zirconium, and vanadium to the alloy (Lankford, 2008).

7.3.1.4 Inclusions

Inclusions in metal generally have only negative influences. They reduce the mechanical properties of the steel, increase porosity, corrosion and increase the internal stress in the steel, resulting in premature failure (Kleber, 2006). Nonmetallic inclusions, particularly sulfide inclusions, are known to initiate corrosion on carbon steels (Robert, 2008).

The CRS sample is very clean with a limited amount of globular aluminum oxides and hardly any manganese sulfides (Figure 76, Table 29). Therefore it can be concluded that there is very little negative influence on the mechanical properties and corrosion resistance of this CRS as a result of inclusions.

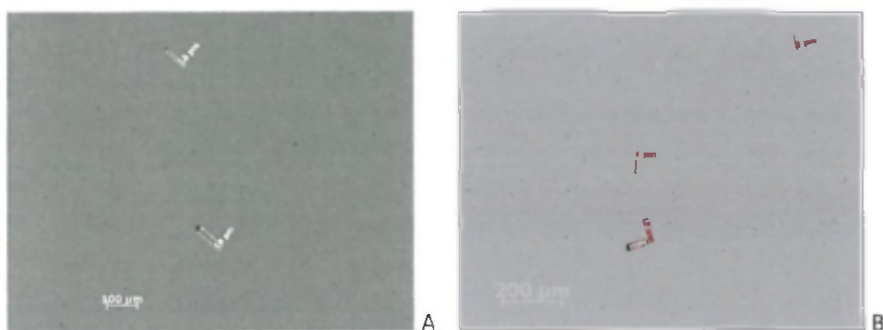


Figure 76: inclusions CRS. A: sample 7 B: sample 32 through SEM-EDX analysis, 100 times enlarged. Very few Aluminum oxide inclusions visible. No manganese sulfide inclusions detected.

Table 29: Total amount and length of inclusions CRS sample 7 and 32 as per ASTM E2142-08, expressed in µm.

a = _____ = manganese sulfide, single; b = = aluminum oxides, line;
c = _____ = manganese sulfide, line; d = . = aluminum oxide, single.

Nr 7/32	line number	max dimension in µm	a -----		b -----		c -----		d .	
			amount	dimen sion	amount	dimen sion	amount	dimen sion	amount	dimen sion
	1	5.5		0.0		0.0		0.0	2	11.0
	2	11.0		0.0		0.0		0.0	1	11.0
	3	22.0		0.0		0.0		0.0		0.0
	4	44.0		0.0		0.0		0.0		0.0
	5	88.0		0.0		0.0		0.0		0.0
	6	176.0		0.0		0.0		0.0		0.0
	7	353.0		0.0		0.0		0.0		0.0
	8	705.0		0.0		0.0		0.0		0.0
	9	1410.0		0.0		0.0		0.0		0.0
total			0		0		0		3	
total length				0		0		0		22

7.3.2 Mechanical properties

7.3.2.1 Hardness

The two CRS samples, respectively 7 & 32, were tested. Each sample was cut into three pieces 7.1, 7.2, 7.3 & 32.1, 32.2, 32.3. The results of the Vickers HV10 and HRB tests are given in Table 30.

Table 30: results KdG hardness measurements, according the Vickers HV10 and HRB tests. no unit.

Sample nr. 7	HV10	HRB	Sample nr. 32	HV10	HRB
7.1	168	85	32.1	171	84
7.2	172	87	32.2	168	84
7.3	165	84	32.3	169	85
Average	168	85,3	Average	169	84,3

By using the ASTM standards prognoses can be made regarding the tensile strength of the CRS steel. 169 HV10 corresponds with a tensile strength of approximately 550MPa satisfying the high tensile steel AH32 standard (Table 25). Since hardness tests are not compulsory for ship construction steel no reference statistical material is available.

7.3.2.2 Notch toughness

The results of the Charpy V-notch tests are presented in Table 31.

Table 31: results KdG notch toughness measurements as per Charpy V-notch test. Impact energy in J and notch impact strength in Jmm⁻².

	Sample nr.	Impact Energy [J]	Notch Impact strength [Jmm ⁻²]
Ambient temperature	7.1	172	2.15
	7.2	88	1.10
	7.3	90	1.12
	Average	(117)	(1.46)
	32.1	94	1.18
	32.2	90	1.13
	32.3	104	1.30
	Average	96	1.20
0°C	32.4	157	1.98
	32.5	170	2.14
	32.6	90	1.13
	Average	139	1.75
-20°C	32.1	188	2.34
	32.2	82	1.02
	32.3	84	1.05
	Average	118	1.47

We consider the impact energy value obtained for sample 7.1 at ambient temperature as an outlier. If we calculate the average value of the impact energy [J] over the remaining five samples we obtain 93.2J. This result and the average impact energy at 0°C is compared to the Bureau Veritas standards (2011) (Table 32).

Table 32: steel mechanical properties for different steel grades, Bureau Veritas, 2011.

Steel grade	Yield stress R _{eH} (MPa) min	Tensile strength R _m (MPa)	El.A ₅ (%) min	Average impact energy [J] min KVL longitudinal – KVT Transverse – t = thickness (mm)						
				Test temp (°C)	t ≤ 50		50 ≤ t ≤ 70		70 ≤ t ≤ 100	
					KVL	KVT	KVL	KVT	KVL	KVT
A	235	400/520	22	+20			34	24	41	27
AH32	315	440/570	22	0	31	22	38	26	46	31
AH36	355	490/630	21	0	34	24	41	27	50	34
AH40	390	510/660	20	0	39	26	46	31	55	37

The average impact energy of the CRS is well above the values as shown in Table 32.

The values AH32 for a thickness < 50mm are most relevant (shown in bold).

To validate the rather high outcome of the notch toughness impact test as performed at Karel de Grote University College (2012) we compared this result with data from a study by Vanderhorn & Wang (2011). Since the results for the five steel mills are very similar we show in Table 33 only one steel mill by way of example.

Table 33: statistical information for impact energy for ship building steels (VanderHorn & Wang, 2011).

Reference	Steel grade	Mean/Rule Value (IACS)	COV	N° of tests
Steel maker 1	A	6.561	0.183	45
	AH32	4.500	0.144	4927
	AH36	3.660	0.179	2067
	AH40	5.145	0.119	348

COV: Coefficient of variation = Standard deviation/Mean. The COV shows the variability in relation to the mean of the population.

The third column (Mean/Rule Value) shows how many times the average impact energy value [J] of the samples produced by steel maker 1, exceeds the minimum imposed by the International Association of Classification Societies (IACS) and this for A, AH32, AH36 and AH40 steel. Based on the totality of tests on the CRS, the average of the mean values was found to be 4.24 times the IACS nominal rule value. It can therefore be assumed that although the measured impact energy is way above the IACS nominal rule value this can be considered as normal.

7.3.2.3 Tensile strength and yield stress

Table 34 gives an overview of the different standards IACS standards, together with the obtained CRS values. Figure 77 shows the tensile strength curve, as obtained at the Karel de Grote Hogeschool, Antwerp.

Table 34: comparison yield stress (MPa), tensile strength (MPa) and elongation (%) of steel grades A, AH32, AH36 and CRS.

	A	AH32	AH36	CRS
Yield Strength R_{eH} ($R_{p0.2\%}$) (MPa)	235	315	335	310
Ultimate tensile strength R_m (MPa)	400-520	440-570	490-630	572.20
Elongation A_5 (%)	22	22	21	29.75

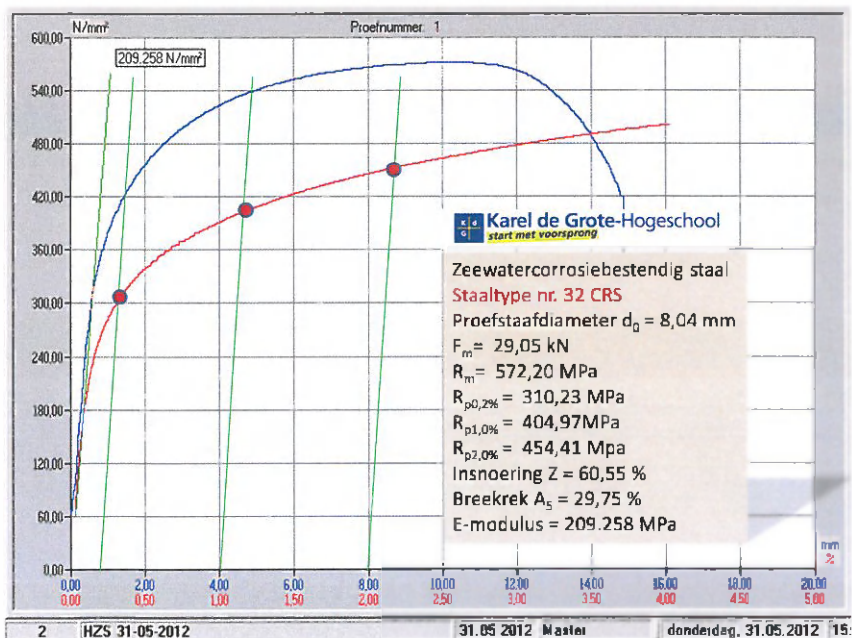


Figure 77: tensile strength (N/mm or MPa) diagram of CRS.

Table 35 represents the yield strength for ship building steel, derived from the Vanderhorn & Wang study (2011). The values given in column two till five show how many times the average yield stress (R_{eH} or $R_{p0.2\%}$ in N/mm^2) of the samples produced by steel maker I till V exceed the minimum imposed by the International Association of Classification Societies (IACS) and this for A, AH32, AH36 and AH40 steel.

Table 35: statistical information for yield strength (MPa) for ship building steels from different steelmakers (2004-2009), related to the IACS standard, based on Vanderhorn & Wang (2011).

Steel grade	Steel maker I	Steel maker III	Steel maker IV	Steel maker V	Average steel maker	IACS value	Average x IACS value
A	1.228			1.287	1.26	235	296.10
AH32	1.204			1.182	1.19	315	374.85
AH36	1.188	1.17	1.199	1.154	1.18	355	418.90
AH40	1.196				1.20	390	468.00

The mean value of the yield stress is, on average, about 1.21 times the nominal value. Separating the data by the steel type, it can be seen that grade A steel is on average 1.26 times the nominal value and high strength steel (AH32) 1.19 times the rule (IACS) nominal value (Vanderhorn & Wang, 2011). The yield stress value of the CRS is 310.23MPa. We note that is this is very close to the minimum IACS value (315MPa) applicable for AH32 steel (Table 35). Compared with the present industrial standard, CRS is situated only slightly above the average grade A value (296.10 MPa).

Table 36 gives the ultimate tensile strength for ship building steel, again derived from the Vanderhorn & Wang study (2011).

Table 36: statistical information for tensile strength for ship building steels from different steelmakers (2004-2009), related to the IACS standards, based on Vanderhorn & Wang (2011).

Steel grade	Steel maker I	Steel maker III	Steel maker IV	Steel maker V	Average steel maker	IACS value min	IACS value max	Average x IACS min	Average x IACS max
A	1.095			1.129	1.112	400	520	444.8	578.24
AH32	1.134			1.202	1.168	440	570	513.92	665.76
AH36	1.094	1.163	1.126	1.11	1.123	490	630	550.39	707.65
AH40	1.11				1.110	510	660	566.1	732.6

The average of the mean value for the tensile strength is 1.13 times the nominal rule value. CRS, which has an ultimate tensile strength of 572.20 MPa, is well within the IACS range of AH36 steel but compared to present industrial standard, it meets only the grade A level. Table 37 shows the percentage elongation for the studied samples by Vanderhorn (2011).

Table 37: statistical information for elongation for ship building steels (2004-2009) related to the IACS standard, based on Vanderhorn & Wang (2011).

Steel grade	Steel maker I	Steel maker III	Steel maker IV	Steel maker V	Average steel maker	IACS value (%)	Average x IACS
A	1.323			1.577	1.45	22	31.90
AH32	1.186			1.382	1.28	22	28.25
AH36	1.119	1.278	1.028	1.417	1.21	21	25.42
AH40	1.08				1.08	20	21.60

The average elongation of the five steelmakers is 1.25 times the IACS nominal rule value. The elongation A_5 of CRS is 29.75%. This can be defined as excellent and is above IACS and present industrial standards.

7.3.2.4 Suitability for welding test

The practical test at Antwerp Ship Repair gave satisfactory results and according the specialist welder this CRS material welded as good as ordinary ship steel.

A Vickers hardness test was done on the weld. The maximum hardness measured is situated between 280 & 350 HV. Therefore the risk of hydrogen induced cold cracking in the heat affected zone is limited and in general welding without heat treatment is possible (Figure 78).

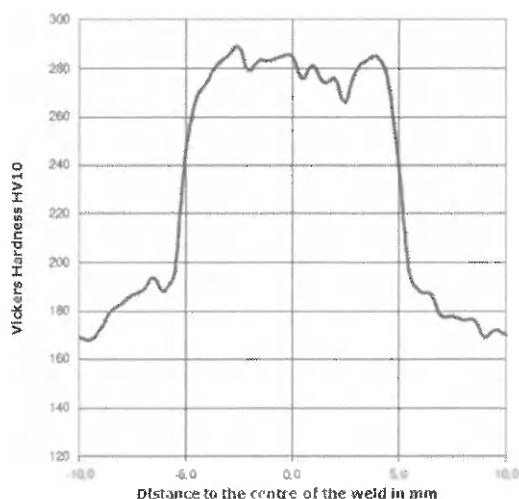


Figure 78: Vickers hardness fluctuations (no unit) in CRS weld, related to the distance to the center of the weld in mm.

The carbon equivalent was calculated with two different methods.

The AWS formula (Eq. 76) generated a carbon equivalent value of 0.76%. This value is rather high. Through experience 0.45% (Lloyds Formula) has been determined to be limiting value at which satisfactory welding results can be obtained under shipyard conditions without excessive preheat (Templeton, 2006).

Since the carbon concentration in the CRS is rather low a more reliable result should be obtained by the Ito and Bessyo equation (Eq. 77) resulting in a carbon equivalent of 0.22269%. With this value, the cracking parameter (PC) and the critical preheating temperature can be calculated (Smet, 2000). We hereby considered two different cases.

First, welding performed with classical rutile electrodes and a H_2 concentration of $10\text{cm}^3/100\text{g}$ and an assumed plate thickness of 15.5mm. This gave a PC of 0.415 and a critical preheating temperature of 206°C.

Then the calculations were done with basic electrodes, MAG or TIG welding with a H_2 concentration of $5\text{cm}^3/100\text{g}$, resulting in a PC of 0.332 and the critical preheating temperature of 85°C.

The above results have been checked with the Yurioka method that takes additionally into account the heat input from the welding process. The outcome of this method shows that the MAG and TIG welding process requires a preheating of 14.8°C which can be considered as negligible while when rutile electrodes are used a preheating temperature of 62°C is necessary (Yurioka, 1981), which is too high for welding operations in a shipyard.

7.4 Conclusions

The present study was designed to determine the chemical and mechanical characteristics of the corrosion resistant steel sample in our possession and to determine the possibility for use as ship construction material in ballast tanks of merchant vessels.

The chemical composition show and increased concentration of chromium, aluminum, and molybdenum and a reduced concentration of carbon and copper, resulting in a weight reduction of 1.5-5%.

We were able to prove a significant better resistance to corrosion in a saline environment compared with ordinary grade A and AH steel. It remains difficult to demonstrate the exact influence of every single alloying element on the corrosion behavior. Most probably the solution lies within the symbioses of the different composing elements of which the activity is function of environment and time.

Our approach was pragmatic. However it would be nice and favorable to have a better understanding of the physical, chemical and even biological processes involved.

We have put considerable effort into revealing the hidden secrets and consulted many national and international corrosion authorities, unfortunately without any result. Most probably the exact mechanisms are yet unknown. At this point this is discouraging but it also indicates that further and deeper research is necessary and most probably this will result in exciting innovative steel grades.

When it comes to the mechanical properties of this steel, the results of this study indicate that the samples are satisfying the applicable international rules and regulations. The notch toughness is rather high, but can be considered as normal. Hardness tests are not compulsory for ship construction steel, but the steel satisfies the standard for high tensile steel. Welding is possible without preheating with TIG or MAG (low H_2 welding system). Therefore, approving this steel for ballast tank construction should not be a problem. 2 major classification societies, ABS and LR, were consulted concerning this matter, but no answer was received at the moment of publication.

8 Discussion and conclusions

The work presented here is part of the research concerning corrosion in ballast tanks of merchant vessels that was developed over the last five years at the Antwerp Maritime Academy. Within the scope of the initial objective, the development of a maintenance free ballast tank, it was the purpose of this particular study to discover which of the physical and/or chemical properties of ship construction steel are most relevant to the corrosion rate. This knowledge might lead to the introduction of innovative steel alloys, resulting in a new methodology of ballast tank construction, including the possibility of a more environmental friendly design.

Improvement of the corrosion resistance of the ship's construction benefits the overall safety of the vessel, its cargo and crew. Moreover, corrosion represents a major cost to the shipping industry (Chapter 1). Maintenance and repair in ballast tanks are very difficult and consequently expensive. Steel replacement jobs, performed under difficult conditions, often create excessive stresses near the inserts and do not always improve the overall condition of the ship (NSRP, 2012). A better corrosion resistance therefore also reduces the expenses of ship maintenance and so the operation cost for the ship-owner. This is a lucky match between ship safety and economics. Usually, the ship owner is not so keen on investing in ship safety, as his investment often fails to pay off directly in terms of profit, but rather results in a reduction of expenses as a result of a decrease in the overall occurrence of accidents on board.

Ship owners that sell their newly built ship after eight to ten years before the first important expenses emerge are not interested in the condition of their vessel on a long term. However, this study is not governed solely by the economic concerns of the first owner. A broader viewpoint should dominate. When sold, these ships keep on trading and should adequately protect crew and cargo. There is an increased economic awareness in the shipping industry. In the future, the lifetime of ships will be stretched beyond the actual accepted 25 years. Often a ship is considered to be a trading commodity and an owner will sell it when the occasion arises. Due to the extreme cyclicity of the shipping markets, important opportunities exist, when cautiously timed, to buy low and sell high (Figure 79) (Tsolakis, 2003).



Figure 79: what matters in shipping, cartoon (Sheppard, 2012).

Previous research at the Antwerp Maritime Academy by the corrosion research team, presented in the Ph. D dissertation of Capt. De Baere (2011), quantified the corrosion in ballast tanks of merchant vessels after in situ investigation of more than 140 vessels by means of a self-developed corrosion index. Using time dependent linear regression, the influence of ship specific parameters such as land of construction, trading area, coating, ship type and length was thoroughly studied. No significant correlations could be established.

The in situ research is definitely not finished and the database is being completed upon arising opportunities. Every ship added to the database results in a more reliable outcome. Today, we can already present a better understanding of the corrosion process and some of the influencing elements. For example, remarkable results were obtained when studying the protection of ballast tanks with sacrificial anodes where the advantage of these anodes could not be established. Further research showed that the positioning and distribution of these anodes plays an important role in the optimal operation.

This aspect required more attention. Hence, in 2012, the Antwerp Maritime Academy started a project investigating this phenomenon more in depth. Through a 3D CAD program, Solid Works, a ballast tank model of an existing ship (2P and SB of the Flanders Harmony, an LPG tanker owned and managed by Exmar) was built including the true to life distribution of the anodes (Figure 80). The theoretical protection of the tank by the sacrificed anodes was calculated through CPmaster (Elsyca, 2012). At this moment, the outcome is being compared with reality, recorded during an in situ inspection of the ship while in dry dock, Bahrain, December 2012.

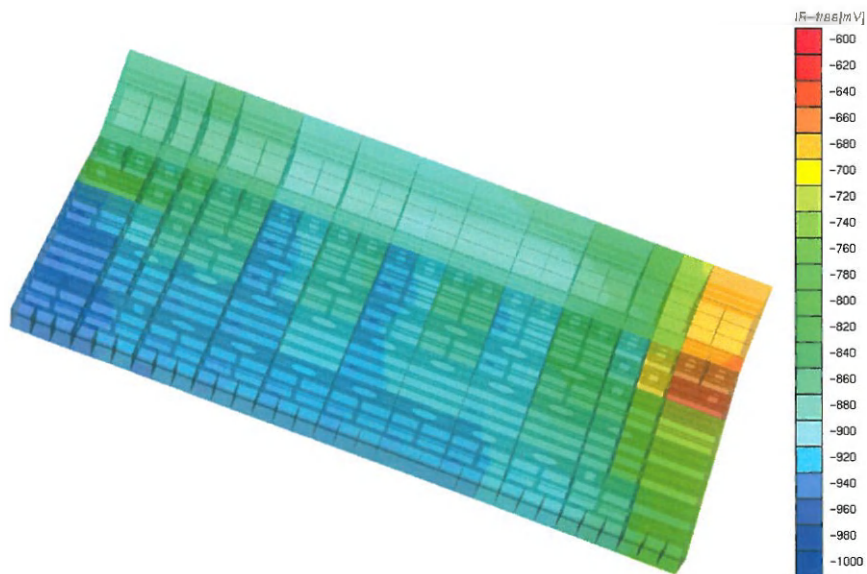


Figure 80: CAD model of ballast tank (18m x 42m), (Elsyca, 2013), with indication of the protection by sacrificial anodes. Blue zones are overprotected, green are well protected zones, red are under protected. Polarization data are based on a current demand of 1.2 mA/m^2 (given a coating in excellent condition).

The work of Capt. De Baere (2011) comprised an economic study comparing five different ways of ballast tank construction. This study was further improved in this work (Chapter 1) through a refinement of the parameters, an actualization of the prices and a modification of the model. A Monte Carlo analysis simulated the probability of certain outcomes by running multiple simulations, using random variables. This study, accepted for publication in *Marine Structures*, forms the link between the work of Capt. De Baere (2011) and the work presented here. Although the study concluded that the present way of ballast tank construction, using grade A steel and corrosion protection with epoxy coating in combination with sacrificial anodes is today the best economic choice, it also confronted us with the possibility that the steel quality used for ballast tanks might have an influence on the corrosion rate and required further investigation.

This brings us to the main objective of this dissertation: to investigate how the steel quality of grades used in ballast tanks influences the corrosion rate and to explain the determining parameters of this process.

With the help of mainly Antwerp Ship Repair, DEME and EXMAR a total of 40 steel plates (30 x 50cm) were gathered, directly cut out of the hulls of ships calling at a dry dock for steel repair work. This sample set comprises plates from various types of vessels and from vessels constructed at different construction yards worldwide. Moreover, with the help of the American Bureau of Shipping we obtained 2 samples (30x50cm) of experimental corrosion resistant steel (CRS), alloyed by POSCO, Korea, especially

developed for use in a saline environment. This added an new dimension to the research and introduced the possibility to test the hypotheses formulated in the economic study.

A test facility was built from scratch at the premises of the Antwerp Maritime Academy (Chapter 5). Natural North Sea water was used. The chemical composition, microstructure and inclusions of every plate were determined (Chapter 4) and the corrosion rates were monitored and evaluated after six, ten, twenty and twenty-four months through weight loss measurement. Electrochemical measurements were used as point of comparison and confirmed the outcomes of these weight loss measurements. A photographic corrosion quantification technique was attempted and together with an ultrasonic thickness loss measurement discarded.

Statistical analysis of the findings suggests that in general IACS grade A and AH steel qualities used for ballast tank construction have similar corrosion rates and that the influences from fluctuations in chemical composition on the corrosion are not significant. Robust PCA analysis applied on the experimental data resulted in three distinguished clusters of steel types A, AH and CRS. The corrosion rates of both grade A and AH steels are nearly identical. The CRS added to the experiment defines the third cluster and forms an exception to this conclusion. A corrosion rate gain between 30% and 50% was noted. The combination of a bainitic layered structure, higher Cr, Al and Mo and lower C and Cu concentrations suggest a better corrosion resistance to seawater exposure.

The observed reduced corrosion rate of the CRS sample raised additional questions. First, an explanation for the significant corrosion moderation must be given. This was done in depth in chapter 6 and the time frame is reflected further in this discussion. Then, it must be assured that the steel is suitable for ballast tanks of merchant vessels. This was confirmed by the outcome of the different physical and mechanical tests of chapter 7.

The results of the experiments determining the mechanical properties of the CRS samples were positive. The values for ultimate tensile strength meet the requirements for high tensile steel. The yield strength of 310MPa is very close to the minimum value of 315 MPa required by IACS. Notch toughness, tensile strength and yield stress tests of the CRS all had a positive outcome. Practical welding tests performed at Antwerp Ship Repair by a qualified welder following standard procedures and in the KdG workshop provided a first impression on the weldability, which was subsequently evaluated as good. The calculations on the carbon equivalent were done with the formula of the American Welding Society and the equation of Yto and Bessyo for low carbon concentrations. The CRS is a low carbon steel and the results of the calculation suggests that the preheating required for MAG and TIG welding with standard rods is negligible.

The microstructures of the A and AH samples show a large diversity. In general it is accepted that small grain sizes have better strength and wear resistance and have an influence on the electrochemical behavior of the steel and consequently on the corrosion rate (Ralston, 2010). Scientists agree on the positive effect of grain refinement, but the work on fundamental understanding of the way grain size affects the corrosion rate is very limited. Ralston states that existing literature is often contradictory, even within the same alloy class, and a coherent understanding of how grain size influences corrosion response is largely lacking (Ralston, 2010).

The grain size of the CRS was defined as being medium sized, and in the context of what is described in the previous paragraph, this cannot be considered as a positively or negatively influencing element in the corrosion performance of this steel grade.

Multiple studies confirm the negative effect of non-metallic inclusions on the corrosion resistance of steel (Wang, 1996, Steward, 1992, Gubenko, 2011). Scientists state that corrosion resistance is higher for clean steel, having little inclusions. During our experiments, we investigated the amount of aluminum oxides and manganese sulfides in the steel samples. The amount of inclusions found in the steel samples varied substantially. The CRS samples proved to be very clean, with almost no inclusion, which is of course a very positive outcome. However, with a very small sample size (<1cm²), transferring results to bulk material must be done with the necessary caution.

The conclusion of chapter 6 and 7 is that CRS is most probably acceptable as ship construction steel. The final decision lies with the Classification Societies. We approached two IACS members with this question but up till now no answers were received.

These CRS test results generated an impact on the generic economical study presented in chapter one. Case IV of this study was based on the supposition that steel replacement during dry dock could be eliminated by using a superior steel quality with limited corrosion rate. Based on the chemical composition and the concentration of the various elements, it was suggested by Arcelor Mittal that this CRS will cost about 30% more than ordinary grade A steel. The conclusions showed that the use of CRS is a valuable economical choice only when the price is not over 110% of the normal grade A steel price. The Monte Carlo analysis, taking into account the variability of the different significant parameters, confirms this.

As all basic resources become scarcer, a price drop this is not likely to occur in the near future. Nevertheless, we are convinced that finally the green public awareness will be reflected in the rules and regulations, so that environmental friendly designs will prevail.

The observed reduced corrosion rate suggests an implication on the plate thickness and the corresponding weight. However, this effect is rather limited. The ballast tanks of our

theoretical Panamax bulkers are constructed in 14mm plate and the classification rules require a minimum of 11mm plate thickness without the corrosion allowance (IACS, 2012). This means that reductions are only applicable on the corrosion allowance of 3mm. Calculations show that this reduction in 25 years is about 0.68mm. Given the reduced density of the steel, calculated based on the composing elements, this results in a weight reduction of approximately 5%. This reduction was incorporated in case IV of the economic model.

The findings presented suggest the feasibility of applying new corrosion resistant materials in ship construction might be confirmed by the appearance on the market of a new steel grade AMLoCor (Arcelor Mittal, 2011) for seaport constructions. The conditions in this environment are comparable with the situation in a ballast tank. AMLoCor is a low carbon steel grade with 1.5% Cr and 0.65% Al and a non-specified concentration of Mo. Arcelor Mittal studies resulted in a substantial reduction in steel loss by a factor three to five, depending on the exposed zones (Arcelor Mittal, 2011). The results in our study were not as spectacular as those of the AMLoCor steel, but they still offer sufficient new opportunities.

The current study was unable to explain in a conclusive way why certain steel grades corrode less fast. Chapter 7 contains an effort to draw parallels between our findings, literature and similar research programs. It is obvious that the answer, when disclosed, will not be as clear-cut as we would like. The secret is most probably a complex symbiosis of alloying elements, physico-chemical characteristics and environmental conditions.

The current research was limited by its time frame. Corrosion was investigated for a period of 2 years. Stretching these results to 25 years or more, with sufficient accuracy, requires longer and/or accelerated experiments. It was assumed that the influences of the different alloy elements will continue to have the same effect in the future. This might however not be true. In his 2003 paper, Melchers gives an overview (Table 38) of several comprehensive test programs for coupons immersed at different locations in a seawater environment. The effect of Cr turned out to be positive for a limited period. Blekkenhorst (1986) specifies a time span of 7.2 years. Southwell (1969) states that “3% and 5% chromium steels had initial corrosion losses in seawater lower than those of carbon steel, but beyond 4 years the advantage was reversed. After 16 years the chromium steels showed 22 to 45% higher losses than ordinary steel”. The studies that investigated the influence of Mo all appointed this element as being beneficial and reduces the corrosion rate. It is interesting to note that Blekkenhorst (1986) combines this Mo effect to a low Cr-Al concentration and that his results show a complex non-linear influence. Additions of Mo up to 0.5% are beneficial, but higher concentrations have no effect on the corrosion rate (Melchers, 2003). The same paper describes Al as being beneficial to the corrosion rate on the long term for concentrations up to 1,5%.

Petersen (1977) especially formulates this effect in the combination with Cr. When combining this with the findings of Blekkenhorst (1986), Cr can have its effect in the first years and then Al can take over, as its effect is more beneficial on the long term. Further experimental investigations are needed to estimate the corrosion performances of the CRS for extended periods.

Table 38: effect of small composition changes to corrosion rate, summary of various long term studies (Melchers, 2003).

Alloying element	Hudson and Stanners (1955)	Forgeson et al. (1960)	Schultze and van der Wekken (1976)	Peterson (1977)	Blekkerhorst et al. (1986)
Cr	<ul style="list-style-type: none"> - Beneficial - More advantages over shorter exposure periods (<2y) 	<ul style="list-style-type: none"> - Initially beneficial, - Negative influence after about 4 years, 	<ul style="list-style-type: none"> - Initially beneficial, - Negative long-term 	<ul style="list-style-type: none"> - Strongly beneficial, certainly in combination with Al 	<ul style="list-style-type: none"> - Beneficial for up to 7.2 years
Mo			<ul style="list-style-type: none"> - Beneficial long term 	<ul style="list-style-type: none"> - Moderately beneficial 	<ul style="list-style-type: none"> - Beneficial for low Cr, Al concentrations - Complex nonlinear influence
Al	<ul style="list-style-type: none"> - No clear effect 		<ul style="list-style-type: none"> - Beneficial long term 	<ul style="list-style-type: none"> - Beneficial, - Particularly with Cr 	<ul style="list-style-type: none"> - Beneficial, particularly long term

When studying the CRS, similarities with Cor-Ten steel were noticed. CRS and Cor-Ten are both passivating alloys, but Cor-Ten does not resist chlorides while CRS does. We believe aluminum plays a key role in this process. To investigate this, very recently a cooperation with the University of Liège was initiated. SEM-EDS and crystalline structure characterization will be applied on 3 samples (2 CRS and 1 reference grade A) to discover the role of aluminum in the oxide layer, to define to the exact position of the aluminum in the goethite and to disclose its function.

The research on corrosion of ballast tanks on board merchant vessels is certainly not finished, but the findings of this study already can have a number of important

implications for future practice. On the other hand, it is too early to formulate specific advices to the ship owner, as there are still a lot of unknown parameters which require further investigation. This Ph. D dissertation can therefore be considered as the second part of an overarching triptych, the overall objective of which is to equip a ship owner with a set of achievable recommendations in order to stretch the lifetime of the ballast tanks on board his ship up to and beyond the economic life time expectancy of 25 years. Already the first steps have been taken to initiate the third and final part. Two new lines of research will be opened. The first one will resume and carry forward the anode story, the second one will concentrate on ballast tank coatings and more exactly on the correct influence of the application conditions on the final quality.

Recommendations for further research

Ship construction is an important steel consumer challenging steel mills to enlarge their research and development on corrosion resistant materials. It is the final objective to find a way of ensuring the 25 years of life expectancy of a ship without steel replacement and maintenance as a consequence of corrosion. Steel degradation is mainly caused by seawater contact. The availability of class approved CRS could limit these corrosion consequences, improve safety and yield an economical advantage. This superior steel quality can also have numerous other applications, where the corrosion resistance is very critical and the reliability of the construction of the utmost importance. In this context, windmills, port constructions and other difficult accessible area in contact with seawater can be given as an example.

To reduce the cost, it might be an option to introduce clad steel into the ballast tanks. Clad steel plate is a composite steel plate made by bonding specific steel material (cladding material) to either or both sides of a carbon steel or low alloy steel plate (base metal) (JFE, 2012). It is maybe possible to combine best of both worlds: the strength of the base material at a low cost, with the specific features such as corrosion resistance of the cladding material, and this at a lower cost compared to products made entirely out of the top layer material. It would therefore be interesting to repeat the experiments described in this work with other steel grades that have increased Al/Cr concentrations. Some of these grades are available on the market for other purposes (such as AmLoCor) but they might perhaps also serve for ballast tank construction. The comparison of these steel grades with the CRS would definitely place the research in a wider context.

Another option to reduce the cost of this CRS is to look at the protection measures. It would therefore be interesting to assess the long term effects if this steel is used without any coating or sacrificial anodes. It is now compulsory by PSPC regulation (IMO, 2006) to have a light epoxy coating on the ballast tanks surface, but this does not mean

that other options for further development are not open for consideration. If a steel quality is produced with a very low corrosion rate thanks to a protective rust layer, sufficiently adhesive to the base material, also in a seawater environment, coating and protection with anodes might become obsolete. Without any doubt this is extremely beneficial to the maritime ecosystem, these days already under ultimate stress by pollution and overfishing. No paint and no anodes means less introduction of heavy metals and solvents. Only iron oxide, which is one of nature's basic materials, is reintroduced into its natural habitat. A possible drawback of the omission of a coating system is the dark color of the ballast tanks. Previous, tanks were coated with coal tar epoxy, which was a good coating, but had some very important downsides. As the coating was black, inspection of the tanks was very difficult. A dark color also increases the risk for slips and trips, a safety concern that cannot be underestimated. Besides this, coal tar is classified as a carcinogen and can cause skin problems, another important negative aspect.

A complete other approach is the N.E.I VOS™ (Ventury Oxygen Stripping) system, which can be used in both empty and filled tanks. They claim to reduce the corrosion rate up to 84% by adding low-oxygen inert gas into the ballast tank, maintaining the oxygen level below 4% (NEI, 2012). The results of experimental data after 30 and 270 days exposure are given in hereunder (Table 39, Figure 81).



Figure 81: corroded plates after 270 days exposure splash zone. Left with VOS, right without VOS (NEI, 2007).

This system is already installed on the Belgian TI tankers and has proven his effectiveness.

Table 39: corrosion reduction in percentage for COS system after 30 and 270 days exposure (NEI, 2007).

Environment	30 days exposure	270 days exposure
Splash zone	-40%	-38%
Humid	-78%	-84%
Buried	-14%	-20%

This study has demonstrated that the development of a superior CRS at a balanced price creates most certainly the possibility to construct maintenance free ballast tanks with a life span of at least 25 years. The principal drawback is that these steel grades require expensive alloying elements ever growing scarcer. Painting is and will remain the principle protection of immersed steel structures for the coming years. A follow-up study could assess the impact of correct coating and coating application on metallic structure degradation. It has been estimated that approximately 75% of all premature coating failures are caused by inadequate or improper surface preparation (Nace, 2012). Surface preparation on new steel includes degreasing, removal of the mill scale,

rounding of edges and removing of weld spatter. During maintenance and repair work on coated surfaces, loose coating has to be removed and the transition between coated and uncoated surface must be feathered. This surface preparation will make the difference between a poor and adequate coating system¹⁴. How this is to be ascertained and controlled in a shipyard environment or by the ships' crew during a sea transit is another important question and start of a complete new research program.

If the coating debate is to be moved forward, a better understanding of epoxy coatings and possible alternatives needs to be developed. At the Antwerp Maritime Academy, experiments have been performed with protective films, today already used to cover airplanes and busses. These films are more flexible than traditional coatings, which harden and become brittle in time. Impact from tugs or loading- and discharging equipment may cause cracks and consequently coating failure, which can be avoided with these films. The application on welds, corners and stiffeners has still to be investigated. Other flexible coatings can be developed too, as an alternative for the traditional PSPC epoxy coating system. The same elements of concern, already mentioned in the previous paragraph, apply.

All the above mentioned elements would benefit from a corrosion friendly design. Nowadays, ship design is concentrated on maximizing the cargo carrying capacity. To ascertain this, all construction elements are removed out of the holds or cargo tanks and relocated in the surrounding compartments, including the ballast tanks. In their final report on commercial ship design and fabrication for corrosion control, Parente et al (1996) already give suggestions for a corrosion friendly design. These include the minimization of horizontal structures which can trap water, the provision of sufficient drain cut-outs and sloping structures to facilitate drainage and prevent accumulation of sediment, the provision of contoured metal surfaces (plate edges) and minimized shadow areas to facilitate application of coatings and modification of scantlings to effect a stiffer structure, which is thought to lead to lower corrosion rates (Parente, 1996).

Another option would be to keep the double hull, surrounding the cargo tanks, dry and to create separated ballast tanks that contain no structural elements. This idea was suggested by the Japanese classification society Class NK (1996) (Figure 82). In this concept, double hull spaces are designed as void spaces and the ballast tanks are incorporated as two pairs of large wing tanks positioned in the inner hull. The initial cost for construction will be higher, but the maintenance cost will drop significantly, as the ballast tanks are simple tanks without structural elements (NRC, 1998).

¹⁴ Lifetime protection with paint is certainly possible. In December 2012, we performed an inspection on board of the Flanders Harmony, a 20 year old LPG tanker. An average corrosion rate of only 3% was noted. This example supports the large variation in corrosion rate for ships older than 15 years.

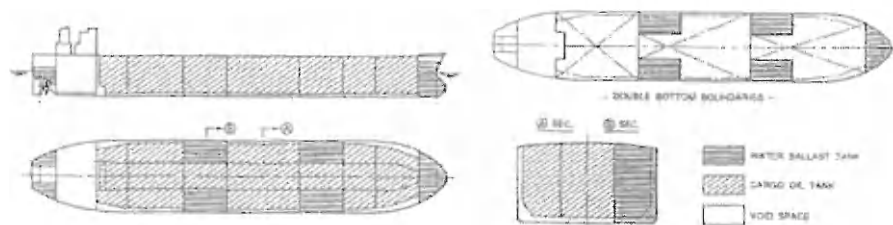


Figure 82: void space overview double hull tanker (Akiba, 1996).

The ultimate solution that will prevent the problem of corrosion in ballast tanks is of course the elimination of the ballast tanks. Projects at the university of Michigan (USA) and the TU Delft (The Netherlands) show that a complete redesign of the traditional ship is possible and makes the need for ballast water superfluous. The Michigan project was proposed back in 2008, mainly as a combined solution to reduce cost and to eliminate the transport of invasive aquatic species through the ballast water (University of Michigan, 2008). The elimination of the corrosion problem in these tanks can only speak in favor of this project. The worldwide economic crisis that started back in 2008 and still continues today however does not create a positive environment to support any new innovative developments that require a drastic change in ship construction.

9 Bibliography

Abbaschian, R., Abbaschian, L., Reed-Hill, R.E., *Physical Metallurgy Principles*, fourth edition, Cengage learning, USA, 2009.

ABS, *Generic rules for condition of classification, materials & welding and survey after construction*, ABS, USA, 2012.

ABS, *Guidance notes on the Inspection, Maintenance and Application of Marine Coating Systems*, Third edition, Houston, USA, 2007.

Agarwal, B.K., *Introduction to Energy Dispersive X-ray Spectrometry (EDS)*, 2nd ed, Springer, Berlin, Germany, 1991.

Ahmad, Z., *Principles of Corrosion Engineering and Corrosion Control*, Oxford, UK, 2006.

Akiba, T., Kitano, K., Yamauchi, Y., Ito, H., Tsukuda, H., Emi, H., Kumano, A., *Void double hull space type VLCC*, ClassNK technical bulletin, Japan, 1996.

All about Science, *Second law of Thermodynamics*, <http://www.allaboutscience.org/second-law-of-thermodynamics.htm>, USA, as per 2012.

Al-Mansour, F., Kozuh, M., *Risk analysis for CHP decision making within the conditions of an open electricity market*, Energy 2007.

Aloui, R., *Development of a generalized life cycle cost/earning model for tanker ship structure based on effective cost assessment of the corrosion, maintenance and scantling design variables*, Master thesis, Université de Liège (ANAST), 2010.

American Chemical Society, *Element-Specific Chromatographic Detection by Atomic Emission Spectroscopy*, American Chemical Society, 1992.

Arab Shipbuilding and Repair Yard Company, <http://www.asry.net>, as per December 2011.

Arcelor Mittal, AMLoCor, *product brochure*, Arcelor Mittal, 2011.

Arcelor Mittal, AMLoCor, *technical data sheet*, Arcelor Mittal, 2011.

ArcelorMittal, *datasheet A 3.5, Lloyd's ship hull steel – 2001 Normal and Higher Strength Steel Plate for Hull Construction*

Arnaud, P., *Chimie Physique*, 6e édition, Dunod, Paris, France, 2007.

Asahi, H., Kushida, T., Kimura, M., Fukai, H., Okano, S, Role of Microstructures on Stress Corrosion Cracking of Pipeline Steels in Carbonate-Bicarbonate Solution, Corrosion, USA, Nace, 1999.

ASM Handbook, Vol. 4, Heat Treating, ASM International, Ohio, USA, 1991.

ASM international, ASM Specialty Handbook: Aluminum and Aluminum Alloys, ASM international, USA, 1993.

ASM International, Weld integrity and performance, ASM international, USA 1997.

ASM, Corrosion, Understanding the Basics, ASM International, Ohio, USA, 2000.

ASTM A131 /A131-M, Standard Specification for Structural Steel for Ships, ASTM, USA, 2008.

ASTM E2142 - 08 Standard Test Methods for Rating and Classifying Inclusions in Steel Using the Scanning Electron Microscope, ASTM, USA, 2011.

ASTM E45 - 11 Standard Test Methods for Determining the Inclusion Content of Steel, ASTM, USA, 2011.

ASTM G46 – 94, Standard Guide for Examination and Evaluation of Pitting Corrosion, ASTM, USA, 2005.

ASTM, ASTM E23, Standard Test Methods for Notched Bar Impact Testing of Metallic Materials, ASTM, 2007.

Atkins, P.W., Beran, J.A., General Chemistry, second edition, Scientific American, New York, USA, 1992.

Baldwin, L., Techno-Economic assessment of New Coating application for New-Building Marine Production, Ph D thesis University of Newcastle Upon Tyne, 1995.

Bangert, A. Introduction to mineralogy, section 3: Crystal structure and crystal system, unpublished course material, University of California, USA, as per 2012.

Bardal, E. Corrosion and Protection, Springer-Verlag, London, UK, 2004.

Bartholomew, R.D., Shifler, D.A., Marks' Standard Handbook for mechanical Engineers, Section 6: Materials of Engineering, 6.5: Corrosion, 2008.

Baumgartner A.W., Practical Engineering of Corrosion Control, Journal of Petroleum Technology, Society of Petroleum Industry, 1964.

Bhadeshia, H.K.D.H., Interpretation of the Microstructure of Steels, University of Cambridge, UK, 2008.

Boardman, A.E., Greenberg, D.H., Vining, A.R., Weimer, D.L., Cost benefit analysis, Upper Saddle River, New Jersey: Pearson Education Inc., 2006.

Bogaerts, W., Zheng, J., Course Corrosion Chapter 3: Corrosion Mechanisms: Some Basic Understanding, KUL, Belgium, 2008.

Bogaerts, W.F.L. e.a., Handboek constructiematerialen, corrosie en corrosiebescherming, Kluwer, Belgium, 2004.

Britz, D., IR Elimination in Electrochemical Cells, Journal of Electroanalytical Chemistry and Interfacial Electrochemistry, Elsevier, 1978.

Brown, R.S., Savage I., The economics of double hulled tankers, Marit. Pol. MGMT 23, 1996.

Brown, T.L., LeMay, H.E., Bursten, B.E., Murphy, C.J., Woodward, P., Chemistry, The Central Science, eleventh ed. Pearson, USA, 2009.

Budinski, K.G., Materiaalkeuze voor technici, 3th ed., The Netherlands, Academic service, 2003.

Bureau Veritas, Mechanical properties of Carbon Steel, Materials and Weldings, chapter 2, Steel and iron products, section 1, Rolled steel plates, sections and bars, article 2, Normal and higher strength structural steels, 2011.

Charlesworth, P., Thermodynamics: Entropy, Free energy and Equilibrium, chapter 17, 2004.

Chieh, C., Nernst equation, University Waterloo, Ontario, Canada, 2010.

Clover, D., Kinsella, B., Pejic, B., Demarco, R., The influence of microstructure on the corrosion rate of various carbon steels, Journal of applied Electrochemistry, 2005.

Community of European Shipyard Associations, Report 24, 2011.

Connors, K.A., Chemical Kinetics, The Study of Reaction Rates in Solutions, VCH Publishers, NY, USA, 1990.

Cottis, B., Corrosion Measurement Techniques, The Centre for Process Integration, Manchester, UK, 1995.

Croux, C., Ruiz-Gazen, A., High breakdown estimators for principal components: the projection-pursuit approach revisited, Journal of Multivariate Analysis, Elsevier, 2005.

Cuproban, <http://www.cuproban.com/anodes.htm>, as per January 2012.

De Baere, K., Corrosion and paint, unpublished course Antwerp Maritime Academy, Antwerpen, Belgium, 2008.

De Baere, K., Corrosion in ballast tanks on board of merchant vessels, In situ study of the significant parameters, UPA University press Antwerp, Belgium, 2011.

De Baere, K., Verstraelen, H., Lemmens, L., Lenaerts, S., Potters, G., In situ study of the parameters quantifying the corrosion in ballast tanks and an evaluation of improving alternatives, NACE Conference Papers, Houston, USA, 2011.

De Baere, K., Verstraelen, H., Rigo, P., Van Passel, S., Lenaerts, S., Potters, G., Study on alternative Approaches to Corrosion Protection of Ballast Tanks using an Economic Model, submitted for publication, Marine Structures, Elsevier, 2012.

Degarmo, E.P., Black, J.T., Kosher, R.A., Materials and Processes in Manufacturing, Wiley, USA, 2007.

Dekkers, R., Nonmetallic inclusions in liquid steel, KU Leuven, Belgium, 2002.

Department of Chemistry, The University of North Carolina at Chapel Hill together with Shodor, Chemical Thermodynamics,
<http://www.shodor.org/unchem/advanced/thermo/index.html>, USA, as per 2012.

Dillion, C.P., Forms of Corrosion-Recognition and Prevention: NACE Handbook 1, Volume 1, NACE, USA, 1982.

DNV, Rules for classification of ships, DNV, Norway, 2012.

Dulski, T.R., A manual for the chemical analysis of metals, ASTM international, USA, 1996.

Edminister, J.A., Schaum's outline of Theory and Problems of Electric Circuits, McGraw-Hill, USA, 1995.

Eijgenraam, C.J.J., Koopmans, C.C., Tang, P. J.G., Verster, A.C.P., Evaluatie van infrastructuurprojecten: leidraad voor kosten-batenanalyse, Centraal Planbureau, Nederlands Economisch Instituut, The Netherlands, 2000.

Elert, G., Density of Steel, Physics Factbook, USA, 2009.

Elgun, S. Z., TTT diagram, Farmingdale State University, New York, USA, 1999.

Eliasson, J., Ballast water tank coatings for the future, NACE Corrosion Conference paper No. 05001, USA, 2005.

Eliasson, J., Personal communication, 2012.

Eliasson, J., Economics of Coatings/Corrosion Protection of Ships. Selecting the correct type of anticorrosion protection for underwater applications on new buildings,

Prevention and Management of Marine Corrosion, Lloyd's List event conference, London, 2003.

European Maritime Safety Agency, Double Hull Tankers, High Level Panel of Experts Report, Lisbon, European Maritime Safety Agency, 2005.

Eurostat, http://epp.eurostat.ec.europa.eu/statistics_explained/index.php/Consumer_prices_inflation_and_comparative_price_levels, as per February 2012.

Eyres, D.J., Ship Construction, 6th ed., USA, Butterworth-Heinemann, 2007.

Filzmoser, Fritz, Kalcher, Robust PCA by Projection Pursuit, 2012.

Fowler, K. A., Elfbaum, G. M., Smith, K.A., Nelligan, T.J., Theory and Applications of Precision Ultrasonic Thickness Gaging, USA, NDT, 1997.

Frimpong, M., Moortgat, E., Van Tender Loo L., Experimentele studie van corrosie van ballasttanks in zeeschepen, Projectwerk chemie- en voedingstechnologie, Universiteit Antwerpen, Belgium, 2009.

Gamry Instruments, Getting started with Electrochemical Corrosion Measurement, 2010.

Gardiner, C.P., Melchers, R.E., Corrosion analysis of bulk carriers, Part I: operational parameters influencing corrosion rates, Marine Structures, 2003.

Garnett, P. J., Treagust, D. F., Conceptual Difficulties experienced by Senior High School Students of Electrochemistry: Electrochemical (Galvanic) and Electrolytic Cells. Journal of Research in Science Teaching, 29 (10), 1992.

Garrels, R.M., Christ, C.L., Minerals, Solutions and Equilibria, Jones and Bartlett, London, UK, 1990.

Goldstein, J. Newbury, D., Joy, D., Lyman, C., Echlin, P., Lifshin, E., Sawyer, L., Michael, J., Scanning Electron Microscopy and X-Ray Microanalysis, Springer, 2003.

Gratsos, G.A., Zachariadis, P., Life cycle cost of maintaining the effectiveness of a ships structure and environmental impact of ships design, Hellenic Chamber of Shipping, Greece, 2007.

Groisman, A., Corrosion for everybody, Springer Science + Business Media, 2010.

Gubenko, S.I., Pinchuk, S.I., Belaya, E.V., Investigation of Non-Metallic Inclusion Effect on Corrosion Behavior of Wheel Steel, Metallurgical and Mining Industry, Vol. 3, No. 2, 2011.

Guedes Soares, C., Garbatov, Y., Reliability of maintained, corrosion protected plates subjected to non-linear corrosion and compressive loads, *Marine Structures* 12, 425–55, 1999.

Guo, J., Wang, J., Ivanov, L., Perakis, A.N., Time-varying ultimate strength of aging tanker deck plate considering corrosion effect, *Marine Structures*, Vol.21, issue 4, 2008.

Hack, H.P., *Designing Cathodic Protection Systems for Marine Structures and Vehicles*, 1999.

Harmonized indices of consumer prices (2005=100) - Monthly data (12-month average rate of change), as per 2012.

Hatano, Y., Yoshida, N., Futagami, H. Tokunaga, T., Glow-Discharge Optical Emission Spectroscopy for Plasma-Surface Interaction Studies, University of Toyama, Kyushu University, poster presentation, as per 2012.

Herman, J.C., Leroy, V., Influence of Residual Elements on Steel Processing and Mechanical Properties, *Metal Working and Steel Processing*, Cleveland, USA, 1996.

Hermans, M., *Afwijkingen van de ideale kristalstructuur*, NIL, The Netherlands, 2007.

Hermans, M., *Materialenkennis, opbouw van de metalen*, NIL, The Netherlands, 2007.

Herring, D.H., *Steel Cleanliness; Inclusions in Steel*, Industrial heating, 2009.

Hinton, R.W., Wiswesser, R.K., Estimating Welding Preheat Requirements for unknown Grades of Carbon and Low Alloy Steels, Supplement to the *Welding Journal*, American Welding Society, 2008.

IACS, Common structural rules for tankers and bulk carriers, International Association of Classification Societies, London, UK, 2005.

Ilseling, F.P., *General Guidelines for Corrosion Testing of Materials for Marine Applications*, The Institute of Materials, 1989.

IMO 1993, Resolution A.744(18), Guidelines on the enhanced program of inspections during surveys of bulk carriers and oil tankers, London, UK, 1993.

IMO, IMO Resolution MSC.215(82), Performance standard for protective coatings for dedicated seawater ballast tanks in all types of ships and double-side skin spaces of bulk carriers, IMO Naval Architectural Group - Maritime Safety Committee, UK, adopted 8 December 2006.

IMO, Tanker familiarization Course, Model 1.01, IMO, UK, 2000.

Impact assessment guidelines, European Commission, 2009.

Iowa State University, Materials, Science and Engineering Department, SEM introduction, <http://www-archive.mse.iastate.edu>, 2012.

ISO 4967, Steel-Determination of Content of Nonmetallic Inclusions--Micrographic Methods Using Standard Diagrams, second edition, ISO, 1998.

Ivanov, L.D., Wang, G.E., Seah, A.K., Evaluating corrosion wastage and structural safety of aging ships. In: Pacific international maritime conference, Sydney, Australia, 2004.

Janssens, K. Chemie II: Fysische en beschrijvende chemie, hoofdstuk 4, Universiteit Antwerpen, Belgium, 2010.

Japan Welding Engineering Society: Online calculation of carbon equivalent, <http://www.jwes.or.jp/en>, as per 2012.

JFE steel corporation, <http://www.jfe-steel.co.jp>, as per 2012.

JFE, Clad steel plate, technical information brochure, JFE, Japan, consulted online 2012.

Jim Erickson, U-M “ballast free ship” could cut costs whil blocking aquatic invaders, University of Michigan, 2008.

Johnson, J., Cost of Corrosion in Ships, Report, CC Technologies Laboratories, Inc., Dublin, Ohio, USA, 2001.

Juvonen, P., Effects of Non-Metallic Inclusions on Fatigue Properties of Calcium Treated Steels, Helsinki University of Technology, Finland, 2004.

Kamimura, T., Hara, S., Miyuki, H., Yamashita, M., Uchida, H., Composition and protective ability of rust layer formed on weathering steel exposed to various environments, Corrosion Science, Elsevier, 2006.

Kasuya, T., Carbon Equivalent to assess hardenability of steel and prediction of HAZ hardness Distribution, Nippon Steel technical report Nr. 95, Japan, 2007.

Kattan, M. R., Corrosion in Ballast Tanks: Is rust a must? Safinah, UK, 2007.

Kawano, H., Hirakata, M., Tanker structure and hull failure strength, PAJ Oil Spill Symposium 2003, Petroleum Association of Japan, Tokyo, February 27-28, 2003.

Kiessling, R., Non-metallic Inclusions in Steel, Parts I-IV, The Metals Society, 1997.

Kim, I., Ten years after the enactment of the Oil Pollution Act of 1990: a success or a failure, Mar. Policy 26, 2002.

Kleber, X., Surface and Subsurface Metallic Inclusions Detected using Hot Tip Thermoelectric Power Measurements, ECNDT, France, 2006.

Koch, H.H., Corrosion Costs and Preventive Strategies in the United States, National Association of Corrosion Engineers, USA, 2002.

Koenker, R., Hallock, K. F., Quantile Regression, *Journal of Economic Perspectives*, vol.15, nr 4, 2001.

Koenker, R., *Quantreg: Quantile Regression, R Package*, 2012.

Kok, M.V., Safety & Environmental Impact, PETE424, unpublished course, United Arab College of engineering, UAE, 2009.

Kopeliovich, dr. D., effect of alloying elements on steel properties, *Substances and technology*, 2011.

Kopeliovich, dr. D., *Solidification, Substances and technology*, 2009.

Kozin, A. Proton binding at the akaganéite/water interface, Department of Chemistry, Umeå University, Umeå, Sweden, as per 2012.

Kroch, L., Ellor, J., Ault, E.P., Life Cycle Predictions for Coating Systems, DoD corrosion conference, USA, 2009.

Kwok YL, *The learning of organic chemistry reactions, ΔG and temperature*, *Journal of the American Chemical Association*, 2012.

Lambert, F., A Student's Approach to the Second Law and Entropy, <http://entropysite.oxy.edu>, 2008.

Langereis, G., *Elektrochemie voor dummies*, personal webpage, 1997.

Langford, G., *Microstructures*, Massachusetts Institute of Technology, Cambridge, UK, 2005.

Lankford, W. T., *The Making, Shaping and Treating of Steel*, Association of Iron and Steel Engineers, Pittsburgh, USA, 2008.

Laque, F.L., *Marine Corrosion : Causes and prevention*, John Wiley and Sons Inc., New York, USA, 1975.

Legacy Shipbroking S.A., *Market Report*, 2010.

Lewis, R.J., *Hawley's Condensed Chemical Dictionary*, thirteenth edition, John Wiley and Sons, Inc., 1997.

Lister, D.H., Cook, W.G., *Kinetics of Aqueous Corrosion*, University of New Brunswick, USA, as pers 2012.

Lloyds Register, Rules and Regulations set appropriate standards for the design, construction and lifetime maintenance of ships, 2001.

Lloyds Register, Tanker Focus, Issue 1, p. 12, UK, 2006.

López, D.A., Pérez, T., Simison, S.N., The influence of microstructure and chemical composition of carbon and low alloy steels in CO₂ corrosion. A state-of-the-art appraisal, Materials & Design, Elsevier, 2003.

Løseth, R., Sekkesæter, G., Valsgård, S., Economics of high-tensile steel in ship hulls, Marine Structures 7, 1994.

Lower, S., chem1 virtual textbook, Simon Fraser University, Canada, 2007.

Luzginova, N., Formation of bainite, TU Delft, The Netherlands, 2012.

Maalekian, M., the effects of alloy elements on steel, TU Graz, France, 2007.

Madou, M.J. Pourbaix VII, Power Point presentation, UC Davis, University of California, USA, 2004.

March, G.A., A review of corrosion and cathodic-protection principles from an electrochemical point of view, Journal of petroleum technology, 1962.

Marcus, P., Corrosion mechanisms in theory and practice, London, UK, 2002.

Massa, W., Crystal Structure Determination, Springer, 2004.

Mattson, E., Basic corrosion technology for scientists and engineers, 2nd edition, Institute of Materials, London, UK, 2004.

McCafferty, E., Introduction to Corrosion Science, Springer, New York, USA, 2010.

McKee, W., Safety and Health guidance note 59, Personal Health Protection during the Application of Tar Containing Coatings, International Paint, 2004.

McNulty, P., Alternatives to PSPC, NEI Treatment Systems, Los Angeles, USA, 2008.

McNulty, P., Life cycle cost of the Venturi Oxygen Stripping ballast tank corrosion protection system in double hull ships, NEI Treatment Systems, Los Angeles, USA, 2007.

Medeiros, F.N.S., Rahamho, G.L.B., Bento, M.P., Medeiros, L.C.L., On the evaluation of texture and color features for nondestructive corrosion detection, EUASIP journal on Advances in Signal Processing, volume 2010, Hindawi Publishing Corporation, 2010.

Melchers, R.E., Corrosion uncertainty Modeling for steel structures, J. Constr. Steel Res. 52, 1999.

Melchers, R.E., Effect of small compositional changes on marine immersion corrosion of low alloy steels, Corrosion science, Elsevier, 2003.

Melchers, R.E., effects of alloying on maximum depth of pits in mild steel in marine environments, Corrosion, Nace International, USA, 2005.

Michaux, N. *Corrosie en coatings, master scriptie, Hogere Zeevaartschool, Antwerpen, Belgium*, 2008.

Moor, J.T., Scheikunde voor dummies, Pearson, USA, 2009.

Morris, J.W., The Influence of Grain Size on the Mechanical Properties of Steel, University of California, USA, 2001.

MSE 300 Materials Laboratory Procedures, Iron-carbon phase diagram, University of Tennessee, USA, 2012.

MUMM, Management unit North Sea mathematical models, 2012.

N.E.I. treatment systems, <http://www.nei-marine.com>, as per 2012.

N.E.I., Life cycle cost of the venture oxygen stripping™ ballast tank corrosion protection system in double hull ships, Nei-marine, USA, 2007.

N.E.I., Life cycle cost Panamax tanker, http://www.nei-marine.com/doc/pub/PeterMcNulty_LifeCycleCost_VOS_Panamax.pdf, as per August 1, 2011.

Nace resource centre, Cathodic protection, <http://events.nace.org/library/corrosion>, USA, as per 2012.

Nace resource centre, FE Reactions, <http://events.nace.org/library/corrosion/Thermo/FeReactions.asp>, Nace International, USA, as per 2012.

Nace, Coating inspector Program Level 1, Student Manual, Nace International, USA, 2012.

Nace, Nace Corrosion Engineer's Reference book, third edition, NACE International, Houston USA, 2002.

National research council, Double hull tanker legislation, an assessment of the oil pollution act 1990, NRC, USA, 1998.

Nave, R., Corrosion as an Electrochemical Process, <http://hyperphysics.phy-astr.gsu.edu/HBASE/CHEMICAL/corrosion.html>, Hyperphysics, Georgia State University, USA, as per 2012.

Neely, J.E., Bertone, T.J., Practical Metallurgy and Materials of Industry, sixth edition, Prentice Hall, Ohio, USA, 2003.

Nei-marine, Life cycle cost Panamax tanker, http://www.nei-marine.com/doc/pub/PeterMcNulty_LifeCycleCost_VOS_Panamax.pdf, as per August 1, 2011.

Nimmo, B., Hinds, G, Beginners guide to corrosion, NPL's Corrosion Group, UK, 2003.

Non Destructive Testing Resource Center, <http://www.ndt-ed.org>, as per 2012.

Noran instruments, Energy-dispersive X-ray microanalysis, an introduction, Noran instruments, USA, as per 2012.

Scholler, S., Huang, T.D., Ship Design and Construction Training Module, NSRP, National Shipbuilding Research Program, NSRP Joint Panel Meeting, 2012.

NSW TAFE Commission, annual report, Australia, 2008.

OCIMF, Factors influencing accelerated corrosion of cargo oil tanks, 1997.

OECD, Directorate for Science, Technology and Industry (STI) – compensated gross ton system, 2006.

Oil Pollution Act, Public Law No 101-380 (33 U.S.C. 2701 et seq.), 104 Stat. 484, 1990.

Olson, G.B., Owen, W.S., Martensite, ASM International, USA, 1992.

Oxforddictionaries.com, as per 2012.

Paik, J. K., Thayamballi, A. K., Park, Y. I., & Hwang, J. S., A time-dependent corrosion wastage model for seawater ballast tank structures of ships. Corrosion Science (46), 2004.

Paik, J.K., Kim, D.K., Advanced method for the development of an empirical model to predict time-dependent corrosion wastage, Corrosion Science, 63, 51-58, 2012.

Paik, J.K., Thayamballi, A.K., Ultimate strength of ageing ships, Proceedings of the Institution of Mechanical Engineers, Part M: Journal of Engineering for the Maritime Environment vol 216, 2002.

Parente, J., Daidola, J.C., Basar, N.S., Rodi, R.C., Final Report, Commercial ship design and fabrication for corrosion control, MR&S Report, Rosenblatt & sons, New York, USA, 1996.

Pearce, D., Groom, B, Hepburn, C, Koundouri, P., Valuing the future: recent advances in social discounting, World Econ. 4, 2003.

Pearce, D., The standard discounting rate EU, <http://ec.europa.eu/governance/impact/>, 2003.

Pedefferri, P., Cathodic protection and cathodic prevention, *Construction and Building Materials*, 10, 1996.

Perez, N., *Electrochemistry and corrosion science*, Boston, USA, 2004.

Perez, T., Fitzsimons, G., Videm, K., *Proceedings of the 13th International Corrosion Conference*, Melbourne, 1996.

Perlibakas, V., Distance Measures for PCA-based face recognition, *Pattern Recognition Letters*, 2004.

Pieters, R., *Materialenkennis, TTT- en CCT-diagram*, NIL, The Netherlands, 2007.

Pissierssens, T. invloed van staalkwaliteit op de corrosiesnelheid, bachelor thesis, Antwerp Maritime Academy, Belgium, 2010.

Psarros G.A., Vassalos, D., Effectiveness of corrosion measures to bulk carriers with Life Cycle Cost Analysis, *International Shipbuilding Progress* 56, 2009.

Qin, S., Cui, W., Effects of corrosion models on the time-dependent reliability of steel plated elements, *Marine Structures*, vol 16, issue 1, 2003.

R Development Core Team, *The R Project for Statistical Computing*, Institute for Statistics and Mathematics of the WU Wien, 2011.

Ralston, K.D., Birbilis, N., Effect of grain size on corrosion: a review, *Corrosion Science*, Nace, Houston, USA, 2010.

Revie, R.W., Uhlig, H.H., *Corrosion and corrosion control; An Introduction to Corrosion Science and Engineering*, 4th edition, John Wiley and Sons Ltd, UK, 2008.

RINA, *Guide for the Structural Design of Oil Tankers*, Registro Italiano Navale, Italy, 2004.

Roberge, P.R., *Corrosion Basics, an Introduction*, second edition, NACE International, Houston, USA, 2006.

Roberge, P.R., *Corrosion Engineering, Principles and Practice*, McGraw-Hill, New York, USA, 2008.

Roberge, P.R., *Corrosion inspection and monitoring*, Royal Military College of Canada, Ontario, Canada, 2007.

Roberge, P.R., *Corrosion Kinetics, Overpotential*, <http://corrosion-doctors.org/Corrosion-Kinetics/Overpotential-concentration.htm>, USA, as per 2012.

Roberge, P.R., Handbook of Corrosion Engineering, McGraw-Hill, New York, USA, 2000.

Roberge, P.R., Types of water, <http://corrosion-doctors.org/Corrosion-by-Water/Types-of-water.htm>, USA, as per 2012.

Roet, D., Analytische scheikunde, Thermodynamica van de chemische reacties, Universiteit Antwerpen, Belgium, 2002-2008.

Rothwell, G., Corrosion phenomena - an introduction, National Physical Laboratory, 2007.

Rousseeuw, P., Struyf, A., Hubert, M., Cluster Analysis, R package, 2012.

Rubi, J.M., Kjelstrup, S., Mesoscopic nonequilibrium Thermodynamics gives the same thermodynamic basis to Buttlar-Volmer and Nernst Equation, Department of Chemistry, Norwegian University of Science and Technology, Norway, 2003.

Russell, B.J., Shelton, J.P., Walsh, A., An atomic-absorption spectrophotometer and its application to the analysis of solutions, Spectrochimica Acta, Elsevier, 1957.

Safinah Newsletter. "Equivalent" Ballast Tank Protection. March 2009. <http://www.safinah.co.uk/news/equivalent-ballast-tank-protection.htm>, as per August 1, 2011.

Schillemans, W. Scheepsbouw deel 1, niet gepubliceerde cursus Hogere Zeevaartschool, Antwerpen, Belgium, 2008.

Schweitzer, P.A., Corrosion and corrosion protection handbook, 2nd edition, New York, USA, 1989.

Schweitzer, P.A., Fundamentals of Corrosion, Mechanisms, Causes and Preventative Methods, CRC Press, Boca Raton, USA, 2010.

Sciencelab, Material Safety Data Sheet Coal Tar, Sciencelab, updated 2012.

Shackleford, J.F., Introduction to materials science for engineers, 6th edition, Pearson Education Inc., 2005.

Shah, K.P., The hand book on mechanical maintenance, classification of alloys, 2010.

SHELL, Ballast tanks: An overview of the TSCF guidelines for ballast tank coating systems and surface preparation, Tanker structure cooperative forum, shipbuilders meeting, Tokyo, 2000.

Sheppard, D., Alper, A., Cartoon, New York Washington, USA, July 3th, 2012.

Shifler, D.A., Understanding material interactions in marine environments to promote extended structural life, Corrosion Science (47), 2005.

- Skrylov, S.N., *Spontaneous change: Entropy and Free energy*, York University, 2010.
- Smallman, R.E., Ngan, A.H.W., *Physical Metallurgy and Advanced Materials*, 7th edition, Elsevier, 2011.
- Smet, J.P., *Corrosie en corrosiepreventie*, Karel de Grote-Hogeschool, Belgium, 2009.
- Smet, J.P., *Lastetechniek*, Unpublished Course, KdG university college, Belgium, 2000.
- Smet, J.P., *Materialenleer: Metaalkunde*, Karel De Grote Hogeschool, Hoboken, unpublished course material, Belgium, 2008.
- Smith, W.F., Hashemi, J., *Foundations of Materials Science and Engineering*, McGraw-Hill, USA, 2006.
- Smoljko, I. et al, *Some new studies of sacrificial anodes*, 1st World Congress on Corrosion in the Military, USA, 2007.
- Soares, C.G., Garbatov, Y., Zayed, A., *Influence of environmental factors on corrosion of ship structures in marine atmosphere*, *Corrosion Science*, vol 51, issue 9, 2009.
- Southwell, C.R., Alexander, A.L., *Corrosion of Metals in Tropical Environments. Part 9 - Structural Ferrous Metals - Sixteen Years' Exposure to Sea and Fresh Water*, Naval Research Laboratory, Washington, USA, 1969.
- Southwell, C.R., Bultman, J.D., Hummer, C.W., *Estimating of service life of steel in seawater*, *seawater corrosion handbook*, Noyes Data Corporation, 1979.
- Speller, F.N., *Corrosion: causes and Prevention - An Engineering Problem*, 2nd Edition, McGraw-Hill, New York, USA, 1935.
- Steelguru, *Information steel market*, <http://www.steelguru.com>, India, as per 2011.
- Stewart, J., Williams, D.E., *The initiation of pitting corrosion on austenitic stainless steel: on the importance of sulphide inclusions*, *Corroisn Science*, Elsevier, U.K., 1992.
- Substances and Technology*, www.substech.com, as per 2012.
- Suzuki, S., Kakita, K., *A comparative Study of GDOES, SIMS and XPS depth profiling of thin layers on metallic materials*, *Journal of surface analysis*, Vol. 12, no.2, 2005.
- Talbot, D. et al., *Corrosion Science and Technology*, Boca Raton, USA, 1998.
- Tator, K.B., *Risk assessment and economic considerations when coating ballast tanks*, *Workshop: Coatings for Corrosion Protection: Offshore Oil and Gas Operation Facilities, Marine Pipeline and Ship Structures*, Mississippi, USA, 2004.

Tavakkolizadeh, M., Galvanic corrosion of carbon steel in aggressive environments, Journal of composites for construction, 2001.

Templeton, J.S. III, Offshore technology in civil engineering, ASCE Publications, 2006.

The Japan Welding Engineering Society, Carbon equivalents and transformation temperature, Japan, 2011.

The Standard Club, Surveyor's notebook, vol. 16, The standard club publications, UK, 2004.

Thermo Scientific ARL 4460 Metals Analyzer, technical information manual, as per 2012.

Thomas, J.G.N., edited by Hinds, G., The electrochemistry of corrosion, 2010.

TI-25M ultrasonic thickness measurement instrument, Check-line Europe, user manual, as per 2012.

Tsolakis, S.D., Cridland, C. Haralambides, H.E., Econometric Modelling of Second-hand Ship Prices, Maritime Economics and Logistics, Palgrave Macmillan Ltd, 2003.

Tutorvista, Classification of electrolytes, <http://www.tutorvista.com/bow/classification-of-electrolytes>, TutorVista.com, USA, as per 2012.

U.S. Department of energy, Doe fundamentals handbook, chemistry, volume 1 of 2, USA, 1993.

Uhlig, H.H., Triadis, D. and Stern, M., Electrochem. Soc, 1995.

Unknown, The Physics Factbook,

<http://hypertextbook.com/facts/2004/KarenSutherland.shtml>, as per July 2012.

Van Der Stichelen, W., Lloyds Register Classification Society, personal communication, 2012.

Van Lierop, K., Experimentele bepaling van de H-huishouding in staal met behulp van thermische desorptie spectroscopie, scriptie tot het behalen van de graad van burgerlijk ingenieur metaalkunde, Universiteit Gent, Belgium, 2007.

VanDerhorn, E., Wang, G., A statistical study on the material properties of shipbuilding steels, Sustainable Maritime Transportation and Exploitation of Sea Resources, CRC Press, London, UK, 2011.

Vantorre, M., Afmetingen en grootte van schepen, unpublished, University Gent, Belgium, 2011-2012.

Vargel, K., Corrosion of Aluminum, Elsevier, 2004.

Veleva, L., Kane, R.D., ASM Handbook Volume 13A, Corrosion: Fundamentals, Testing, and Protection, ASM International, 2003.

Verboven, J., Opstelling van een piping inspectieprogramma, Katholieke Hogeschool Kempen, Belgium, 2003.

Vercauteren, P., Bepaling van edele metalen in elektronisch schroot via vonk-optische-emissie-spectrometrie, Proefschrift tot het behalen van de graad van industrieel ingenieur in de Chemie, Hoboken, Belgium, 2005.

Verstraelen, H., De Baere, K., Schillemans, W., Lemmens, L., Dewil, R., Lenaerts, S., Potters, G., In situ study of ballast tank corrosion on ships —Part 2, Mater. Performance 48 (11), 54-57, 2009b.

Verstraelen, H., De Baere, K., Schillemans, W., Lemmens, L., Dewil, R., Lenaerts, S., Potters, G., In situ study of ballast tank corrosion on ships—Part 1, Materials Performance 48 (10) 48-51, 2009a.

Verstraelen, H., Potters, G., Lemmens, L., Luyckx, D., Lenaerts, S., De Baere, K., Impact of ship construction steel properties on ballast tank corrosion rate: methodological choices, submitted for publication, Materials Performance, Nace, 2012.

Videm, K., Kvarekval, J., Perez, T.E., Fitzsimons, G., Surface Effects on the Electrochemistry of Iron and Carbon Steel Electrodes in Aqueous CO₂ Solutions, Corrosion '96, USA, Denver, Nace, 1996.

Von Baeckmann, W., Handbook of cathodic protection, Gulf Professional Publishing, 1997.

Walsh, The application of atomic absorption spectra to chemical analysis, Spectrochimica Acta, Elsevier, 1955.

Walton, O., Making Modern Shipping: Making the modern world, Pandi, UK, 2005.

Wang, G.E. et al, A statistical investigation of time-variant hull girder strength of aging ships and coating life, Marine Structures 21, 240-256, 2008.

Wang, G.E. et al., Estimation of corrosion rates of structural members in oil tankers, Proceedings 22nd International Conference on Offshore Mechanics and Arctic Engineering, 2003.

Wang, W., Sacrificial anode polarization of steel in seawater: Part 1 – A novel experimental and analysis methodology, NACE International, 1996.

Wang, Y., Akid, R., Role of non-metallic inclusions in fatigue, Pitting and Corrosion Fatigue, Corrosion, Nace, Houston, USA, 1996.

Weidmann, G. Lewis, P., Structural materials, Materials in action series, Butterworth-Heinemann, Elsevier, 1990.

Yurioka N., Okumura M, Oshita S., Shoja S., On the method of determining preheating temperature necessary to avoid cold cracking in welding, IIW Doc., Nippon, Japan, 1981.

Z-guard, The A-Z of cathodic protection, <http://www.z-guard.co.uk/zguardcart/product2.asp?pid=410>, as per December 2011.

Zou, Y., Wang, J., Zheng, Y.Y., Electrochemical techniques for determining corrosion rate of rusted steel in seawater, Corrosion science, Elsevier, 2010.

10 List of figures

Figure 1: steel replacement (tonnes) in function of the age (y) of the ship (Alaoui (2010) + Løseth (1994))	10
Figure 2: C1 (portion steel replacement due to corrosion (%)) in function of the age (y) of the ship (graphical presentation by Kawano & Hirakata 2003).....	11
Figure 3: results (€) of the basic model for each of the five cases, inflated with 2% and discounted with 4% per year.	20
Figure 4: result of the Monte Carlo analysis (€) after 5,000 trials.....	24
Figure 5: time-energy diagram iron (adapted from Smet, 2008).	29
Figure 6: electron and current flow of corrosion cell (http://amudugowripalan.blogspot.com).	31
Figure 7: simplified Pourbaix diagram for iron with assumed concentration of $[\text{Fe}^{2+}]$, $[\text{Fe}^{3+}]$ and $[\text{HFeO}_2^-]$ of $10^{-6} \text{ mol l}^{-1}$ (adapted from Bogaerts, 2008, Smet, 2008).	34
Figure 8: electric double layer formed at the metal surface in water, - = electrons, + = metallic cations, E_a = absolute electric potential (Groysman, 2010).....	38
Figure 9: diffusion of O_2 near the electrode surface (Roberge, 2010). Metal surface at ordinate axis, x-axis expresses the distance (x) from the surface, y-axis gives concentration of chemical species being reacted. for well mixed solutions, the concentration is constant for the convection region.	39
Figure 10: polarization curves, A: overpotential – current density; B: overpotential, logarithmic absolute value current = Tafel diagram (adapted from Smet, 2008).....	41
Figure 11: LPR measurement. X axis: external current (i), y-axis: potential (η).	42
Figure 12: LPR plot. x-axis: current in μA , y-axis potential in mV.	42
Figure 13: apparent polarization curves (adapted from corrosion center Ohio, 2012). $i_a = i_c = i_{\text{corr}}$ at the corrosion potential E_{corr}	43
Figure 14: Tafel curve. x-axis: current (μA), Y-axis: potential (mV). Orange lines represent tangents to the curves, red lines are the measured values. E_{corr} is given at the intersection of the tangents.	44
Figure 15: crystal structure and amorphous structure (Atkins, 1992).	47
Figure 16: BCC structure (Smallman, 2011).	48
Figure 17: FCC structure (Smallman, 2011).	48
Figure 18: HCP structure (Smallman, 2011).	49
Figure 19: BCT structure, Orthorhombic structure (Smallman, 2011)	49
Figure 20: monoclinic structure (Smallman, 2011).....	50
Figure 21: simplified presentation Fe-C diagram.	52
Figure 22: nucleation (NDT- resource center, 2011).	52
Figure 23: diagram of grain boundaries in a metal (ASM International, 2000).....	53
Figure 24: Fe-C diagram (adapted from Neely, 2003).	53
Figure 25: time temperature ($^{\circ}\text{C}$) curve pure iron.....	56

Figure 26: lattice representation of an alloy. (A) Substitutional; (B) Interstitial; (C) Vacancies (Hermans, 2007).	57
Figure 27: TTT diagram, logarithmic scale on X axis. M_s : starting of transformation; M_f : finish of transformation, (adapted from S. Z. Elgun, 1999).	58
Figure 28: SEM image, magnification 500x, ferrite structure. clear grains, no cementite present.	58
Figure 29: SEM image, magnification 500x, pearlite: white zones ferrite and dark zones cementite.	59
Figure 30: cross section of pearlite (University of Tennessee, 2012).	59
Figure 31: SEM image, magnification unknown, of martensite. Thin plates are visible (Olson, 1992).	59
Figure 32: SEM image, magnification unknown, of bainite. plates with limited size are visible, resulting in strong and stable combination of ferrite and cementite, less internal stress than martensite (Luzginova, 2012).	60
Figure 33: classification alloy types: (a) open field; (b) closed field; (c) expanded field; (d) contracted field (adapted from Maalekian, 2007).	62
Figure 34: effect of alloy addition on eutectoid temperature of 723°C at 0.83%wt carbon concentration (Maalekian, 2007).	63
Figure 35: diagrams of isothermal transformation. (a) Carbon steel and steel alloyed with non-carbide-forming elements; (b) carbon steel and steel alloyed with carbide-forming elements (ASM, 1991).	64
Figure 36: influence of carbon content on the martensite transformation. M_s : start of transformation; M_f : finish of transformation (Abbaschian, 2009).	65
Figure 37: example determination inclusions,	67
Figure 38: sample preparation: A: grinding; B: sample before and after grinding.	69
Figure 39: atomic emission spectrum. Electrons promoted to higher energy level (n levels) return to lower level (arrows pointing down), I.E = internal energy. Under: different emission lines shown with increasing frequencies (www.avogadro.co.uk, 2012).	70
Figure 40: monochromator. Separation of the different wavelengths through diffraction. (Shimadzu, 2012).	71
Figure 41: electrode. A: cleaning; B: positioning; C: samples after test.	71
Figure 42: GD-OES principle. Plasma used on sample to obtain emission and identification of the atoms (Hatano, 2012).	72
Figure 43: Electron microscope source. Specimen is scanned with thermal energy (Iowa State University, 2012).	74
Figure 44: different types of inclusions found in studied steel samples: A = _____ = manganese sulfide, single; B = = aluminum oxides, line; C = _____ = manganese sulfide, line; D = . = aluminum oxide, single.	75
Figure 45: XRD diffraction pattern on weathering steel after different exposure periods (1, 3, 6 and 15 years) (Kamimura, 2005).	76

Figure 46: SEM microstructure steel sample images. A: side, 100 enlarged; B: Center, 100 times enlarged; c: Side, 500 times enlarged; D: Center, 500 times enlarged.	77
Figure 47: SEM image 100% ferrite.	78
Figure 48: SEM image ferrite-pearlite structure.....	78
Figure 49: SEM images showing microstructure: A: layered structure; B: non layered structure.....	78
Figure 50: SEM images showing grain size: A: small grain size <20µm; B: medium grain size between 20µm and 30µm; C: large grain size >30µm.....	78
Figure 51: A: steel plate example approximately 50x60cm, B: sample preparation DEME Zeebrugge.	79
Figure 52: experimental set-up: sample numbering and positioning in cube container.	80
Figure 53: test facility at Antwerp Maritime Academy. A: laboratory, B: compartment with cube containers.	81
Figure 54: test facility at Antwerp Maritime Academy. A: 25m ³ tank with seawater, B: collecting seawater at vessel (8/3/2010).....	81
Figure 55: schematic overview of the test facility with 25m ² seawater tank, 1 and 3 are cube container with permanent immersion, 2 is a cube container with spray system. Water circulating, passing through UVC lamp to kill organisms. Constant measurement of pH, oxygen concentration in ppm and temperature in °C.	82
Figure 56: electrochemical measurement set up. Green is working electrode (sample), red is counter electrode (platinum), white is reference electrode (Ag/AgCl).....	83
Figure 57: potential measurement principle at certain time. Potential of working electrode related to reference electrode (197mV).....	84
Figure 58: potential measurement principle. Current related to potential.	84
Figure 59: potential measurement (mV) at a given time with respect to reference electrode (197mV).	85
Figure 60: weight measurement procedure. A: samples after 2 years immersion; B: rust scraping; C: etching of samples; D: sample after etching; E: weight measurement; F: measurement of dimensions with caliper.	86
Figure 61: photographical measurement set up at Antwerp Maritime Academy.	88
Figure 62: photos of same sample after different periods of immersion; a: start of experiment, b: 1 day, c: 7 days, d: 31 days.....	88
Figure 63: quantile regression of weight loss (g m ⁻² year ⁻¹) on comp 1 and comp 2, with indication of three clusters 1: CRS steel, 2: High tensile steel, 3: Grade A steel.....	96
Figure 64: clusters based on steel composition. The first division is given by the C content, the second by the Mn concentration. Further divisions are related to Si, Ni and Cu concentrations.	97
Figure 65: scatter plot of the weight loss measurement in function of respectively Tafel & LPR values. Green dots representing CRS, blue dots grade AH and grey dots grade A steel.....	100

Figure 66: Tafel curves A: grade A, B: grade AH and C: CRS steel after 145 hours. Tangents to the slopes are the β values.	102
Figure 67: stress-strain diagram, in MPa function of elongation in %.	109
Figure 68: corrosion time dependent model (Melchers, 2004).	112
Figure 69: relation corrosion rate in mm y^{-1} to carbon content in %wt (Pleshivtse, 2009).	113
Figure 70: overview of rust film formed in the initial stage of corrosion (Tamura, 2008).	114
Figure 71: formation of FeOOH layers after exposure (adapted from Kimura, 2005).	115
Figure 72: relation corrosion rate, composition rust layer (Shuichi, 2007).	115
Figure 73: schematic illustration of goethite crystal, where CrO_x^{3-2x} complex ion adsorbs at the surface (Yamashita, 2004).	117
Figure 74: GD-OES analysis of CRS steel oxide layer. Dark blue line is Al line. An almost linear increase in Al concentration is visible.	119
Figure 75: microstructure CRS. A: sample 7 B: sample 32 through optical microscope at (10x50) magnification. Bainite structure (OCAS, 2011).	120
Figure 76: inclusions CRS. A: sample 7 B: sample 32 through SEM-EDX analysis, 100 times enlarged. Very few Aluminum oxide inclusions visible. No manganese sulfide inclusions detected.	121
Figure 77: tensile strength (N/mm or MPa) diagram of CRS.	124
Figure 78: Vickers hardness fluctuations (no unit) in CRS weld, related to the distance to the center of the weld in mm.	126
Figure 79: what matters in shipping, cartoon (Sheppard, 2012).	130
Figure 80: CAD model of ballast tank (18m x 42m), (Elsyca, 2013), with indication of the protection by sacrificial anodes. Blue zones are overprotected, green are well protected zones, red are under protected. Polarization data are based on a current demand of 1.2 mA/m^2 (given a coating in excellent condition).	131
Figure 81: corroded plates after 270 days exposure splash zone. Left with VOS, right without VOS (NEI, 2007). Table 39: corrosion reduction in percentage for COS system after 30 and 270 days exposure (NEI, 2007).	137
Figure 82: void space overview double hull tanker (Akiba, 1996).	139

11 List of tables

Table 1: summary of the five cases in the economic analysis in terms of construction, equipment and maintenance criteria.	6
Table 2: TCB variables per model and per equation, used in the economic model.	8
Table 3: number of days needed for recoating in function of ship's age (y).	13
Table 4: parameters used in the economic model.	17
Table 5: minimum, maximum and most plausible value of the uncertain parameters used during the Monte Carlo Analysis together with the probability distribution.	19
Table 6: influence on the real TCB (€) of the evolution of the steel price and coating cost. Cells with grey shading refer to values used in the basic model.	22
Table 7: influence on the real TCB (€) of the price ratios of CRS to grade A steel and TSCF ₂₅ to PSCF ₂₅ . Cells with grey shading refer to values used in the basic model.	23
Table 8: statistical outcome of the Monte Carlo Analysis after 5,000 trials.	25
Table 9: contribution to the variance of certain assumptions in Monte Carlo analysis.	25
Table 10: standard reduction potentials 298K, volts vs. hydrogen electrode (Schweitzer, 2010).	32
Table 11: systems of crystal symmetry (Smallman, 2011).	50
Table 12: carbon concentration in different carbon steels (NSW Tafe Commission, 2008).	54
Table 13: chemical requirements ordinary strength hull structural steel (ABS, 2012).	61
Table 14: influence of the alloying elements on the properties of steel (ODS metals, 2007).	61
Table 15: overview inclusions types and appearance (based on ISO 4967, 1998).	67
Table 16: Cross reference table between steel class types and abbreviations used by different classification societies and the ASTM A 131 standard (Phione Limited, 2010). ..	90
Table 17: Chemical requirements ordinary strength hull structural steel (ABS, 2012).	91
Table 18: Overview of the steel composition and structure in the different steel samples. Division in three cluster. Average per cluster given, as well as standard deviation per element.	94
Table 19: overview corrosion rates for the 6, 10, 20 and 24 months permanent immersion. % gain of CRS to A and AH steel. Corrosion rates based on calculated density (weight/volume).	98
Table 20: corrosion rate after 6 months wet/dry situation. % gain of CRS to A and AH steel. Corrosion rates based on calculated density (weight/volume).	99
Table 21: Electrochemical determination of the corrosion rate. LPR and Tafel, expressed in $\text{mmy}^{-1}10^{-3}$	100
Table 22: β values as per Tafel curve of A, AH and CRS steel after 145 hours, expressed in volt.	101
Table 23: prolonged electrochemical measurements for 20, 44, 68, 121 and 145 hours. R_p , i_{corr} and corrosion speed are given for A, AH and CRS steel.	102

Table 24: chemical composition as specified by Lloyd's Rules (2001). Elements are given in %wt.....	106
Table 25: Mechanical properties for hull steels (Common Structural Rules for Bulk Carriers, IACS). ReH : minimum yield stress, in MPa, of the material, Rm : ultimate minimum tensile strength, in MPa, of the material, t : thickness in mm.....	107
Table 26: chemical composition traditional steel compared with JFE-Marin 400, experimental POSCO CRS and Corten A steel (ASTM, JFE, POSCO, 2012).....	111
Table 27: composition H16 (Melchers, 2003) and CRS, expressed in %wt.	112
Table 28: corrosion rate of H16 (Melchers, 2003) and CRS, expressed in mm y^{-1}	113
Table 29: Total amount and length of inclusions CRS sample 7 and 32 as per ASTM E2142-08, expressed in μm	121
Table 30: results KdG hardness measurements, according the Vickers HV10 and HRB tests. no unit.	122
Table 31: results KdG notch toughness measurements as per Charpy V-notch test. Impact energy in J and notch impact strength in Jmm^{-2}	122
Table 32: steel mechanical properties for different steel grades, Bureau Veritas, 2011.	123
Table 33: statistical information for impact energy for ship building steels (VanderHorn & Wang, 2011).....	123
Table 34: comparison yield stress (MPa), tensile strength (MPa) and elongation (%) of steel grades A, AH32, AH36 and CRS.	124
Table 35: statistical information for yield strength (MPa) for ship building steels from different steelmakers (2004-2009), related to the IACS standard, based on Vanderhorn & Wang (2011).....	125
Table 36: statistical information for tensile strength for ship building steels from different steelmakers (2004-2009), related to the IACS standards, based on Vanderhorn & Wang (2011).....	125
Table 37: statistical information for elongation for ship building steels (2004-2009) related to the IACS standard, based on Vanderhorn & Wang (2011).	126
Table 38: effect of small composition changes to corrosion rate, summary of various long term studies (Melchers, 2003).....	135
Figure 81: corroded plates after 270 days exposure splash zone. Left with VOS, right without VOS (NEI, 2007).Table 39: corrosion reduction in percentage for COS system after 30 and 270 days exposure (NEI, 2007).....	137

12 Abbreviations

a	Number of anodes	
A	Frequency factor	
AA	number aluminum anodes	
ABS	American Bureau of Shipping	
AES	Atomic emission spectroscopy	
AH	High tensile steel	
AS	Purchase price grade A steel	[€/ton]
ASA	Useful surface area of the anode	[m ²]
ASR	Quantity of steel replaced per dry dock, per age of the ship.	
ASTM	American Society for Testing and Materials	
BCC	Body centered cubic	
BCT	Body-centered tetragonal	
BOF	Bijzonder onderzoeks fonds	
BV	Bureau Veritas	
C	Concentration in the bulk solution	[mol ² /m ²]
CA	Corrosion allowance in	[mm]
CAN	Cost new building in grade A steel quality	[€/ton]
CCRS	Cost coating /re-coating CRS	[€]
CDD	Cost rental dry dock	[€/day]
CNCRS	Cost new building in CRS quality	[€/ton]
CNCRS	Cost new building corrosion resistant steel	[€]
CP	Breakdown of coating or area rusted on plates	
CRS	Corrosion resistant steel	
Cs	Specific heat	[J/(K·kg)]
CT	Continuous transformation	

D	Diffusion coefficient	[m ² /s]
DENS	Density	[kg/m ³]
DR	Discount rate	[%]
DRC	Days re-coating	
DWT	Deadweight	[ton]
E	Driving potential	[V]
E	Internal energy	[J]
E	Reduction potential	[V]
E_{298}^0	Standard reduction potential (25°C & 1bar)[V]	
E_a	Activation energy	[J]
E_{corr}	Corrosion potential	[V]
EDX	Energy-dispersive X-ray spectroscopy	
E_{eq}	Equilibrium potential	[V]
E_k	Kinetic energy	[J]
EMF	Electromotive Force	[V]
E_p	Passivation potential	[V]
E_r	Reversible potential	[V]
E_t	Transpassive potential	[V]
F	Faraday's constant	[C/Mol]
FCC	Face centered cubic	
FE-C	Iron- Cementite diagram	
G	Gibbs energy (Free energy)	[J]
G_{298}^0	Free energy (25°C & 1bar)	[J]
GDOES	Glow discharge optical emission spectroscopy	
GL	Germanisher Lloyd	
H	Enthalpy	[J]

H_{298}^0	Enthalpy (25°C & 1bar)	[J]
HCP	Hexagonal close-packed	
HTS	High tensile steel	
i	Current density	[A/m ²]
I	Current	[A]
i_0	Exchange current density	[A/m ²]
i_0	Exchange current	[A]
IA	Installation cost anodes	[€/piece]
i_a	Anodic current density	[A/m ²]
I_a	Anodic current	[A]
IAA	Initial installation cost aluminum anodes	[€]
IACS	International Association of Classification Societies	
I_{anode}	Delivered current per sacrificial anode	[A]
I_c	Cathodic current	[A]
i_c	Cathodic current density	[A/m ²]
I_{corr}	Corrosion current	[A]
i_{corr}	corrosion current density	[A/m ²]
i_{cp}	Current density at critical passivation	
i_g	Layer current density	[A/m ²]
I_g	Layer current	[A]
IMO	International Maritime Organization	
i_p	Current density at passivation	[A/m ²]
IR	inflation rate	[%]
i_{required}	Required current density	[A]
IZA	Initial installation cost zinc anodes	[€]
J	flux or movement	[mol/m ² s]

K	Equilibrium constant	
LOA	Length over all	[m]
LPR	Linear Polarization Resistance	
LR	Lloyds Register	
LWT	Lightweight	[ton]
LWT _T	Lightweight tank type I, III and IV	{ton}
LWT _{TII}	Lightweight tank type II	[ton]
M	Molar mass	[gmol ⁻¹]
m, n.....	Number of atoms, mol, electrons	
Nital	Nitric Acid in Methanol	
OES	Optical emission spectroscopy	
OPP	Surface ballast tanks	[m ²]
ORP	Oxidation/reduction potential	
P	coefficient of stiffness	
P	inflation rate	[%]
PA	Price aluminum	[€]
PCA	Principal Component Analysis	
PSPC	Performance Standard for Protective Coatings	
PSPC ₁₅	Coating according PSPC standards – 15 years lifetime expectancy	
PT	plate thickness	[m]
PZ	Price zinc	[€]
q	Electrical charge	[C]
q	Heat	[J]
Q	Reaction quotient	
R	Ideal gas constant	[JK ⁻¹ mol ⁻¹]
RA	Replacement of anodes	[€/piece]

RACRS	Ratio CRS versus grade A	
RAS	Replacement of steel	[€/ton]
RCCRS	Cost repairing CRS	[€/m ²]
RINA	Registro Italiano Navale	
R _p	polarization resistance	[Ω]
RPSPC	Cost of repairing PSPC ₁₅	[€/m ²]
RS	Russian Maritime Register of Shipping	
RTSCF	Cost of repairing TSCF ₂₅	[€/m ²]
S	Entropy	[J/K]
SA	Surface appearance	
SA _{total}	Total surface area to be protected	[m ²]
SD	Standard deviation	
SCE	Saturated Calomel Electrode	
SCI	Scrap per ton grade A steel	[€/ton]
SCRS	Scrap per ton CRS steel	[€/ton]
SEM	Scanning electron microscope	
SHE	Standard Hydrogen Electrode	
T	Temperature	[K]
TC	Time charter equivalent	[€/day]
TCB	Total cost of ballast tanks	[€]
TSCF	Tanker Structure Cooperative Forum	
TSCF ₂₅	Coating according TSCF standards – 25 years lifetime expectancy	
TTT curve	Time-Temperature-Transformation Curve	
U	Internal energy	[J]
u	Specific internal energy	[Jmol ⁻¹]
UTS	Ultimate Tensile Strength	

v	Speed	[m/s]
V	Volume	[m ³]
W	Number of microstates	
w	Work	[J]
WA	Weight anodes	[kg]
XRD	X-Ray diffraction	
ZA	Number zinc anodes	
α	Transfer coefficient	
δ	layer thickness	[m]
η	Overpotential ($E-E_{eq}$)	[V]

Publications

2009: Helen Verstraelen, Kris De Baere, Lucien Lemmens, Raf Dewil, Willy Schillemans, Silvia Lenaerts, Geert Potters; In situ study of ballast tank corrosion on ships – part 1 – Materials performance (NACE) october 2009

2009: Helen Verstraelen, Kris De Baere, Lucien Lemmens, Raf Dewil, Willy Schillemans, Silvia Lenaerts, Geert Potters; In situ study of ballast tank corrosion on ships – part 2 – Materials performance (NACE) november 2009

2009: Kris De Baere, Helen Verstraelen; Textbook of maritime medicine – Norwegian maritime directorate – Chapter 14 - ship control published 2010 + peer review hoofdstuk 2 – The shipping Industry – Prof. Siri Strandenes

2010: Kris De Baere, Helen Verstraelen, Geert Potters; Het schip gaat zo lang te water tot het doorroest – De Grote Rede 27 – Vlaams Instituut voor de zee – juni 2010 + Galois Genootschap jan-feb 2011

2010: Kris De Baere, Helen Verstraelen; De Belgische driekleur wappert weer als weleer – De Grote Rede 27 – Vlaams Instituut voor de zee – april 2010

2010: Kris De Baere, Helen Verstraelen, Raf Dewil, Lucien Lemmens, Silvia Lenaerts, Tharcisse Nkuzimana, Geert Potters; Impact of tank construction on corrosion of ship ballast tanks Materials Performance (NACE) mei 2010

2011: Kris De Baere, Helen Verstraelen, Lucien Lemmens, Silvia Lenaerts, Geert Potters; In situ study of the parameters quantifying the corrosion in ballast tanks and an evaluation of improving alternatives - Paper 11419, published NACE corrosion conference Houston, maart 2011

2011: Kris De Baere, Helen Verstraelen, Lucien Lemmens, Silvia Lenaerts, Geert Potters; In situ study of the parameters quantifying the corrosion in ballast tanks and an evaluation of improving, Eurocorr corrosion conference, Stockholm, September 2011
Reproduced Nautilus, Journal of Koninklijk Belgisch Zeemanscollege

2011: Kris De Baere, Helen Verstraelen; Roest slaapt nooit – Vlaams Instituut voor de Zee, "Zeekrant" juli 2011

2011: Kris De Baere, Helen Verstraelen; Roest slaapt nooit – De Wetenschap van De Zee, over een onbekende wereldoceaan, Vlaams Instituut voor de Zee, Acco, 175p.

2011: Kris De Baere, Helen Verstraelen, Geert Potters, Quantifying ballast tank Corrosion, Seawaysn The Nautical Institute, oktober 2011.

Reproduced by: The French Institute Of Navigation in their journal "Navigation"

Reproduced by: Ahrenkiel Shipmanagement in their newsletter

2011: Kris De Baere, Geert Potters, Helen Verstraelen; Corrosion control on new steel sheet piles in harbor waters – studie in opdracht van Acotec.

2013: Kris De Baere, Helen Verstraelen, Lucien Lemmens, Silvia Lenaerts, Steven Van Passel, Philippe Rigo, Geert Potters; The cost of corrosion – accepted for publication Marine Structures, Elsevier.

2013: Helen Verstraelen, Geert Potters, Lucien Lemmens, Deirdre Luyckx, Silvia Lenaerts, Kris De Baere, Impact of ship construction steel properties on ballast tank corrosion rate: methodological choices, accepted for publication Materials Performance, Nace.

2013: Kris De Baere, Helen Verstraelen , Lucien Lemmens, Silvia Lenaerts, Geert Potters; Does sacrifice guarantee a longer life? An in situ study of the effect of sacrificial anodes on the life expectancy of ballast tanks on board merchant vessels – Under review

Helen Verstraelen

CORROSION IN BALLAST TANKS ON BOARD OF MERCHANT VESSELS

Study of the relation between steel quality and corrosion

Corrosion in ballast tanks represents a major cost in the operation of merchant vessels. Reducing corrosion in these tanks increases the ship's lifetime expectancy. One of the defining elements of the corrosion process is the steel quality used for tank construction. It is therefore interesting to understand whether a relation exists between the steel characteristics and the corrosion rate.

To investigate this phenomenon, a test facility to study the corrosion behavior of different steel grades was built and used for a period of two years. The samples, immersed in real North Sea water for different periods of time and under different conditions, were collected on board ships performing steel work in dry-dock. An experimental corrosion resistant steel sample was added to the sample set allowing comparison.

This true to life investigation enlarges considerably the theoretical knowledge on ballast tank corrosion.

ABOUT THE AUTHOR

Helen Verstraelen studied Nautical Sciences. She specialized in safety at the University of Leuven. Presently she lectures Maritime Safety and Ecology at the Antwerp Maritime Academy.

Since 2007 she has been engaged in research on corrosion in the ballast tanks of merchant ships together with capt. dr. Kris De Baere and dr. Geert Potters.

www.upa-editions.be

ISBN 978 90 5718 278 5



9 789057 182785